PNNL-16683

Interim Report: Uranium Stabilization Through Polyphosphate Injection

300 Area Uranium Plume Treatability Demonstration Project

D. M. Wellman
E. M. Pierce
E. L. Richards
B. C. Butler
K. E. Parker
J. N. Glovack
S. D. Burton
S. R. Baum
E. T. Clayton
E. A. Rodriguez

July 2007

Prepared for the U.S. Department of Energy
under Contract DE-AC05-76RL01830

DISCLAIMER

This report was prepared as an account of work sponsored by an agency of the United States Government. Neither the United States Government nor any agency thereof, nor Battelle Memorial Institute, nor any of their employees, makes **any warranty, express or implied, or assumes any legal liability or responsibility for the accuracy, completeness, or usefulness of any information, apparatus, product, or process disclosed, or represents that its use would not infringe privately owned rights**. Reference herein to any specific commercial product, process, or service by trade name, trademark, manufacturer, or otherwise does not necessarily constitute or imply its endorsement, recommendation, or favoring by the United States Government or any agency thereof, or Battelle Memorial Institute. The views and opinions of authors expressed herein do not necessarily state or reflect those of the United States Government or any agency thereof.

PACIFIC NORTHWEST NATIONAL LABORATORY
operated by
BATTELLE
for the
UNITED STATES DEPARTMENT OF ENERGY
under Contract DE-AC05-76RL01830

Printed in the United States of America

Available to DOE and DOE contractors from the
Office of Scientific and Technical Information,
P.O. Box 62, Oak Ridge, TN 37831-0062;
ph: (865) 576-8401
fax: (865) 576-5728
email: reports@adonis.osti.gov

Available to the public from the National Technical Information Service,
U.S. Department of Commerce, 5285 Port Royal Rd., Springfield, VA 22161
ph: (800) 553-6847
fax: (703) 605-6900
email: orders@ntis.fedworld.gov
online ordering: http://www.ntis.gov/ordering.htm

This document was printed on recycled paper.
(9/2003)

PNNL-16683

Interim Report: Uranium Stabilization Through Polyphosphate Injection

300 Area Uranium Plume Treatability
Demonstration Project

D. M. Wellman
E. M. Pierce
E. L. Richards
B. C. Butler
K. E. Parker
J. N. Glovack
S. D. Burton
S. R. Baum
E. T. Clayton
E. A. Rodriguez

July 2007

Prepared for
the U.S. Department of Energy
under Contract DE-AC05-76RL01830

Pacific Northwest National Laboratory
Richland, Washington 99352

Summary

For fiscal year 2006, the United States Congress authorized $10 million dollars to Hanford for "…analyzing contaminant migration to the Columbia River, and for the introduction of new technology approaches to solving contamination migration issues." These funds are administered through the U.S. Department of Energy Office of Environmental Management (specifically, EM-22). After a peer review and selection process, nine projects were selected to meet the objectives of the appropriation. As part of this effort, Pacific Northwest National Laboratory (PNNL) is performing bench- and field-scale treatability testing designed to evaluate the efficacy of using polyphosphate injections to reduce uranium concentrations in the groundwater to meet drinking water standards (30 μg/L) in situ. This technology works by forming phosphate minerals (autunite and apatite) in the aquifer, which directly sequesters the existing aqueous uranium in autunite minerals and precipitates apatite minerals for sorption and long-term treatment of uranium migrating into the treatment zone, thus reducing current and future aqueous uranium concentrations. Polyphosphate injection was selected for testing based on technology screening as part of the 300-FF-5 Phase III Feasibility Study for treatment of uranium in the 300 Area.

The overall objectives of the treatability test include the following:

- Optimize the use of multi-length polyphosphate amendment formulations, quantify the hydrolysis rates of polyphosphate, quantify the kinetics of autunite and apatite formation, and determine the long-term immobilization of uranium by apatite and longevity for polyphosphate injections to remediate uranium such that costs for full-scale application can be estimated effectively.

- Inject polyphosphate to evaluate reduction of aqueous uranium concentrations and to determine the longevity of treatment of the process at full scale.

- Demonstrate field-scale application of polyphosphate injections to evaluate whether a full-scale process can be implemented.

This report presents results from bench-scale treatability studies conducted under site-specific conditions to optimize the polyphosphate amendment for implementation of a field-scale technology demonstration to treat aqueous uranium within the 300 Area aquifer of the Hanford Site. The general treatability testing approach consisted of conducting studies with site sediment and under site conditions, to develop an effective chemical formulation for the polyphosphate amendments and evaluate the transport properties of these amendments under site conditions. Phosphorus-31 nuclear magnetic resonance was used to determine the effects of Hanford groundwater and sediment on the degradation of inorganic phosphates. Static batch tests were conducted to optimize the composition of the polyphosphate formulation for the precipitation of apatite and autunite, and to quantify the kinetics, loading, and stability of apatite as a long-term sorbent for uranium. Dynamic column tests were used to further optimize the polyphosphate formulation for emplacement within the subsurface and the formation of autunite and apatite. In addition, dynamic testing quantified the stability of autunite and apatite under relevant site conditions. Results of this investigation provide valuable information for designing a full-scale remediation of uranium in the 300 Area aquifer.

Acknowledgments

Funding for this project was provided by the U.S. Department of Energy (DOE), Office of Environmental Management, EM-20 Environmental Cleanup and Acceleration. This work was conducted in part at the William R. Wiley Environmental Molecular Sciences Laboratory (EMSL), a DOE Office of Science User Facility, under proposal number 5592.

Acronyms

ASTM	American Society for Testing and Materials
BET	Brunauer-Emmett-Teller
BTC	breakthrough curve
CAS	
DCL	deuterated hydrochloric acid
DIW	deionized water
DOE	U.S. Department of Energy
EDS	energy dispersive spectroscopy
EPA	U.S. Environmental Protection Agency
EXAFS	extended x-ray absorption fine structure (spectroscopy)
FAP	fluorapatite
FY	fiscal year
GHR	calcium-autunite
HGW	Hanford groundwater
HPDE	high-density polyethylene
ICP-OES	inductively coupled plasma-optical emission spectrometry
ICP-MS	inductively coupled plasma-mass spectrometry
MCL	maximum concentration limit [in groundwater reports, MCL = maximum contaminant level]
M&TE	materials and test equipment
NBS	National Bureau of Standards
OCP	octacalcium-phosphate
PFA	perfluoroalkoxide
PNNL	Pacific Northwest National Laboratory
^{31}P NMR	phosphorus-31 nuclear magnetic resonance
ROD	record of decision
SEM	scanning electron microscope
SI	saturation index
SPFT	single-pass flow-through (test)

TRIS	tris hydroxymethyl aminomethane
UV	ultraviolet
XRD	x-ray diffraction

Contents

Summary iii

Acknowledgments v

Acronyms vii

1.0 Introduction 1.1

1.1 Background 1.1

1.1.1 300 Area Uranium Plume 1.1

1.1.2 Polyphosphate Remediation Technology 1.6

1.2 Objectives 1.8

2.0 Laboratory Testing – Materials and Methods 2.1

2.1 Polyphosphate Hydrolysis Experiments 2.1

2.2 Autunite and Apatite Formation 2.3

2.2.1 Batch Experiments 2.3

2.2.2 Column Experiments 2.4

2.3 Immobilization of Uranium by Apatite 2.5

2.3.1 Apatite Pre-Equilibration 2.5

2.3.2 Kinetic Experiments 2.6

2.3.3 Loading Experiments 2.6

2.3.4 Desorption Experiments 2.7

2.3.5 Column Experiments 2.8

2.4 Apatite Barrier Longevity 2.8

2.4.1 Single-Pass Flow-Through Test Methods 2.8

2.5 Effect of pH and Temperature on the Dissolution Kinetics of Meta-Autunite Minerals 2.11

2.5.1 Starting Materials 2.12

3.0 Results and Discussion 3.1

3.1 Polyphosphate Hydrolysis Experiments 3.1

3.2 Apatite and Autunite Formation 3.3

3.2.1 Batch Experiments 3.3

3.2.2 Column Experiments 3.8

3.3 Immobilization of Uranium via Apatite 3.19

3.3.1 Sorption Kinetics 3.20

3.3.2 Loading and Sorption Isotherms 3.22

3.3.3 Desorption of Uranium 3.23

3.3.4 Column Transport Experiments 3.25
3.4 Apatite Barrier Longevity 3.26
3.4.1 Hydroxyapatite Single-Pass Flow-Through Dissolution Experiments 3.26
3.4.2 Column Experiments 3.32
3.5 Effect of pH and Temperature on the Dissolution Kinetics of Meta-Autunite Minerals 3.33
3.5.1 Interlayer Cation Release Rates 3.37
3.5.2 Structural Dissolution 3.37
3.6 Polyphosphate Amendment 3.39
4.0 Conclusions 4.1
5.0 References 5.1
Appendix A.1

Figures

1 Map of the Hanford Site 1.2
2 300 Area Detail Map Showing Uranium Plume in December 2005 and Test Site Location 1.4
3 300 Area Detail Map Showing Uranium Plume in June 2006 ..... 1.5
4 Schematic Depicting the 300-FF-5 Operable Unit Geology and Proposed Treatability Test of Polyphosphate to Sequester Uranium 1.6
5 Schematic Depicting the Step-Wise Hydrolysis of Sodium Tripolyphosphate 1.7
6 Hydrolysis Rate of Polyphosphate Molecules as a Function of pH 1.7
7 Photo Displaying the Apatite Barrier Placed in the Middle of a Sediment Column Composed of the <2-mm Fraction from the 300 Area 2.8
8 Schematic of the Single-Pass Flow-Through Dissolution Test System 2.9
9 A ^{31}P NMR Spectrum of a Buffered Aqueous Solution of 0.2 M Pyro- and Tripoly-Phosphate Solutions 3.1
10 A ^{31}P NMR Spectrum Integrated Peak Area as a Function of a Known Aqueous Concentration of Tripolyphosphate 3.2
11 Percentage of Phosphorus as Tripolyphosphate as a Function of Time for Homogeneous Experiments Conducted with Aqueous Cations, Al^{3+}, Ca^{2+}, Fe^{3+}, Mg^{2+}, and Hanford Site Groundwater; and Heterogeneous Experiments Conducted with Solids, FeOOH, and Hanford Site Sediment 3.2
12 Percent Removal of Calcium and Phosphorus as a Function of Calcium-to-Phosphorus Molar Ratio 3.9

13 Representative Photo of Sediment Sectioned from the Effluent End of Column 1 Illustrating the Visual Identification of Uranium-Phosphate under Shortwave UV Radiation 3.11

14 Photo Showing Disperse Precipitation of Calcium-Phosphate Throughout Column 1 and Discrete Precipitation of Calcium-Phosphate within Column 4 ..... 3.13

15 Graphs Depicting Aqueous Uranium Concentrations from Columns Saturated with 1,000 μg/L Uranium as a Function of the Number of Pore Volumes of Polyphosphate Remedy Displaced Through Columns 11, 12, 13, and 4 ..... 3.15

16 Photos of Column Sections Taken under Shortwave UV Radiation. 3.15

17 Graphs Depicting Aqueous Uranium Concentrations from Columns Saturated with 1,000 μg/L Uranium as a Function of the Number of Pore Volumes of Polyphosphate Remedy Displaced Through Columns 15, 16, 17, and 18 ..... 3.16

18 Representative Plot Depicting the Removal of Phosphorus by Sorption and Precipitation Reactions 3.17

19 Breakthrough Curves for Sodium Ortho-, Pyro-, Tripolyphosphate, Calcium, the Phosphorus Amendment Formulation as Mixed, and the Phosphorus Amendment Formulation pH Adjusted to ~7 ..... 3.18

20 Rate of Aqueous Uranium Sorption on Hydroxyapatite in Apatite Equilibrated Water 3.21

21 Sorption of Aqueous Uranium on Hydroxyapatite as a Function of the Solution-to-Solid Ratio under the pH Range of 6 to 7 ..... 3.23

22 Percent Desorption of Uranyl from Hydroxyapatite as a Function of the Cumulative Volume of Apatite-Equilibrated Water and Hanford Groundwater 3.24

23 A Scanning Electron Photomicrograph of Hydroxyapatite in Apatite-Equilibrated Water Reacted with 100 ppm Uranium at pH 7 ..... 3.25

24 Experimental Migration of Uranium in Hydraulically Saturated Columns Through 300 Area Sediment and Sediment Containing an Apatite Barrier 3.26

25 Heat of Dissolution for Fluor-, Chlor-, and Hydroxyapatite 3.27

26 Aqueous Effluent Concentration of Calcium and Phosphorus as a Function of Reaction Time 3.28

27 Effect of the Variation in *q/S* as Indexed by the Release of Calcium and Phosphorus from Hydroxyapatite 3.29

28 Rate of Hydroxyapatite Dissolution as Indexed by the Release of Calcium and Phosphorus as a Function of Temperature-Corrected pH 3.30

29 The Ca:P ratio as a Function of pH as Measured in Effluent Samples During Dissolution Testing 3.30

30 Predicted Saturation State Based on Effluent Solution Concentrations for the Dissolution of Hydroxyapatite in 0.05 M THAM at 40°C 3.31

31 Predicted Phosphorus Mineral Saturation Indices Based on the Reaction of Hydroxyapatite at 40°C, pH 8 ..... 3.31

32 Scanning Electron Photomicrograph of Hydroxyapatite Reacted at 40°C, pH = 8, Illustrating the Re-Precipitation of Hydroxyapatite on the Surface of the Starting Material 3.32

33 Predicted Calcium Mineral Saturation Indices Based on the Reaction of Hydroxyapatite at 40°C 3.33

34 Experimental Release of Calcium and Phosphorus from 300 Area Sediment Containing a 5-wt% Hydroxyapatite Barrier 3.33

35 Log_{10} Uranium Release Rate as a Function of Temperature-Corrected pH for Na-Autunite in 0.01 M THAM solution, and Log_{10} Uranium Release Rate as a Function of Temperature-Corrected pH for GHR in 0.01 M THAM Solution 3.35

36 Log_{10} Phosphorus Release Rate as a Function of Temperature-Corrected pH for Na-Autunite in 0.01 M THAM Solution, and Log_{10} Phosphorus Release Rate as a Function of Temperature-Corrected pH GHR in 0.01 M THAM Solution 3.36

37 Log_{10} Sodium Release Rate as a Function of Temperature-Corrected pH for Na-Autunite in 0.01 M THAM solution, and Log_{10} Calcium Release Rate as a Function of Temperature-Corrected pH for GHR in 0.01 M THAM Solution 3.37

38 A SEM Photomicrograph of Reacted Na-Autunite Illustrating Basal Cleavage of the Autunite Plates from Attack During Dissolution 3.39

39 Viscosity of Polyphosphate Amendment 3.41

Tables

1 Proposed Phosphate Sources for Polyphosphate Amendment 2.4

2 Composition of Solutions Used in Sorption Experiments 2.6

3 Composition of Solutions Used in Single-Pass Flow-Through Experiments 2.10

4 Source, Particle Size, and Surface Area of Autunite Minerals. 2.12

5 Possible Sources and Associated Solubility for Polyphosphate Amendment 3.3

6 Experimental Batch Conditions for Polyphosphate Amendment Optimization 3.4

7 Down-Selected Experimental Batch Conditions for Polyphosphate Amendment Optimization 3.6

8 Experimental Parameters for Polyphosphate Amendment Optimization Column Tests 3.10

9 Transport Parameters Determined by Direct Measurement or from Laboratory-Derived Breakthrough Curve on the <2-mm Sediment Fraction 3.17

10 Field Transport Parameters Calculated from Laboratory-Derived Transport Parameters 3.19

11 Uranium Speciation in Sorption Experiments at 23°C Were Calculated Using the EQ3NR Code V8.0 Database 3.22

12 Mineral Saturation Indices Based on Effluent Solution Compositions from Dissolution of GHR in 0.01 M THAM Buffer 3.36

13 Release Rates from Autunite Samples in H_2O and D_2O at pH(D) = 8, T = 40°C 3.38

14 Pilot Scale Field Test Amendment Formulation 3.40

1.0 Introduction

This report covers work elements associated with the integration of site-specific characterization data with laboratory testing, in order to optimize the polyphosphate amendment for implementation of a field-scale technology demonstration to treat aqueous uranium within the 300 Area aquifer of the Hanford Site. The polyphosphate treatability test will evaluate the efficacy of using polyphosphate injections to reduce uranium concentrations in the groundwater to meet drinking water standards (30 µg/L) in situ. The technology works by forming phosphate minerals (autunite and apatite) in the aquifer, which directly sequesters the existing aqueous uranium in autunite minerals and precipitates apatite minerals for sorption and long-term treatment of uranium migrating into the treatment zone, thus reducing current and future aqueous uranium concentrations (Wellman et al. 2005, 2006). Polyphosphate injection was selected for testing based on previous lab-scale investigations. In situ treatment of uranium contamination is consistent with the results of technology screening, identifying a viable remedial action alternative for uranium in 300 Area groundwater, as part of the 300-FF-5 Phase III Feasibility Study (DOE 2005).

The field site for the polyphosphate treatability test, which is located around well 399-1-23, was selected from four detailed characterization wells installed during fiscal year (FY) 2006 as part of the 300 Area limited field investigation (Williams et al. 2007). The polyphosphate treatability test site is composed of a single injection well (399-1-23) surrounded by a network of monitoring wells within the targeted injection volume as well as a network of downgradient monitoring wells. The monitoring wells were installed in November and December 2006 as part of the initial site characterization as described by Vermuel et al. (2006). Additional downgradient monitoring wells were installed to facilitate monitoring of amendment/tracer plume drift under the groundwater flow regime expected during spring high river stage conditions.

1.1 Background

This section provides background information on the 300 Area uranium plume and selection of polyphosphate remediation technology for further site-specific evaluation and treatability testing. In 1996, a record of decision (EPA 1996) identified the following interim actions for remediation of the uranium contaminant plume beneath the site:

- continued groundwater monitoring to determine how contaminant conditions may change with time
- institutional controls to limit the use of groundwater.

Interim action results determined that uranium concentrations in the groundwater plume have been generally declining, but still persist at concentrations above the drinking water standard (remediation goal); therefore, re-evaluation of the remedy for uranium contamination was necessary. During the 300-FF-5 Phase III Feasibility Study technology screening process, polyphosphate treatment was judged to be the most promising among five other active remedial technologies for uranium at this site for reducing the concentration of dissolved uranium, and it was selected for further testing.

1.1.1 300 Area Uranium Plume

During the period spanning the startup of Hanford reactors in 1944 through the late 1980s, facilities in the 300 Area of the Hanford Site were primarily involved with fabrication of nuclear fuel for plutonium

production, which included some research and development activities (Young and Fruchter 1991). The range of activities produced a wide variety of waste streams that contained chemical and radiological constituents (Gerber 1992; DeFord et al. 1994). Since the early 1990s, extensive remediation of liquid waste disposal sites and solid waste burial grounds has taken place. As of March 2004, most liquid waste disposal sites, which are located in the north half of the 300 Area (shown in Figure 1), have been excavated, backfilled, and the ground surface restored. Some unknown amount of contamination remains in the vadose zone beneath the lower extent of the excavation activities. Additional contamination may also remain beneath buildings and facilities in the southern portion of the 300 Area, where decontamination and decommissioning activities have not yet taken place.

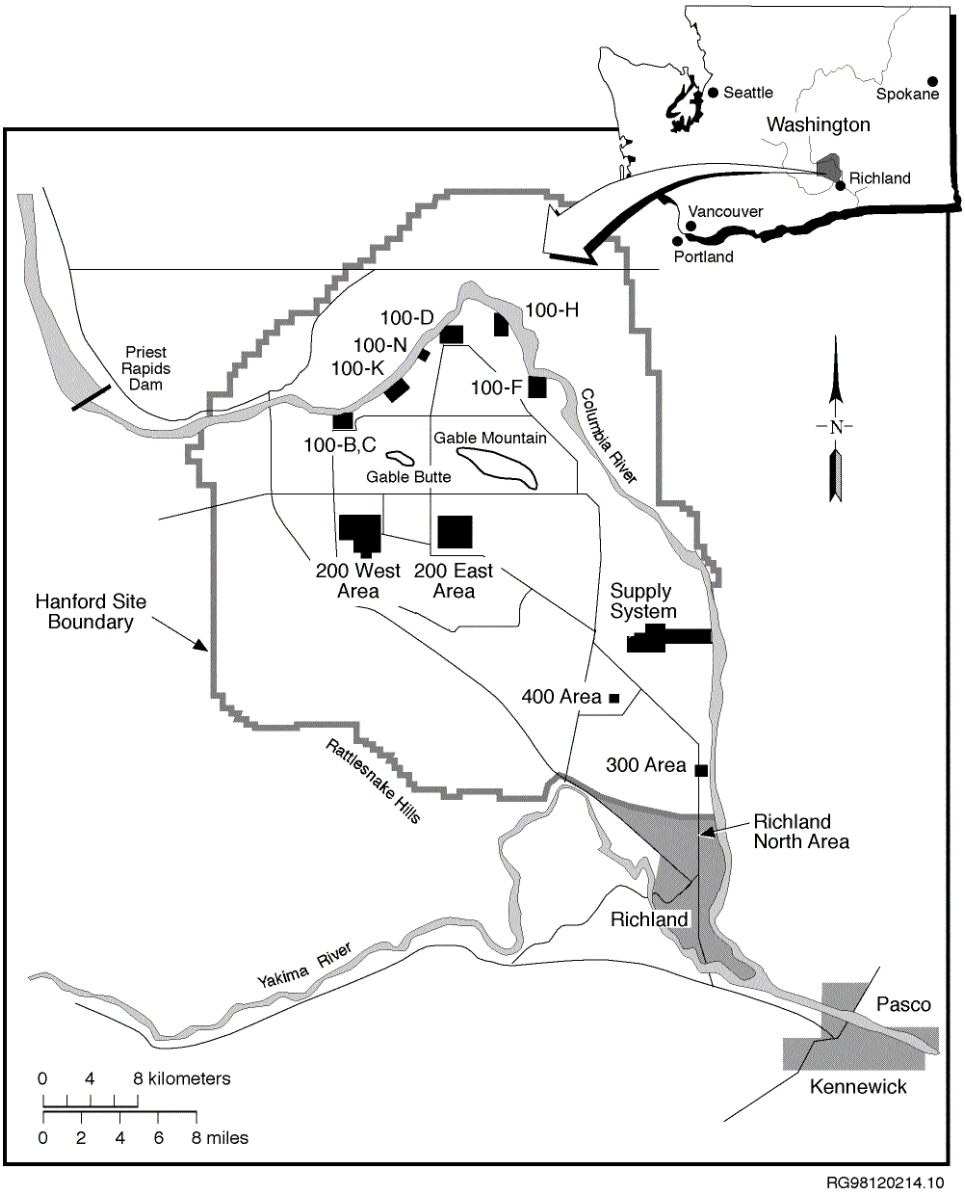

Figure 1. Map of the Hanford Site

The 300-FF-5 Operable Unit, a groundwater operable unit, includes the water and solids that constitute the aquifer. The 300-FF-5 Operable Unit, located in the southeast portion of the Hanford Site, includes groundwater affected by contaminants released from waste sites in three geographic sub-regions of the operable unit: the 300 Area, 618-11 burial ground, and 316-4 cribs/618-10 burial ground.

Groundwater beneath the 300 Area and the two outlying geographic sub-regions (618-11 burial ground and 316-4 cribs/618-10 burial ground) contain contaminants from past-practice disposal activities at concentrations that exceed the U.S. Environmental Protection Agency (EPA) standards for drinking water supplies (Figure 2 and Figure 3). Uranium is the most prominent waste constituent remaining in the environment, and it has persisted in waste sites and groundwater during the years following the shutdown of most fuel fabrication activities and cessation of liquid effluent disposal to the ground. Uranium in its soluble form is of concern because of its chemical toxicity and risk of radiological exposure, even though the concentrations in groundwater for chemical toxicity are lower than those associated with exceeding radiological dose standards. Specific criteria for the toxicity to freshwater aquatic organisms are not currently established, so by default, the criteria for the protection of aquatic organisms are the same as those applied for the protection of human health.

The uranium plume is just upstream of the City of Richland municipal water supply intake on the Columbia River. Elevated uranium concentrations enter the river along the shoreline and enter the riparian and river biota through seeps. The 1996 record of decision (ROD) for the 300-FF-5 Operable Unit (EPA 1996) stipulated an interim action program of a natural attenuation process accompanied by increased groundwater monitoring. The remedial action objective of the ROD is reduction of groundwater uranium to the EPA maximum contaminant level (MCL). The EPA's MCL in groundwater for drinking water supplies is currently 30 μg/L uranium, measured as total uranium in the water sample. During the remedial investigation in the early 1990s and the development of the initial ROD, the proposed standard for uranium was 20 μg/L.

As indicated through comparison of Figures 2 and 3, during high river stage conditions in June 2006, uranium concentrations were elevated in localized areas farther inland than indicated during December 2005. It is thought that these increases in uranium concentration are associated with contamination remaining in the deep vadose zone and capillary fringe. The polyphosphate treatability test site is located near one of the two delineated deep vadose sources. The persistence of this plume is enigmatic for several reasons, including: 1) discharges containing uranium-bearing effluent to ground disposal sites ended in the mid-1980s; 2) contaminated soil associated with these waste sites was removed during the 1990s, with backfilling complete by early 2004; and 3) the aquifer is composed of highly transmissive fluvial sediment, suggesting rapid movement of groundwater. Also, a water supply well, located within the plume has been in operation since 1980, with no observable effect on the plume. The current conceptual site model assumes that re-supply of the plume is occurring, with continuing release from the vadose zone beneath waste sites, the capillary fringe zone, and possibly from aquifer solids, as source candidates (Peterson et al. 2005).

Maximum concentrations in the plume are currently less than 250 μg/L, with mode values ranging from 30 to 90 μg/L. The plume (>30 μg/L) currently covers an area of ~0.4 km^2 (0.15 mi^2). Assuming a representative thickness of the contaminated layer of 3.3 m (10.8 ft) and 27% porosity, the volume of

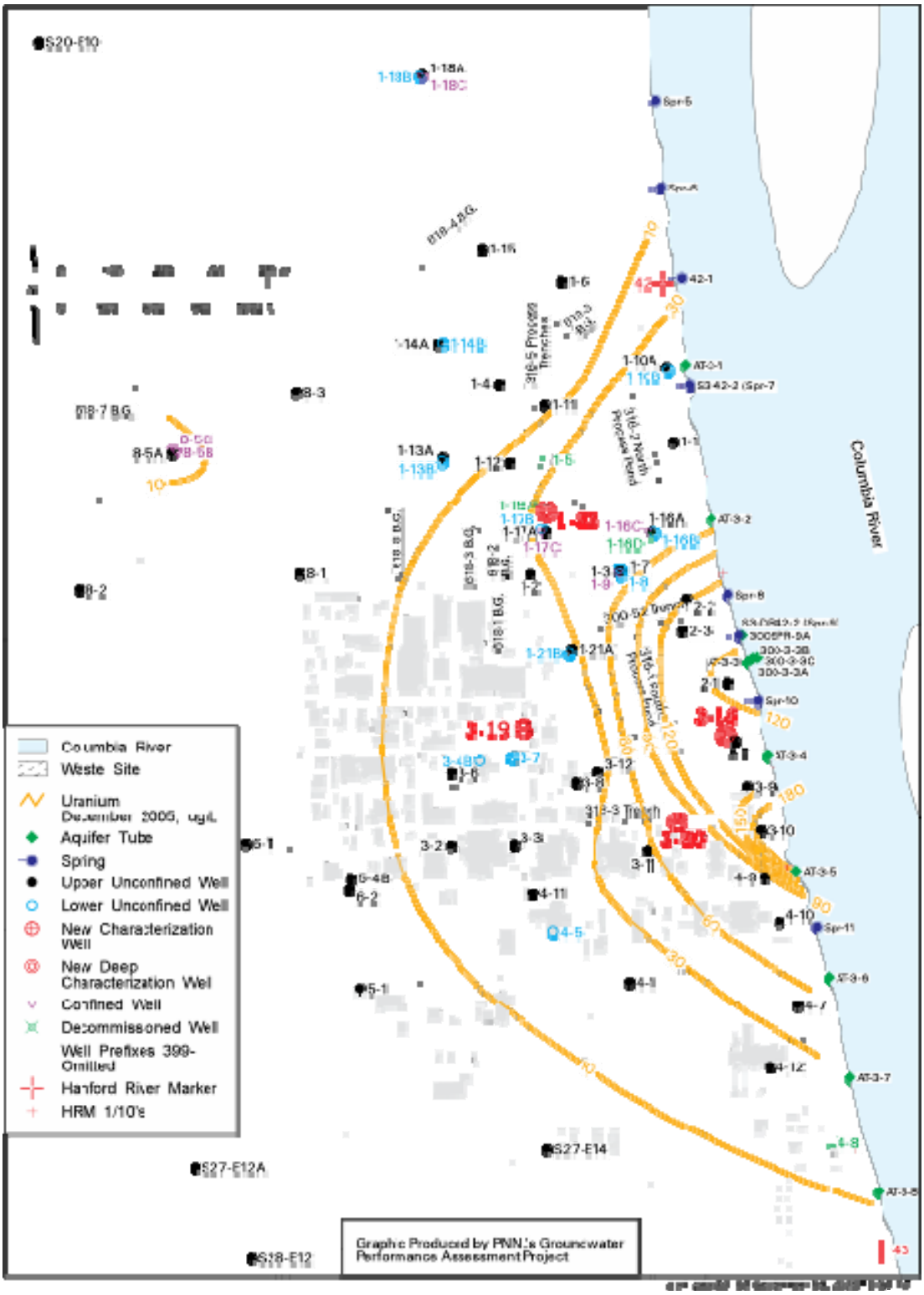

Figure 2. 300 Area Detail Map Showing Uranium Plume in December 2005 and Test Site Location (around well 399-1-23)

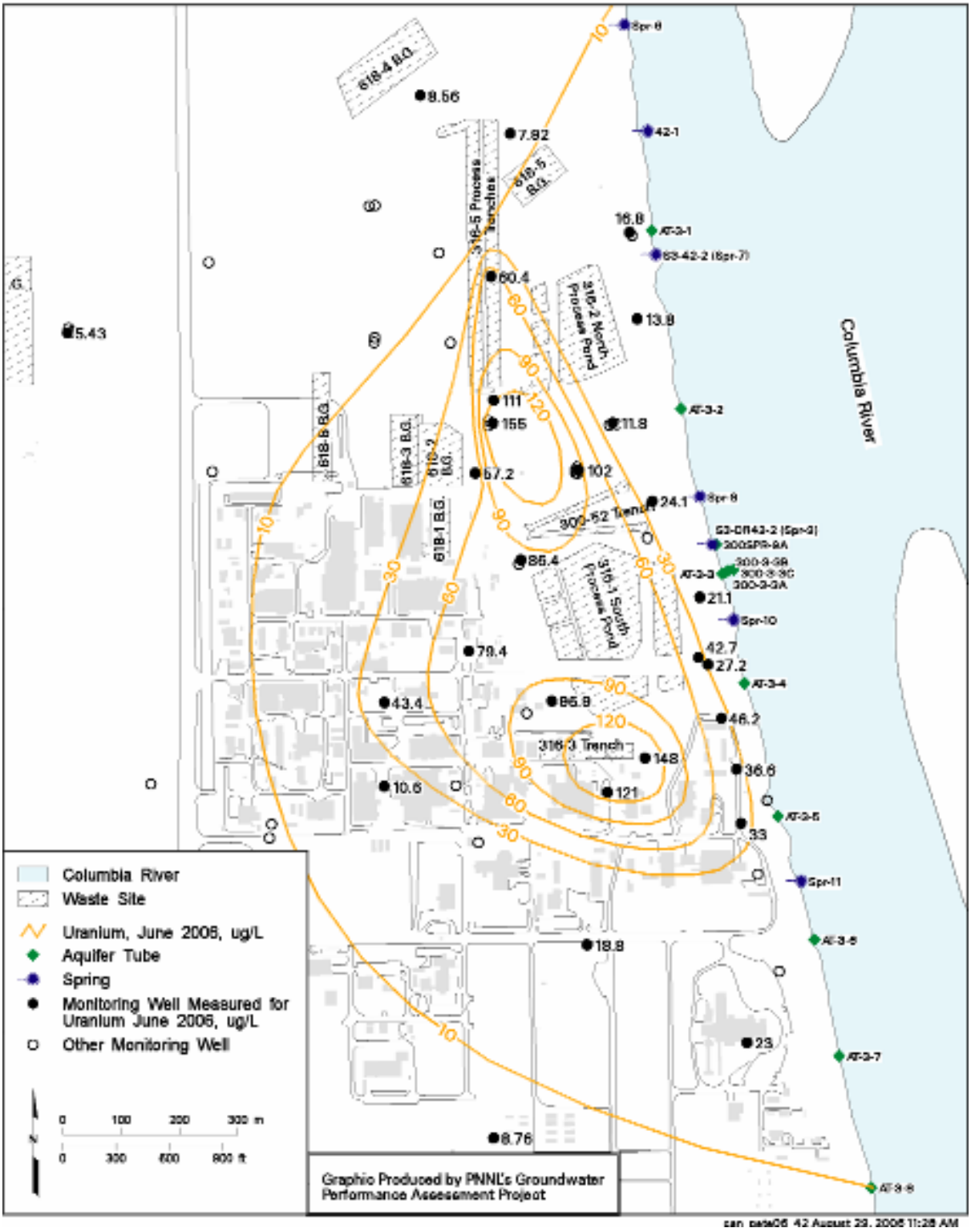

Figure 3. 300 Area Detail Map Showing Uranium Plume in June 2006

contaminated groundwater is ~350,000 m^3 (460,000 yd^3) and the mass of dissolved uranium is ~20 kg (44 lb) (Peterson et al. 2005). The length of Columbia River shoreline impacted is ~1,500 m (4,900 ft). Uranium removal via a water supply well for the 331 Life Sciences Building is ~21 kg (46 lb) per yr, based on monitoring data.

Despite the cessation of uranium releases and the removal of shallow vadose zone source materials, the second five-year review of the ROD will state that as of 2006, dissolved uranium concentration below the cleanup criteria established by the ROD have not been achieved within the anticipated 10-year time period. A Phase III feasibility study was begun in 2005 to identify and evaluate remedial alternatives that will accelerate monitored natural attenuation of the uranium plume. Polyphosphate application is judged to be the most promising among five other active remedial technologies for uranium at this site. Presently focused application of polyphosphate is proposed in source or "hot spot" areas that would significantly reduce the inventory of available uranium that contributes to the groundwater plume (Figure 4).

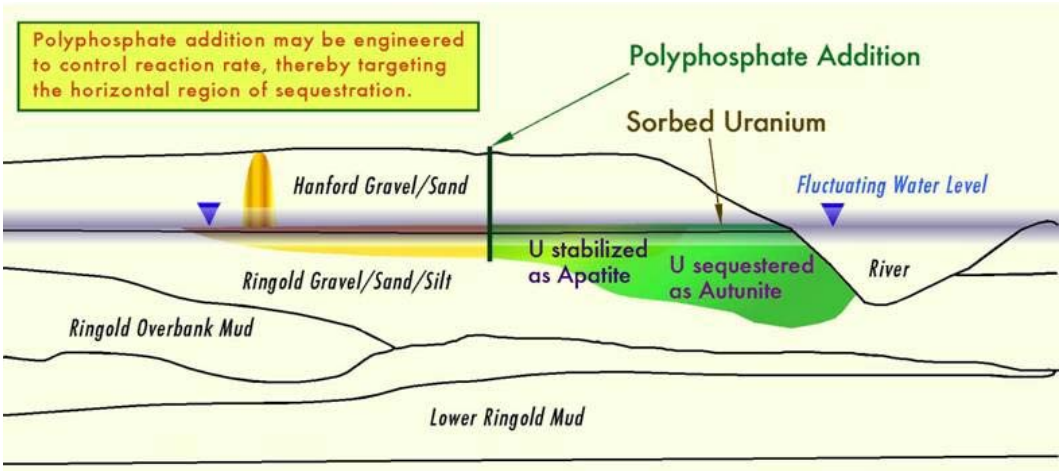

Figure 4. Schematic Depicting the 300-FF-5 Operable Unit Geology and Proposed Treatability Test of Polyphosphate to Sequester Uranium

1.1.2 Polyphosphate Remediation Technology

Numerous approaches have been proposed to sequester uranium, in situ, with solid-phase hydroxyapatite, $Ca_5(PO_4)_3OH$, (Conca 1996; Arey et al. 1999; Wright et al. 1995; Seaman et al. 2001; Moore et al. 2001; Gauglitz and Holterdorf 1992), and water-soluble phosphate compounds, such as tribasic sodium phosphate [$Na_3(PO_4)\cdot nH_2O$] (Lee et al. 1995) or phytic acid (Jensen et al. 1996; Nash et al. 1998b; Nash et al. 1998a; Nash et al. 1999), which could be injected into contaminant plumes from strategically placed wells, acting as a chemical stabilizer for uranium and other radionuclides and heavy metals. The advantages of soluble amendments is that they allow for treatment of plumes situated deep within the subsurface and act to sequester uranium by precipitating insoluble uranium minerals rather than by reversible sorption mechanisms. However, Wellman et al. (2006b) demonstrated that compounds including tribasic sodium phosphate and phytic acid result in the rapid formation of phosphate phases. Formation of these phases occludes ~30% of the fluid-filled pore space within the sedimentary formation. Rapid reduction in the hydraulic conductivity will have a significant effect on subsequently injected amendment solutions, the targeted groundwater plume, or both, by deflecting flow from the natural path.

Conversely, the use of soluble long-chain polyphosphate materials have been demonstrated to delay the precipitation of phosphate phases (Wellman et al. 2005b; Wellman et al. 2006b) (Figure 5). Precipitation of phosphate minerals occurs when phosphate compounds degrade in water, due to hydrolysis, to yield the orthophosphate molecule (PO_4^{3-}). The longer the polyphosphate chain, the slower the hydrolysis reaction leading to orthophosphate production (Shen and Morgan 1973) (Figure 6). Accordingly, use of a long-chain polyphosphate compound does not result in a drastic change in hydraulic conductivity of the target aquifer.

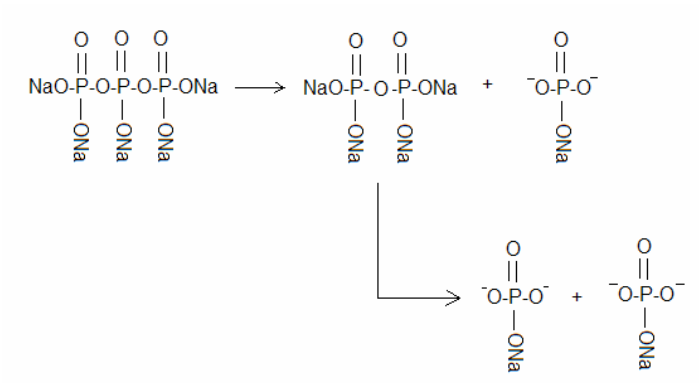

Figure 5. Schematic Depicting the Step-Wise Hydrolysis of Sodium Tripolyphosphate

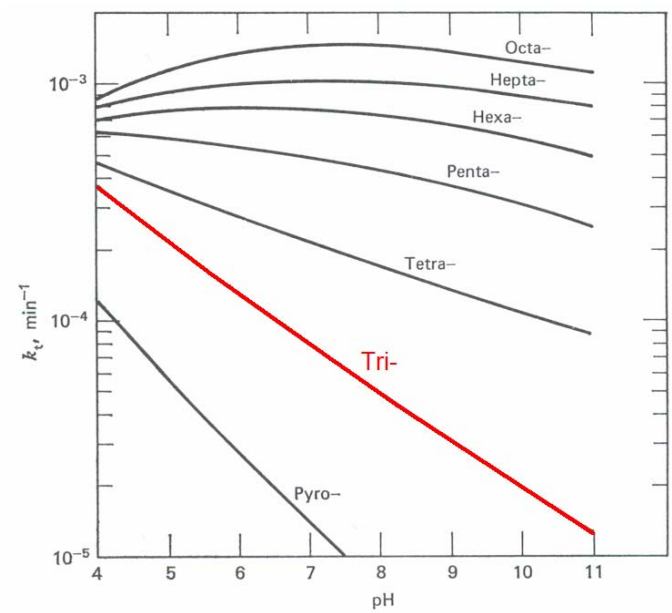

Figure 6. Hydrolysis Rate of Polyphosphate Molecules as a Function of pH (Shen and Morgan 1973)

Injection of a sodium tripolyphosphate amendment into the uranium-bearing saturated porous media has been shown to immobilize uranium through the formation of an insoluble uranyl phosphate mineral, autunite $X_{1-2}[(UO_2)(PO_4)]_{2-1} \bullet nH_2O$, where X is any monovalent or divalent cation. Because autunite sequesters uranium in the oxidized form, U^{6+}, rather than forcing reduction to U^{4+}, the possibility of re-oxidation and subsequent re-mobilization of uranium is negated. Release of uranium from the autunite structure may only occur through dissolution of the autunite structure. Extensive testing demonstrates the very low solubility and slow dissolution kinetics of autunite under conditions relevant to the Hanford subsurface (Wellman et al. 2006b). In addition to autunite, excess phosphorous can result in apatite mineral formation, providing a long-term source of treatment capacity.

Research beginning in the mid-1960s underscored the efficacy of using calcium and/or lime to precipitate stable calcium-phosphate solid phases including apatite for direct removal of phosphate (Ferguson et al. 1973; Ferguson et al. 1970; Schmid and McKinney 1968; Jenkins et al. 1971). By complexing calcium and sorbing to mineral surfaces, polyphosphate compounds effectively enhance the rate of calcium-phosphate precipitation by reducing competing reactions, such as the formation of calcium-carbonate, and "direct" calcium to participate in reactions resulting in calcium-phosphate precipitation (Ferguson et al. 1973).

Fuller et al. (2002a and 2003) demonstrated the efficacy of hydroxyapatite for reducing the aqueous uranium concentration to <0.05 μM under the pH range of 6.3 to 6.9 in the presence of carbonate. Results suggested the binding of uranium, irrespective of dissolved carbonate concentration or aqueous uranium concentration, occurred via surface complexation; long-term retention occurs through the transformation of sorbed apatite to H-autunite (chernikovite). Similar evidence for the long-term retention of uranium via initial sorption and subsequent transformation to uranium mineral phases of low solubility has been observed downgradient of the uranium ore deposit at Koongarra, Australia (Murakami et al. 1997).

1.2 Objectives

Critical to successful execution of the treatability test is 1) the evaluation and optimization of multi-length polyphosphate amendment formulations, 2) the hydrolysis rates of polyphosphates, 3) kinetics of autunite and apatite formation, and 4) long-term immobilization of uranium by apatite. The stability of autunite under conditions relevant to the 300 Area aquifer (Wellman et al. 2006a), the efficacy of soluble sodium tripolyphosphate for in situ immobilization of uranium via formation of autunite (Wellman et al. 2005b; Wellman et al.[(a)], and the efficacy of polyphosphate to control in situ precipitation kinetics, precluding changes in hydraulic conductivity (Wellman et al. 2006b), have been discussed in detail elsewhere. As such, although the in situ formation of autunite is discussed and the results of autunite dissolution kinetic testing are briefly summarized in this report, the majority of the results presented here regard the migration and emplacement of polyphosphate amendments and the formation, stability, and efficacy of apatite for the sequestration of uranium under conditions relevant to the 300 Area aquifer. This document describes a laboratory testing program performed at PNNL in support of the in support of the 300-FF-5 treatability test. The objective of the proposed treatability test was to evaluate the efficacy of using polyphosphate injections to treat uranium-contaminated groundwater in situ.

These activities were conducted in parallel with a limited field investigation, which was conducted to more accurately define the vertical extent of uranium in the vadose zone, capillary fringe zone, and laterally throughout the plume. The treatability test establishes the viability of the method and, along with characterization data from the limited field investigation, provides the means to determine how best to implement the technology in the field. By conducting the treatability work in parallel with the limited field investigation, the resulting feasibility study will provide, site-specific information for evaluating polyphosphate addition and will select a suitable remediation strategy for the uranium plume within both the feasibility study time frame and at an overall cost savings.

(a) Wellman DM, EM Pierce, and MM Valenta. *submitted*. "Efficacy of Soluble Sodium Tripolyphosphate Amendments for the in Situ Immobilization of Uranium." *Environmental Chemistry*.

2.0 Laboratory Testing – Materials and Methods

2.1 Polyphosphate Hydrolysis Experiments

A long-chain polyphosphate molecule is required to forestall the hydrolysis reaction and release of the orthophosphate molecule (PO_4^{3-}). However, a balance between the rate of polyphosphate degradation, groundwater flow rate, autunite/apatite precipitation, and injection rate must be met in order to optimize the remediation strategy. Thus, a clear understanding of polyphosphate hydrolysis kinetics is necessary to select the best chain or mix of polyphosphate chain lengths in order to directly precipitate autunite for immediate mitigation of aqueous uranium concentrations, and further precipitate apatite to control the long-term release of uranium from the sedimentary source.

In a homogeneous environment, the release of PO_4^{3-} is dependent upon both the chain length and the pH of the solution; as the length of the phosphate chain increases, the hydrolysis rate decreases (Shen and Morgan 1973). However, surface-mediated processes affect reaction rates in heterogeneous systems by lowering the activation energy, E_a, of the system, as expressed in the Arrhenius equation:

$$\log k_+ = A\exp\left(\frac{-E_a}{RT}\right) \tag{1}$$

where k_+ = the rate constant
A = the frequency factor (also called the Arrhenius constant)
R = the gas constant (J mol^{-1} K^{-1})
T = the temperature (K).

Therefore, it is essential to quantify the hydrolysis rates of long-chain phosphates in porous media before a remediation strategy can be implemented effectively.

Aqueous cations are believed to accelerate the hydrolysis reaction for tripolyphosphate by withdrawing the electron density from around the central phosphorus atom, thereby allowing nucleophilic attack by water molecules more energetically favorable (Kura 1987; Kura and Tsukuda 1993; Shen and Dyroff 1966; Watanabe et al. 1975; Wazer and Griffith 1955). Although much research has been conducted on cation-accelerated processes, experimental conditions applicable to the Hanford saturated zone have not been examined. The goal of this investigation was to elucidate the effect of aqueous cations, pure minerals, and native Hanford Site sediment on the hydrolysis of tripolyphosphate using phosphorus-31 nuclear magnetic resonance (^{31}P NMR).

The speciation of inorganic phosphate and its chemical affinity for other species in solution can be readily assessed with ^{31}P NMR. Controlled ^{31}P NMR experiments were conducted to quantify the kinetic degradation rate of the tripolyphosphate molecule under conditions present within the Hanford 300 Area subsurface. The effect of aqueous cations (e.g., Al^{3+}, Ca^{2+}, Fe^{3+}, Mg^{2+}, and Na^+) and sedimentary materials (e.g., FeOOH, and native Hanford sediment) on the hydrolysis of polyphosphates was evaluated in potassium carbonate (K_2CO_3) buffered solutions at 23°C. The K_2CO_3 buffer was used 1) to maintain the pH in a range near that of Hanford groundwater, pH = 7.5 to 8.5, 2) because carbonate is a major component of Hanford subsurface and groundwater, and 3) because potassium has been shown to have a low catalytic effect on phosphate hydrolysis (Wieker and Thilo 1960).

Homogeneous hydrolysis experiments were conducted by first preparing buffered metal chloride stock solutions. These solutions were prepared by mixing 700 mL of 0.1 M K_2CO_3 in deuterated water (D_2O) and adjusting the pH by adding 4.86 mL of HCl. Prior to pH-adjusting the influent solutions, the pH probe was calibrated with National Bureau of Standards (NBS) buffers (pH = 7.00, 10.00, and 12.00 at 23°C). Precision of the pH measurement was ±0.02. Once prepared, the stock buffer was then divided into five 100-mL fractions and one 200-mL fraction. To each 100-mL fraction was added 1 mM equivalent of one of the following metal chlorides: $AlCl_3$, $CaCl_2$, $FeCl_3$, and $MgCl_2$. Precipitation occurred in the $AlCl_3$, $CaCl_2$, and $FeCl_3$ stock solutions; probably as $Al(OH)_3$, $CaCO_3$, and $Fe(OH)_3$, respectively, so the final dissolved concentration for aluminum (4.10×10^{-16} M), iron (8.36×10^{-22} M), and calcium (4.0×10^{-8} M) are based upon the solubility limit of the aforementioned phases. All chemicals used in these experiments were reagent grade. Cations used for these experiments are representative of some of the major components of Hanford Site sediment and groundwater. Each homogeneous hydrolysis experiment began by mixing approximately 5 mL of the appropriate buffered metal solution with 0.366 g of solid sodium tripolyphosphate, which corresponded to 0.2 M tripolyphosphate solution.

Unlike the homogeneous experiments, each heterogenous solid experiment contained 2.5 g of Hanford sediment and 44 mg of FeOOH per 5 mL of 0.2 M sodium tripolyphosphate carbonate buffered solution. Each experiment was sampled weekly for four weeks. Approximately 1.5 mL of sample was removed, filtered, and placed in a 5-mm outer-diameter thin-walled precision Wilmad® glass NMR tube and analyzed immediately.

Non-proton decoupled ^{31}P NMR spectra were recored on a two-channel Varian-VXR, operating at 300 MHz proton frequency (i.e., 7.0T). A 4.5-µsec 90° pulse was used with a 0.5-sec pulse delay, 1.813-sec acquisition time, a frequency of 121.43 MHz, and 300 acquisitions per sample. Spectra were referenced to the resonance peak of 85% phosphoric acid (H_3PO_4, 37.9 ppm), which was used as an external chemical shift standard. All ^{31}P NMR experiments were conducted at room temperature in D_2O.

Analysis of the D_2O/phosphate controls, which should have yielded constant peak areas over the course of the experiment (Willard et al. 1975; Wazer 1958), indicated there were fluctuations in the measured areas. Accordingly, this artifact was also reflected in the analysis of the experimental results. However, the ratios of the peak areas within the standards were constant. This consistency implied the peak areas of each sample were being influenced by an analytical artifact which could be correlated to a constant determined from the D_2O/phosphate controls and used to "scale" the sample peak, thus allowing a single set of standard curves to be used to calculate concentration information for each sample.

Peak areas for all phosphate species were computed and tallied. The standard curves indicated the phosphate per peak area ratio was different for each phosphate species. Therefore, ratios of the slopes of the standard curves were used to normalize all peak areas to a single concentration per peak area ratio. Each peak area was then multiplied by the number of phosphate molecules contained in the corresponding species to yield a single phosphate per peak area ratio. Peak areas were then divided by the sum of all peak areas in the sample to yield the percent total dissolved phosphate represented by each species. For tripolyphosphate, the doublet area was used instead of the triplet area because of its greater size and differentiation from other peaks.

2.2 Autunite and Apatite Formation

In homogeneous systems the precipitating phase first forms stable nuclei and then grows via crystallization to macroscopic size. The nucleation rate can be expressed as

$$B = \beta \exp\left(\frac{-A}{\ln^2 s}\right) \tag{2}$$

where B = the rate
β = the frequency factor
A = a parameter that depends on interfacial energy
s = the degree of supersaturation of the solution.

However, heterogeneous nucleation on foreign or heterogeneous surfaces lowers the interfacial energy, *A*. Equation (3) can be used to understand the increase in precipitation rates due to heterogeneous nucleation (Avrami 1939; 1940). The rate of heterogeneous nucleation can be expressed as

$$B(t) = kN(t) = kN_{\circ} \exp(-kt) \tag{3}$$

in which the nucleation rate as a function of time, *B(t)*, is equivalent to the product of a constant times the nucleation density as a function of time, *kN(t)*, and is equal to the product of a constant, *k*, the number of heterogeneous germ nuclei, N_o, and exponentially to the negative product of the constant, *k*, and time, *t*. Note that the degree of supersaturation of the solution is still important and is accounted for in the parameter *k*. The nucleation rate is directly proportional to the number of nucleation sites available, a number that should be large for a solution percolating through porous media. This equation also suggests that nucleation rates should be fastest at early times and will diminish exponentially.

These equations are relevant to the understanding of surface-mediated catalysis of autunite and apatite precipitation kinetics. Rapid initial rates are critical for the successful deployment of a soluble polyphosphate amendment. The above equations imply that catalysis of polyphosphate hydrolysis and solid-phase precipitation should be immediate after orthophosphate contacts porous media. Furthermore, they highlight the importance of quantifying kinetic precipitation data for systems in more realistic column experiments containing actual 300 Area sediments coupled with knowledge regarding the degradation of proposed polyphosphates (Table 1).

2.2.1 Batch Experiments

Prior to conducting tests with 300 Area sediment cores, batch experiments were conducted over a range of polyphosphate sources and concentrations to identify the required conditions to obtain maximum precipitation of autunite and/or apatite. The thermodynamic geochemical code EQ3NR (Wolery 1992) was used to assess the necessary concentration of phosphorus to precipitate hydroxyapatite and autunite given the minimum and maximum saturation state measured within the aquifer. Thermodynamic databases from numerous literature sources were used to update the computer code (Sergeyeva et al. 1972; Langmuir 1978; Alwan and Williams 1980; O'Hare et al. 1976; O'Hare et al. 1988; Vochten 1990; Nguyen et al. 1992; Grenthe et al. 1992; Finch 1997; Chen et al. 1999; Kalmykov and Choppin 2000). It

Table 1. Proposed Phosphate Sources for Polyphosphate Amendment

Phosphate Source	Formula
Sodium Orthophosphate	$Na_3PO_4 \cdot nH_2O$
Sodium Pyrophosphate	$Na_4P_2O_7 \cdot nH_2O$
Sodium Tripolyphosphate	$Na_5P_3O_{10} \cdot nH_2O$
Sodium Trimetaphosphate	$(NaPO_3)_3 \cdot nH_2O$
Sodium Hexametaphosphate	$(NaPO_3)_6 \cdot nH_2O$
Calcium Dihydrogen Phosphate	$Ca(H_2PO_4)_2 \cdot nH_2O$
Calcium Hydrogen Phosphate	$CaHPO_4 \cdot nH_2O$
Calcium Pyrophosphate	$Ca_2P_2O_7 \cdot nH_2O$
Calcium Hypophosphite	$Ca(H_2PO_2)_2 \cdot nH_2O$

is important to note that because of the complex chemistry of uranium, there is significant debate within the literature regarding the stoichiometry and the thermodynamic values assigned to aqueous uranium species and secondary mineral phases. As such, the geochemical calculations are based on current knowledge, but may have significant uncertainty associated with them. Batch experiments evaluated the potential composition of the polyphosphate amendment based on the extreme (i.e., 10 to 1000 ppb) uranium concentration range measured within the 300 Area aquifer. The use of multi-length polyphosphate chain amendments was evaluated to afford rapid precipitation of autunite and/or apatite. All experiments were conducted in Hanford groundwater and in the presence of 300 Area sediments for one week at room temperature. Aqueous concentrations were monitored by inductively couple plasma-mass spectrometry (ICP-MS) and inductively couple plasma-optical emission spectrometry (ICP-OES).

2.2.2 Column Experiments

Tripolyphosphate is a primary ingredient in detergents, which, as illustrated above, degrades to pyro- and orthophosphate. As such, the removal of these phosphate compounds from wastewater has been the subject of several investigations conducted over more than five decades. Research beginning in the mid-60s demonstrates the efficacy of using calcium and/or lime to precipitate stable calcium-phosphate solid phases including apatite for direct removal of phosphate (Ferguson et al. 1973; Ferguson et al. 1970; Schmid and McKinney 1968; Jenkins et al. 1971). However, results of these early investigations also underscore the importance of conducting site-specific tests to optimize the formation of apatite based on environmental parameters, including pH and carbonate concentration. Saturated column experiments were conducted to quantify the following:

- polyphosphate treatment efficiency – amount of polyphosphate required to treat a pore volume of uranium contaminated groundwater

- polyphosphate treatment emplacement efficiency – evaluate mixing problem (i.e., effective contact or tendency for the reagent to push contaminated groundwater ahead of the treatment volume).

2.2.2.1 Amendment Formulation, Efficacy, and Emplacement

The use of multi-length polyphosphate chain amendments, optimized through ^{31}P NMR hydrolysis and batch precipitation experiments, was evaluated to afford rapid precipitation of autunite and/or apatite without negatively impacting the hydraulic conductivity of the formation. Briefly, polyvinyl chlorinate columns (length, L = 30.48 cm; radius, r = 2.54 cm; and bulk volume, V_b = 194.04 to 202.20 cm^3) were packed uniformly with sediment from 300 Area cores and were saturated with Hanford groundwater to ensure chemical equilibrium. Preliminary characterization results indicated that the uranium concentration within the aqueous and solid matrix of the sediment cores is below the MCL for uranium. Therefore, to effectively evaluate polyphosphate amendments for uranium remediation, it was necessary to use a solution of Hanford groundwater spiked with aqueous uranium as the influent solution. The uranium concentration in the pore fluid was 1000 ppb, allowing the efficacy of the polyphosphate amendment to be evaluated under maximum uranium concentrations.

Several injection scheme variations were investigated and are discussed in further detail below. However, in general, following saturation and attainment of chemical equilibrium with uranium-spiked groundwater, the influent solution was changed to Hanford groundwater containing the polyphosphate amendment or calcium followed by the other respective solution. Aqueous concentrations were monitored by ICP-MS and ICP-OES; solid-phase formation was evaluated by fluorescence spectroscopy using short wave ultraviolet (UV) radiation, 254 nm.

2.2.2.2 Transport

The saturated column technique used here has been previously described (Gamerdinger et al. 2001b; 2001a; 1994). However, briefly, borosilicate glass columns (length, L = 10.5 cm; radius, r = 1.25 cm; and bulk volume, V_b = 53.71 cm^3) were packed uniformly with the < 2.00 mm fraction of sediment from cores collected from the 300 Area. The columns were saturated with Hanford groundwater (HGW) until stable water content was attained; syringe pumps were used to control the flow rate. Sediment bulk density, ρ_b (g cm^{-3}), and volumetric water content, θ (cm^3 cm^{-3}), were determined from the mass of the sediment and/or water. The percent saturation was calculated from the ratio of θ (water-filled porosity) to the total porosity, ϕ, which was calculated from the bulk density and particle density.

2.3 Immobilization of Uranium by Apatite

Batch tests were conducted to quantify the effectiveness of uranium retention by apatite. Batch uranium sequestration tests were conducted over a narrow pH range comparable to the expected pH range in the 300 Area, pH 6.0 to 8.0, to quantify the following:

- the rate of uranium sorption on apatite as a function of pH
- the stability of uranium sorbed to apatite as a function of pH
- the capacity of apatite for uranium sequestration.

2.3.1 Apatite Pre-Equilibration

To assess only the interaction between aqueous uranium and solid apatite, the apatite must be in a state of thermodynamic equilibrium with the aqueous matrix. However, because apatite has an exceedingly low solubility, experimentally prohibitive timeframes are required for apatite to equilibrate

naturally with an aqueous matrix. Therefore, the thermodynamic geochemical code EQ36 (Wolery 1992) was used to evaluate the aqueous speciation of the solutions in equilibrium with apatite over the pH range being investigated (6 to 8) (see Table 2). The aqueous matrix used for all experiments was prepared by equilibrating 18 MΩ deionized water with calcite for 4 days, followed by vacuum filtration using a 0.45-μm Nalgene filter. Phosphoric acid was added to the respective solutions based on the concentrations given in Table 2. The solutions were pH adjusted using Optima nitric acid, HNO_3, obtained from Fisher.

Table 2. Composition of Solutions Used in Sorption Experiments. Aqueous calcium and phosphorus concentrations in equilibrium with hydroxyapatite at 23°C were calculated using the EQ3NR Code V7.2b database.

pH	[Ca], M	[P], M
6	9.76×10^{-3}	1.92×10^{-4}
6.5	4.85×10^{-3}	3.73×10^{-5}
7	2.50×10^{-3}	8.99×10^{-6}
8	7.14×10^{-4}	1.10×10^{-6}

Prior to experimental testing, apatite was equilibrated with the respective test solution by shaking overnight, centrifuging, measuring the pH, and decanting the supernatant. This was repeated until the pH of the added solution was constant after contacting the hydroxyapatite. The process of pre-equilibration isolated the uranium sorption reaction from any other reaction that may occur while the apatite and aqueous solutions equilibrate.

2.3.2 Kinetic Experiments

Kinetic experiments were conducted to evaluate the rate of uranium uptake by hydroxyapatite. Nalgene high-density polyethylene (HDPE) bottles had 500 mL of apatite equilibrated solution, at respective pH values ranging from 6 to 8, containing 100 mg/L of uranyl nitrate and 0.25 g of apatite. Control solutions were prepared using the same testing conditions in the absence of hydroxyapatite to evaluate the loss of uranium to the test apparatus. Sorption of uranium to the test containers was not measured over the pH range investigated. All solutions were placed on a shaker table for predetermined time intervals ranging from 2 to 1,440 minutes, then centrifuged at 2,000 rpm for 5 minutes to remove any colloidal apatite from suspension. Immediately after centrifugation 3-mL aliquots of the supernatant were removed and filtered through a 0.2-μm syringe filter. Inductively coupled plasma-mass spectroscopy was used to measure the concentration of aqueous uranium.

2.3.3 Loading Experiments

Loading experiments were conducted in a manner similar to kinetics experiments (ASTM 2001). Hydroxyapatite equilibrated solution at respective pH values ranging from 6 to 8 was spiked with uranyl nitrate to the desired concentration. The respective solutions were added to Nalgene HPDE bottles containing apatite. The solution to solid ratio for loading experiments varied from 100 to 20,000. The initial aqueous uranium concentration was 100 mg/L. Control solutions were prepared using the same testing conditions in the absence of apatite to evaluate the loss of uranium to the test apparatus. Sorption

of uranyl to the test containers was not measured over the pH range investigated. All solutions were placed on a shaker table. The samples were centrifuged at 2,000 rpm for 5 minutes to remove any colloidal apatite from suspension prior to removing 3-mL aliquots of the supernatant. The supernatant was filtered through a 0.2-μm syringe filter and analyzed using ICP-MS to measure the concentration of aqueous uranium.

The percent sorption and distribution coefficients were calculated as follows:

$$\% \, Sorption = \frac{C_i - C_f}{C_i} * 100 \tag{4}$$

where C_i and C_f = the initial and final concentrations of aqueous uranium (mg/L)
V = the volume of solution (mL)
m = the mass of hydroxyapatite (g).

Determining the standard deviation requires accounting for the uncertainty associated with each parameter in Equation (4).

The standard deviation of a function for uncorrelated random errors is given by

$$\sigma_f = \sqrt{\sum_{i=1}^{n} \left(\frac{\partial f}{\partial x_i} \right)^2 \sigma_i^2} \tag{5}$$

where σ_f = standard deviation of the function *f*,
x_i = parameter *i*,
σ_i = standard deviation of parameter *i*.

Substituting Equation (4) into (5) and converting to relative standard deviations, $\hat{\sigma}_r = \sigma_f / \bar{x}$, yields

$$\hat{\sigma}_r = \sqrt{\frac{\left(\hat{\sigma}_{c_i} c_i\right)^2 + \left(\hat{\sigma}_{c_f} c_f\right)^2}{\left(c_i - c_f\right)^2} + \hat{\sigma}_{c_i}^2 c_i^{\,2}} \tag{6}$$

Errors for $\hat{\sigma}_{c_i}, \hat{\sigma}_{c_f}, \hat{\sigma}_V$, and $\hat{\sigma}_m$ are 10%, 10%, 5%, and 5%, respectively. This error analysis results in typical 2σ uncertainties. All experiments were conducted in duplicate to ensure the system yielded reproducible results.

2.3.4 Desorption Experiments

Batch desorption experiments were performed by separating the hydroxyapatite with its sorbed uranium from the liquid phase by centrifugation. The uranyl loaded on hydroxyapatite at a solution-to-solid ratio of 100 with an initial aqueous uranium concentration of 100 mg/L, was ~5.0×10^{-3} g/g. After the supernatant liquid was decanted, 10 mL of Hanford groundwater, adjusted to the respective pH of 6 to 8, was added to each sample and the bottles were placed on a shaker table for one week. The samples

were centrifuged, the supernatant was passed through a 0.2-μm syringe filter, and analyzed using ICP-MS to quantify the aqueous uranium concentration. This was repeated four times for a total desorption time interval of one month. The percent desorption was calculated from the total amount of uranium sorbed on the apatite and the concentration of uranium desorbed during each successive interval (Equation 7).

$$\% \ Desorption = \frac{C_d}{C_s} * 100 \tag{7}$$

where C_d is the concentration of uranium desorbed (mg/L) and C_s is the concentration of uranium sorbed (mg/L).

2.3.5 Column Experiments

Borosilicate glass columns (length, L = 5 cm; radius, r = 1.25 cm; and bulk volume, V_b = 28.55 cm^3) were packed uniformly with the <2.00-mm fraction of sediment from cores collected from the 300 Area; one column had a 5-wt% barrier of hydroxyapatite placed within the middle of the sediment bed (Figure 7). The columns were saturated with Hanford groundwater until stable water content was attained. Syringe pumps were used to control the flow rate. Effluent solution was collected continuously and aliquots of the fluid sample were retained for both pH measurement and analysis of calcium and phosphorus concentrations by ICP-OES and uranium using ICP-MS.

Figure 7. Photo Displaying the Apatite Barrier Placed in the Middle of a Sediment Column Composed of the <2-mm Fraction from the 300 Area

2.4 Apatite Barrier Longevity

The Hanford subsurface does not contain a sufficient amount of naturally occurring phosphate to support precipitation of phosphate minerals such as apatite. An artificially created apatite barrier will be in a state of thermodynamic disequilibrium. Consequently, it is necessary to understand the processes that will determine how long an apatite barrier can function. The long-term stability of minerals is controlled by the solubility and the dissolution rate of the mineral. Under highly advective conditions where transport is greater than the solubility, the stability of the mineral is controlled by dissolution kinetics. Alternatively, in low to moderately advective environments solubility is greater than transport and the long-term stability of the mineral is based on the solubility of the phase. The former conditions are relevant to the 300 Area saturated zone. Therefore, to quantify longevity of an apatite barrier, and therein the performance of polyphosphate technology, it is necessary to evaluate apatite dissolution under conditions representative of the 300 Area aquifer.

2.4.1 Single-Pass Flow-Through Test Methods

Evaluation of the dissolution of apatite was performed with the single-pass flow-through (SPFT) test method. The SPFT apparatus provides for experimental flexibility allowing each of the kinetic test

parameters to be isolated and quantified. Temperature, flow rate, solution composition, and sample mass and size can all be manipulated to assure accurate rate determinations.

In general, the SPFT system (Figure 8) consists of a programmable pump that transports solutions from an influent reservoir via Teflon lines. Solution is transferred into 60-mL capacity *perfluoroalkoxide* (PFA) reactors (Savillex). The reactors are situated within constant temperature ovens, whose temperature is controlled to ±2°C by tested and calibrated thermocouples. The powdered specimen rests at the bottom of the reactor and influent and effluent solutions enter and exit, respectively, from fluid transfer lines that protrude through two separate ports at the top of the reactor. The residence time of aqueous solutions in the reactor varies with the flow rate, which is adjusted in accordance with the needs of the experiment. The effluent line carries solution to collection vials that are positioned outside the oven. See McGrail et al. (2000) for a detailed description of the SPFT system.

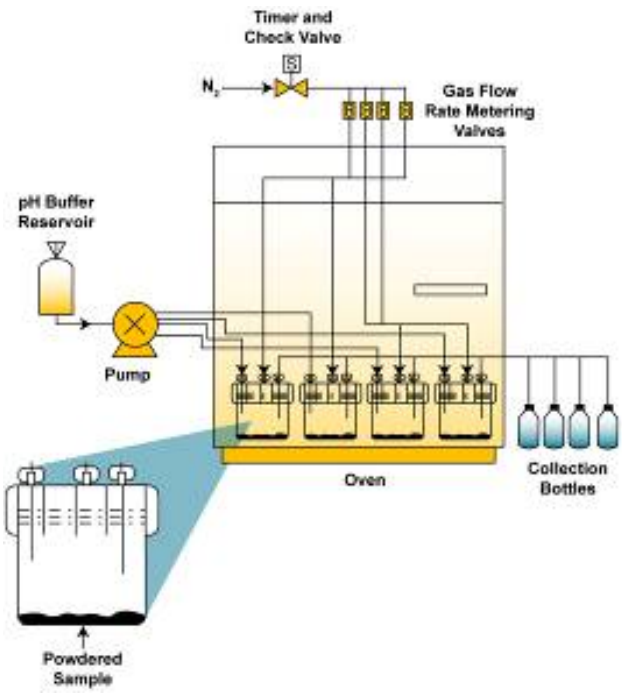

Figure 8. Schematic of the Single-Pass Flow-Through Dissolution Test System

Effluent solution was collected continuously and aliquots of the fluid sample were retained for both pH measurement and analysis of dissolved element concentrations by ICP-OES. Solutions earmarked for analysis by ICP-OES methods were preserved in Optima™ nitric acid. Concentrations of aqueous calcium and phosophorus were used to quantify the dissolution rates as a function of pH and temperature. Before the sample specimens were added to the reactor, blank solution samples were collected and used to establish the concentration of background analytes. The blank samples were treated in exactly the same manner as the samples.

The dissolution rate of hydroxyapatite was quantified using the average flow rate within the 300 Area aquifer (Waichler and Yabusaki 2005). Because reactions involving dissolution of hydroxyapatite involve breaking of strong Ca-P bonds, there is a strong dependency of the dissolution rate on temperature. In the present case, the temperature of the subsurface is too low (15°C) for direct tests. Because reaction rates at this temperature are prohibitively slow, the duration of the experiments are impracticable. An alternative strategy is to conduct experiments at higher temperatures, where rates are faster, and then extrapolate the results down to the temperature of interest (15°C).

The hydroxyapatite sample used in this study was obtained from Sigma-Aldrich Chemical and prepared by sieving into the desired size fractions with ASTM standard sieves (ASTM 2002). The pH values of the solutions that will be used in these experiments spanned the range from 6 to 12. Maintaining a constant temperature and flow rate, while varying the solution pH, allows the value of the pH power law coefficient, η, to be determined. The solutions used to control the pH during the SPFT experiments are summarized in Table 3. Table 3 also contains a summary of the in situ pH values

computed at each test temperature using EQ3NR (Wolery 1992). It is important to take into account the change in pH that occurs at different temperatures when computing dissolution rates from SPFT data because the in-situ pH can vary by as much as 1.5 pH units over the temperature range from 23º to 90ºC. By quantifying temperature and pH-dependent rate parameters the dissolution rate of hydroxyapatite can be extrapolated to conditions representative of the subsurface. Buffer solutions were prepared by adding small amounts of the organic tris hydroxymethyl aminomethane (THAM) buffer to deionized water (DIW) and adjusting the solution to the desired pH value using 15.8M HNO_3 or 1 M LiOH. The THAM buffer range is between pH 7 to 10; therefore the alkaline solutions, pH range 11 and 12, will be prepared by adding of LiOH and LiCl to DIW and adjusting the solution to the desired pH value using 15.8 M HNO_3 or 1M LiOH.

Table 3. Composition of Solutions Used in Single-Pass Flow-Through Experiments. Solution pH values above 23°C were calculated using the EQ3NR Code V7.2b database.

Solution	Composition	pH @			
		23ºC	40ºC	70ºC	90ºC
1	0.05 M THAM + 0.047 M HNO_3	7.01	6.57	5.91	5.55
2	0.05 M THAM + 0.02 M HNO_3	8.32	7.90	7.25	6.89
3	0.05 M THAM + 0.0041 M HNO_3	8.99	8.67	8.08	7.72
4	0.05 M THAM + 0.003 M LiOH	9.99	9.55	8.88	8.52
5	0.0107 M LiOH + 0.010 M LiCl	11.00	10.89	10.43	10.06
6	0.0207 M LiOH + 0.010 M LiCl	12.02	11.74	11.08	10.70
THAM = Tris hydroxymethyl aminomethane buffer.					

2.4.1.1 Rate Calculations and Uncertainty

Dissolution rates, based on steady-state concentrations of elements in the effluent, are normalized to the amount of the element present in the sample by the following formula:

$$r_i = \frac{\left(C_i - \overline{C}_{i,b}\right) q}{f_i S} \tag{8}$$

where r_i = the normalized dissolution rate for element i (g m^{-2} d^{-1})
C_i = the concentration of the element i in the effluent (g L^{-1})
$\overline{C}_{i,b}$ = the average background concentration of the element of interest (g L^{-1})
q = the flow rate (L d^{-1})
f_i = the mass fraction of the element in the metal (dimensionless)
S = the surface area of the sample (m^2).

The surface area was determined using N_2-adsorption Brunauer-Emmett-Teller (BET) analysis (Brunauer et al. 1938), 74.25 m^2/g. The value of f_i was calculated from the chemical composition of the sample. Flow rates are determined by gravimetric analysis of the fluid collected in each effluent collection vessel upon sampling. The background concentration of the element of interest is determined, as previously discussed, by analyses of the starting input solution and three blank solutions. Typically, background

concentrations of elements are below their respective detection threshold. The detection threshold of any element is defined here as the lowest calibration standard that can be determined reproducibly during an analytical run within 10%. In cases where the analyte is below the detection threshold, the background concentration of the element is set at the value of the detection threshold.

Determining the experimental uncertainty of the dissolution rate takes into account uncertainties of each parameter in Equation (8). For uncorrelated random errors, the standard deviation of a function $f(x_1, x_2, \ldots x_n)$ is given by

$$\sigma_f = \sqrt{\sum_{i=1}^{n} \left(\frac{\partial f}{\partial x_i} \right)^2 \sigma_i^2} \tag{9}$$

where σ_f = the standard deviation of the function f
x_i = parameter i
σ_I = the standard deviation of parameter i.

Substituting Equation (8) into (9) results in the following:

$$\sigma_{r_i} = \sqrt{\left(\frac{q}{f_i S} \right)^2 (\sigma_{C_i}^2 + \sigma_{\bar{C}_{i,b}}^2) + \left(\frac{C_i - \bar{C}_{i,b}}{f_i S} \right)^2 \sigma_q^2 + \left(\frac{(C_i - \bar{C}_{i,b})q}{f_i^2 S} \right)^2 \sigma_{f_i}^2 + \left(\frac{(C_i - \bar{C}_{i,b})q}{f_i S^2} \right)^2 \sigma_S^2} \tag{10}$$

Equation (9) can also be expressed in terms of the relative error, $\hat{\sigma}_{r_i} = \sigma_{r_i} / r_i$, and is given by

$$\hat{\sigma}_{r_i} = \sqrt{\frac{\left(\hat{\sigma}_{C_i} C_i\right)^2 + \left(\hat{\sigma}_{\bar{C}_{i,b}} \bar{C}_{i,b}\right)^2}{\left(C_i - \bar{C}_{i,b}\right)^2} + \hat{\sigma}_q^2 + \hat{\sigma}_{f_i}^2 + \hat{\sigma}_S^2} \tag{11}$$

Relative errors of 10%, 10%, 5%, 3%, and 15% for C_i, $\bar{C}_{i,b}$, q, f_i, and S, respectively, are typical for measurements conducted at PNNL. But to reduce the error associated with mass fraction (f_i), the samples to be used in these experiments will be ground, homogenized, sub-sampled, and analyzed at least three times to obtain a more accurate composition with a better estimate of the uncertainty. The conservative appraisal of errors assigned to the parameters in Equation (11), in addition to the practice of imputing detection threshold values to background concentrations, results in typical uncertainties of approximately ±35% on the dissolution rate.

2.5 Effect of pH and Temperature on the Dissolution Kinetics of Meta-Autunite Minerals, $(Na, Ca)_{2-1}[(UO_2)(PO_4)]_2 \cdot 3H_2O$

The dissolution of sodium and calcium meta-autunite minerals was quantified as a function of pH and temperature using the SPFT test method as described above.

2.5.1 Starting Materials

Synthetic sodium meta-autunite I, $Na_2[(UO_2)(PO_4)]_2 \cdot 3H_2O$ (herein designated Na-autunite), was prepared by direct precipitation from a mixture of uranyl nitrate with sodium phosphate, dibasic. The precipitated phase was characterized using extended x-ray absorption fine structure (EXAFS) spectroscopy, chemical digestion followed by ICP-OES and ICP-MS for elemental analyses, x-ray diffraction (XRD), scanning electron microscopy (SEM), and multi-point BET analyses (Wellman et al. 2005a).

Natural calcium meta-autunite I, $Ca[(UO_2)(PO_4)]_2 \cdot 3H_2O$ (herein designated GHR) was obtained from northeastern Washington State. The material was characterized using ICP-OES and ICP-MS analyses, XRD, and SEM to confirm the composition, structure, and morphology of the autunite minerals as 98 to 99% pure autunite with calculated anhydrous structural formula consistent with Ca-autunite: $Ca[(UO_2)(PO_4)]_2$. Electron microprobe analyses further indicated that the autunite mineral contains ~3 waters of hydration per formula unit (p.f.u.). Powdered samples of Na-Autunite and calcium-autunite (GHR) were prepared to be within the same size fraction, 25 to 45 μm (-325 to +500 mesh); however, the surface cracking, fractures, and basal plane cleavage of the GHR resulted in a greater surface area relative to Na-autunite (Table 4). Therefore, a second size fraction of GHR (75 to 150 μm, or -100 to + 200 mesh), was prepared that had a comparable surface area to Na-autunite (Table 4).

Table 4. Source, Particle Size, and Surface Area of Autunite Minerals.

Autunite Composition	Sample I.D.	Source	Particle Size	Surface Area, m^2/g
$Na_2[(UO_2)(PO_4)]_2 \cdot 3H_2O$	Na-Autunite	Synthetic	-325 +500	0.78
$Ca[(UO_2)(PO_4)]_2 \cdot 3H_2O$	GHR	Natural	-325 +500	2.30
$Ca[(UO_2)(PO_4)]_2 \cdot 3H_2O$	GHR	Natural	-100 +200	0.88

3.0 Results and Discussion

3.1 Polyphosphate Hydrolysis Experiments

Figure 9 shows the ^{31}P NMR spectra of 0.2 M tripolyphosphate and 0.2 M pyrophosphate in carbonate buffered D_2O. Tripolyphosphate spectra shows three distinct signals at ~-3 ppm, -4.7 ppm, and ~-18 ppm. The resonant signal at -3 ppm (doublet) and -18 ppm (triplet) represent tripolyphosphate, whereas the single peak observed at -4.7 ppm represents the degradation reaction product pyrophosphate. Tripolyphosphate degrates to pyro- and orthophosphate as shown in Equation (12); once formed pyrophosphate can undergo further hydrolysis to orthophosphate, Equation (13).

$$\underbrace{P-O-P-O-P}_{Tripoly} \rightarrow \underbrace{P-O-P}_{Pyro} + \underbrace{P}_{Ortho} \tag{12}$$

$$\underbrace{P-O-P}_{Pyro} \rightarrow \underbrace{P}_{Ortho} + \underbrace{P}_{Ortho} \tag{13}$$

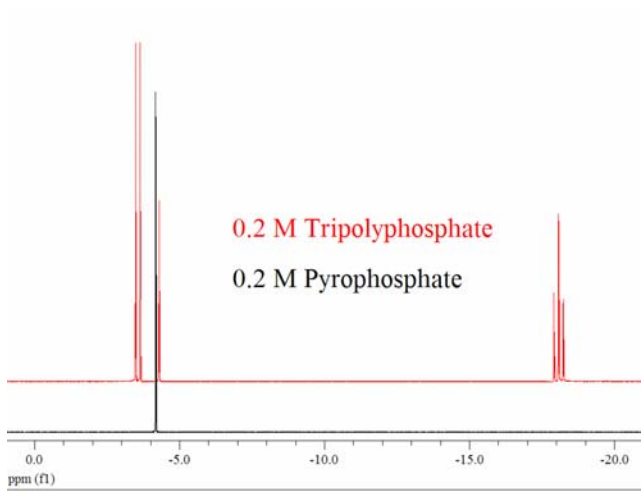

Figure 9. A ^{31}P NMR Spectrum of a Buffered Aqueous Solution of 0.2 M Pyro- and Tripoly-Phosphate Solutions. A single peak is displayed in the pyrophosphate spectra at -4.2 ppm, whereas the tripolyphosphate spectra show three signals: 1) the tripolyphosphate triplet (~ -18 ppm), 2) the tripolyphosphate doublet (~ -3 ppm), and 3) the pyrophosphate degradation compound (~ -4.7 ppm).

Prior to conducting the homogeneous and heterogeneous degradation experiments, a series of ^{31}P NMR experiments were conducted with known amounts of tripolyphosphate. The results from these experiments provided the required information needed to develop a linear relationship between the concentration of tripolyphosphate and integrated peak area. Equation (14) is based on the spectra obtained for the tripolyphosphate doublet and the results of a linear regression are shown in Figure 10.

$$P\,Conc. = \frac{Integrated\ Peak\ Area}{\left(2.94\times10^{6}\right)} \tag{14}$$

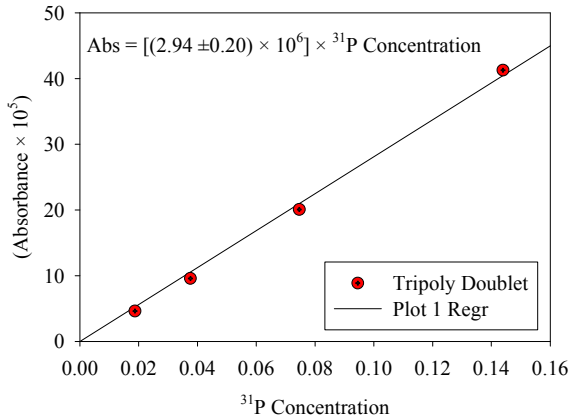

Figure 10. A ^{31}P NMR Spectrum Integrated Peak Area as a Function of a Known Aqueous Concentration of Tripolyphosphate. These results are based on the tripolyphosphate doublet and were used to develop a linear equation that could be used to quantify the amount of tripolyphosphate at a given time.

The resulting regression coefficient is (2.94 ± 0.20) × 10^6 with a $R^2 = 0.99$. A similar technique was used for developing equations to quantify the degradation products, pyro- and orthophosphate.

Results from homogeneous ^{31}P NMR experiments suggest the presence of aqueous cations; Al^{3+}, Ca^{2+}, Fe^{3+}, and Mg^{2+} do not have any significant effect on the rate of tripolyphosphate hydrolysis at the cation concentrations used for these experiments (Figure 11). These results are consistent with the findings of an independent homogeneous experiment conducted with Hanford Site groundwater, where the groundwater had no catalytic effect on tripolyphosphate degradation (Figure 11). Also shown in Figure 11 are the results collected for the heterogeneous experiments conducted with naturally occurring mineral FeOOH, as well as with native Hanford sediments. The only statistically significant deviations in the phosphate percentages were for the heterogeneous experiments. These results suggest the presence of FeOOH and native Hanford Site sediment had a measurable catalytic effect on the hydrolysis of sodium tripolyphosphate, evident by a 12% and 24% decrease in the tripolyphosphate concentration, respectively.

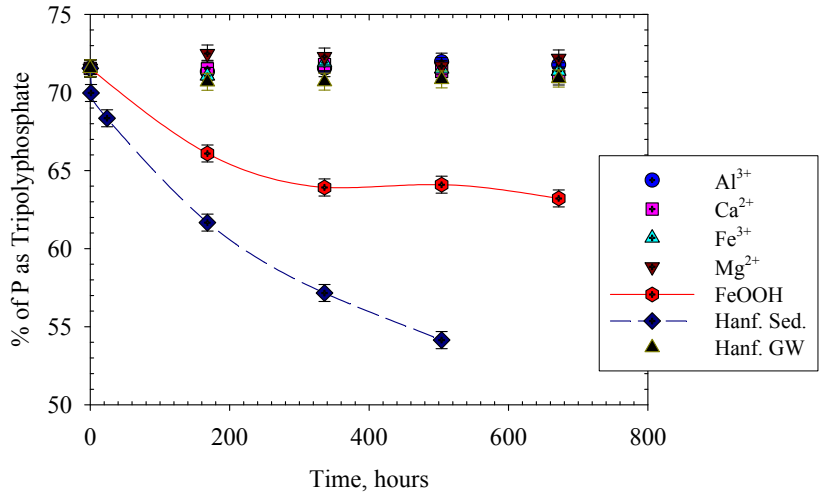

Figure 11. Percentage of Phosphorus as Tripolyphosphate as a Function of Time for Homogeneous Experiments Conducted with Aqueous Cations, Al^{3+}, Ca^{2+}, Fe^{3+}, Mg^{2+}, and Hanford Site Groundwater; and Heterogeneous Experiments Conducted with Solids, FeOOH, and Hanford Site Sediment

3.2 Apatite and Autunite Formation

3.2.1 Batch Experiments

Preliminary field tracer investigations indicated a field flow rate of ~50 ft/day, suggesting rapid formation of autunite and apatite was required within the 300 Area subsurface for remediation. Therefore, nine potential phosphate compounds were selected for investigation as possible components to the polyphosphate amendment formulation (Table 5). Selection of the amendment sources was based on the solubility, hydrolysis rate, and amount of phosphorus and/or calcium provided by the respective compounds. Prior to conducting column tests, heterogeneous batch experiments were conducted, in the presence of 300 Area sediment, over a range of polyphosphate sources and concentrations to identify the optimum source of phosphorus and calcium to obtain maximum precipitation of autunite and/or apatite. Batch experiments evaluated the potential composition of the polyphosphate amendment based on the extreme (i.e., 10 to 1,000 ppb) uranium concentration range previously measured within the 300 Area aquifer. The use of multi-length polyphosphate chain amendments was evaluated to afford rapid precipitation of autunite and/or apatite. All experiments were conducted in Hanford groundwater and in the presence of 300 Area sediments for one week at room temperature. Aqueous concentrations were monitored by ICP-MS and ICP-OES. The exact details constituting the multiple nucleation and growth process that may occur during the formation of calcium-phosphate or the assignment of absolute limits of mineralization potential for any given set of reaction conditions was beyond the scope of this investigation. Rather, the intent was to identify the optimum sources of calcium and phosphorous to precipitate autunite and apatite within a saturated sedimentary matrix through static batch tests.

Table 5. Possible Sources and Associated Solubility for Polyphosphate Amendment

Amendment Source	Formula	Solubility, g/L Cold H_2O
Sodium orthophosphate	$Na_3PO_4 \cdot 12H_2O$	40.2
Sodium pyrophosphate	$Na_4P_2O_7 \cdot 10H_2O$	54.1
Sodium tripolyphosphate	$Na_5P_3O_{10}$	145.0
Sodium trimetaphosphate	$(NaPO_3)_3 \cdot 6H_2O$	Soluble
Sodium hexametaphosphate	$(NaPO_3)_6 \cdot nH_2O$	Very soluble
Calcium dihydrogen phosphate	$Ca(H_2PO_4)_2 \cdot H_2O$	18
Calcium hydrogen phosphate	$CaHPO_4 \cdot 2H_2O$	0.32
Calcium pyrophosphate	$Ca_2P_2O_7 \cdot 5H_2O$	Slightly soluble
Calcium hypophosphite	$Ca(H_2PO_2)_2$	154
Calcium chloride	$CaCl_2$	745

Initial batch tests were conducted based on the minimum amendment concentration as defined by previously conducted, preliminary column tests, which indicated a 1,000-ppm sodium tripolyphosphate solution would reduce the aqueous concentration of uranium to near the MCL in ~12 pore volumes (Wellman et al.[(a)]. This established the initial upper limit for the concentration of phosphorus at 1,000 ppm. Additionally, lower concentrations of 100, 250, and 500 ppm were investigated to ensure the amendment did not contain excessive phosphorus that may not be used in remediation efforts. The initial matrix of batch tests is given in Table 6.

(a) Wellman DM, EM Pierce, and MM Valenta. *submitted*. "Efficacy of Soluble Sodium Tripolyphosphate Amendments for the in Situ Immobilization of Uranium." *Environmental Chemistry*.

Table 6. Experimental Batch Conditions for Polyphosphate Amendment Optimization

Phosphate Source	Phosphorus Conc. (ppm)	Calcium Source	Calcium Conc. (ppm)	Uranium Conc. (μg/L)	
Sodium orthophosphate	1,000	Not applicable	Not applicable	10	1,000
				0.00	
Sodium pyrophosphate	1,000	Not applicable	Not applicable	10	1,000
				0.00	
Sodium tripolyphosphate	1,000	Not applicable	Not applicable	10	1,000
				0.00	
Sodium orthophosphate	500	Not applicable	Not applicable	10	1,000
				0.00	
Sodium pyrophosphate	500	Not applicable	Not applicable	10	1,000
				0.00	
Sodium tripolyphosphate	500	Not applicable	Not applicable	10	1,000
				0.00	
Sodium trimetaphosphate	1,000	Not applicable	Not applicable	10	1,000
				0.00	
Sodium trimetaphosphate	500	Not applicable	Not applicable	10	1,000
				0.00	
				0.00	
Sodium hexametaphosphate	1,000	Not applicable	Not applicable	10	1,000
				0.00	
Sodium hexametaphosphate	500	Not applicable	Not applicable	10	1,000
				0.00	
				0.00	
Calcium hypophosphite	1,000	Not applicable	Not applicable	10	1,000
				0.00	
Calcium hypophosphite	500	Not applicable	Not applicable	10	1,000
				0.00	
Calcium hypophosphite	250	Not applicable	Not applicable	10	1,000
				0.00	
Sodium orthophosphate	1,000	Calcium chloride	500	10	1,000
				0.00	
Sodium orthophosphate	500	Calcium chloride	500	10	1,000
				0.00	
Sodium pyrophosphate	1,000	Calcium chloride	500	10	1,000
				0.00	
Sodium pyrophosphate	500	Calcium chloride	500	10	1,000
				0.00	
Sodium tripolyphosphate	1,000	Calcium chloride	500	10	1,000
				0.00	
Sodium tripolyphosphate	500	Calcium chloride	500	10	1,000
				0.00	
Sodium trimetaphosphate	1,000	Calcium hypophosphite	500	10	1,000
				0.00	

Table 6. (contd)

Phosphate Source	Phosphorus Conc. (ppm)	Calcium Source	Calcium Conc. (ppm)	Uranium Conc. (μg/L)	
Sodium trimetaphosphate	1,000	Calcium chloride	500	10	1,000
				0.00	
				0.00	
Sodium trimetaphosphate	500	Calcium chloride	500	10	1,000
				0.00	
Sodium hexametaphosphate	1,000	Calcium hypophosphite	500	10	1,000
				0.00	
Sodium hexametaphosphate	1,000	Calcium chloride	500	10	1,000
				0.00	
				0.00	
Sodium hexametaphosphate	500	Calcium chloride	500	10	1,000
				0.00	
Calcium hypophosphite	1,000	Calcium chloride	1,000	10	1,000
				0.00	
Calcium hypophosphite	1,000	Calcium chloride	500	10	1,000
				0.00	
Calcium hypophosphite	500	Calcium chloride	1,000	10	1,000
				0.00	
Calcium hypophosphite	500	Calcium chloride	500	10	1,000
				0.00	
Calcium hypophosphite	250	Calcium chloride	1,000	10	1,000
				0.00	
Calcium hypophosphite	250	Calcium chloride	500	10	1,000
				0.00	

Initial batch test results suggested a concentration of at least 1,000 ppm was required to remove more than 50% of the aqueous uranium using sodium phosphate compounds. Results further indicated the availability of calcium from 300 Area Hanford sediments and groundwater was insufficient to precipitate calcium-phosphate solid phases, resulting in the need for an additional calcium source.

All potential calcium-phosphate sources were eliminated from further consideration during the initial round of batch testing. Results indicated the solubility limits of calcium dihydrogen phosphate, calcium hydrogen phosphate, and calcium pyrophosphate did not provide a sufficient source of phosphate or calcium to be included in the amendment formulation. Although, calcium hypophosphite provides a sufficient source of calcium and phosphorus, rather than forming discrete precipitates it produced fine floccules. The formation of fine floccules as a result of phytic acid remediation has been previously shown to provide sorption sites for uranium (Nash 2000; Nash et al. 1998a; Nash et al. 1997; 1998b; Nash et al. 1999). Fine floccules may be highly mobile in the 300 Area subsurface under the high flow conditions. Alternatively, it has been previously shown that rapid flocculation, due to heterogeneous nucleation, in regions of moderate to low hydraulic conductivity may occlude pore space (Wellman et al. 2006b). Either of these results would be detrimental and, therefore, calcium hypophosphite was eliminated from further consideration. Table 7 presents the down-selected formulations.

Table 7. Down-Selected Experimental Batch Conditions for Polyphosphate Amendment Optimization

Phosphate Source	Phosphorus Conc. (ppm)	Calcium Source	Calcium Conc. (ppm)	Uranium Conc., (μg/L)	
Sodium orthophosphate	1,500	Not applicable	Not applicable	10	1,000
				0.00	
Sodium orthophosphate	2,000	Not applicable	Not applicable	10	1,000
				0.00	
Sodium orthophosphate	2,500	Not applicable	Not applicable	10	1,000
				0.00	
Sodium pyrophosphate	1,500	Not applicable	Not applicable	10	1,000
				0.00	
Sodium pyrophosphate	2,000	Not applicable	Not applicable	10	1,000
				0.00	
Sodium pyrophosphate	2,500	Not applicable	Not applicable	10	1,000
				0.00	
Sodium tripolyphosphate	1,500	Not applicable	Not applicable	10	1,000
				0.00	
Sodium tripolyphosphate	2,000	Not applicable	Not applicable	10	1,000
				0.00	
Sodium tripolyphosphate	2,500	Not applicable	Not applicable	10	1,000
				0.00	
Sodium trimetaphosphate	1,500	Not applicable	Not applicable	10	1,000
				0.00	
Sodium trimetaphosphate	2,000	Not applicable	Not applicable	10	1,000
				0.00	
				0.00	
Sodium trimetaphosphate	2,500	Not applicable	Not applicable	10	1,000
				0.00	
Sodium hexametaphosphate	1,500	Not applicable	Not applicable	10	1,000
				0.00	
Sodium hexametaphosphate	2,000	Not applicable	Not applicable	10	1,000
				0.00	
Sodium hexametaphosphate	2,500	Not applicable	Not applicable	10	1,000
				0.00	
Sodium orthophosphate	1,500	Calcium chloride	1,000	10	1,000
				0.00	
Sodium orthophosphate	1,500	Calcium chloride	1,500	10	1,000
Sodium orthophosphate	2,000	Calcium chloride	1,000	10	1,000
				0.00	
Sodium orthophosphate	2,000	Calcium chloride	1,500	10	1,000
				0.00	

Table 7. (contd)

Phosphate Source	Phosphorus Conc. (ppm)	Calcium Source	Calcium Conc. (ppm)	Uranium Conc., (μg/L)	
Sodium orthophosphate	2,500	Calcium chloride	1,000	10	1,000
				0.00	
Sodium orthophosphate	2,500	Calcium chloride	1,500	10	1,000
				0.00	
Sodium pyrophosphate	1,500	Calcium chloride	1,000	10	1,000
				0.00	
Sodium pyrophosphate	1,500	Calcium chloride	1,500	10	1,000
				0.00	
Sodium pyrophosphate	2,000	Calcium chloride	1,000	10	1,000
				0.00	
Sodium pyrophosphate	2,000	Calcium chloride	1,500	10	1,000
				0.00	
Sodium pyrophosphate	2,500	Calcium chloride	1,000	10	1,000
				0.00	
Sodium pyrophosphate	2,500	Calcium chloride	1,500	10	1,000
Sodium tripolyphosphate	1,500	Calcium chloride	1,000	10	1,000
				0.00	
Sodium tripolyphosphate	1,500	Calcium chloride	1,500	10	1,000
				0.00	
Sodium tripolyphosphate	2,000	Calcium chloride	1,000	10	1,000
				0.00	
Sodium tripolyphosphate	2,000	Calcium chloride	1,500	10	1,000
				0.00	
Sodium tripolyphosphate	2,500	Calcium chloride	1,000	10	1,000
				0.00	
Sodium tripolyphosphate	2,500	Calcium chloride	1,500	10	1,000
Sodium trimetaphosphate	1,500	Calcium chloride	1,000	10	1,000
				0.00	
Sodium trimetaphosphate	1,500	Calcium chloride	1,500	10	1,000
				0.00	
Sodium trimetaphosphate	2,000	Calcium chloride	1,000	10	1,000
				0.00	
Sodium trimetaphosphate	2,000	Calcium chloride	1,500	10	1,000
				0.00	
Sodium trimetaphosphate	2,500	Calcium chloride	1,000	10	1,000
				0.00	
Sodium trimetaphosphate	2,500	Calcium chloride	1,500	10	1,000

Table 7. (contd)

Phosphate Source	Phosphorus Conc. (ppm)	Calcium Source	Calcium Conc. (ppm)	Uranium Conc., (μg/L)	
Sodium hexametaphosphate	1,500	Calcium chloride	1,000	10	1,000
				0.00	
Sodium hexametaphosphate	1,500	Calcium chloride	1,500	10	1,000
				0.00	
Sodium hexametaphosphate	2,000	Calcium chloride	1,000	10	1,000
				0.00	
Sodium hexametaphosphate	2,000	Calcium chloride	1,500	10	1,000
				0.00	
Sodium hexametaphosphate	2,500	Calcium chloride	1,000	10	1,000
				0.00	
Sodium hexametaphosphate	2,500	Calcium chloride	1,500	10	1,000
				0.00	

Figure 12 displays the percent of calcium and phosphorus removed from solution as a function of the calcium to phosphorus molar ratio in the presence of 10 and 1,000 ppb uranium. The objective of these tests was to identify the calcium-to-phosphorus molar ratio for maximum removal from the aqueous phase. The mechanisms of removal may include sorption and precipitation; however, no attempt was made to discern the degree of removal based on these respective mechanisms. Greater than 90% removal of calcium and phosphorus from solution was achieved in the presence of sodium orthophosphate, sodium pyrophosphate, sodium tripolyphosphate, respectively, with calcium-chloride (Figure 12). The optimum molar ratio of calcium to phosphorus for sodium orthophosphate and sodium pyrophosphate is 1.5; whereas, the optimum calcium-to-phosphorus molar ratio for sodium tripolyphosphate is ~2.4. Moreover, the uptake of uranium was rapid (<2 min) and complete, ~100%, which is discussed in detail below.

3.2.2 Column Experiments

Column experiments were conducted to

- quantify the mobility of ortho-, pyro-, and tripolyphosphate, individually and as a mixed formulation, to evaluate differences in retardation due to interaction between the various phosphate compounds
- evaluate the mobility of calcium
- optimize amendment formulation based on results of batch tests for amendment emplacement and the formation of autunite and apatite.

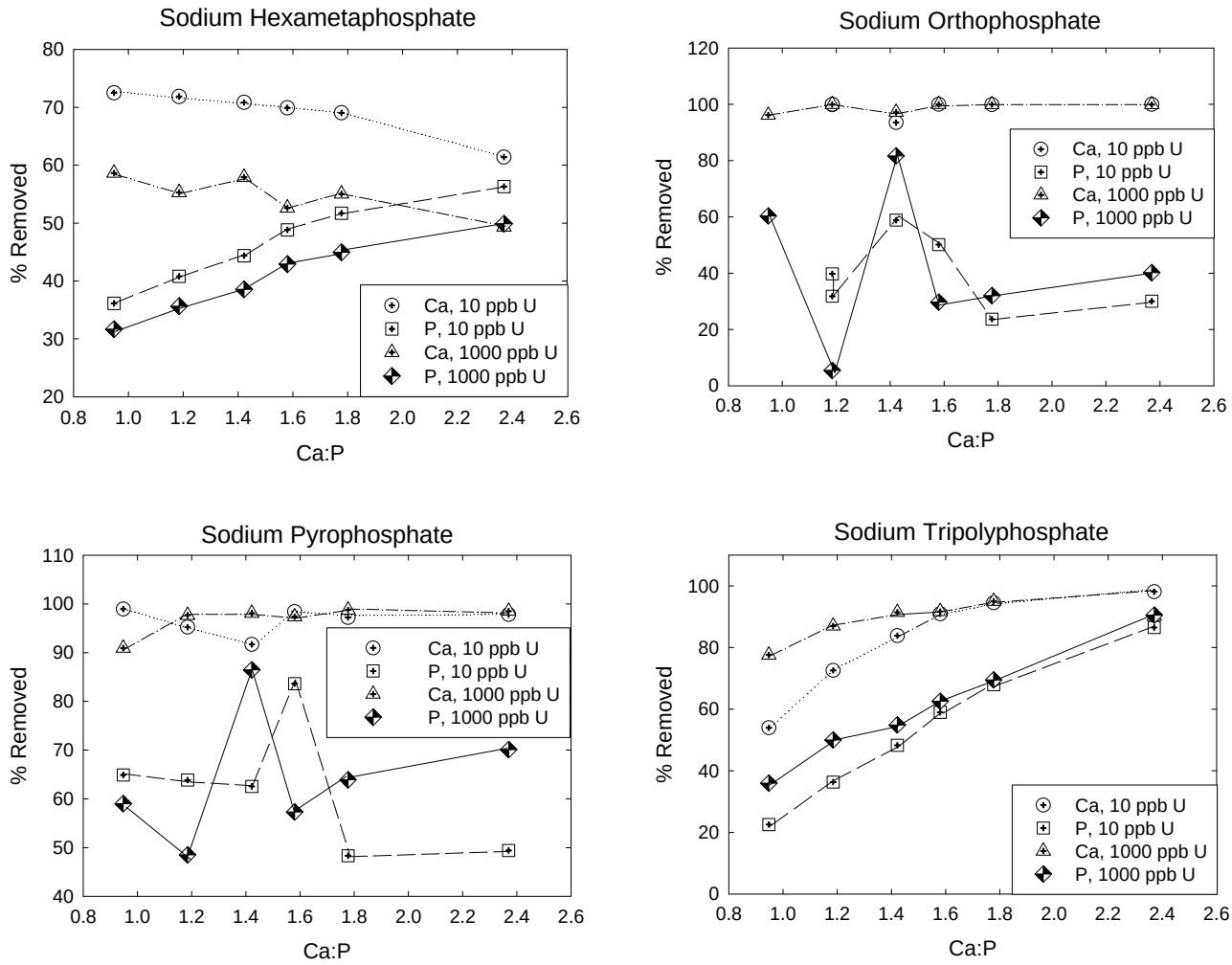

Figure 12. Percent Removal of Calcium and Phosphorus as a Function of Calcium-to-Phosphorus Molar Ratio

3.2.2.1 Amendment Formulation, Efficacy, and Emplacement

Saturated column tests were conducted to evaluate the concentration of total phosphorus and calcium, the ratio of ortho-, pyro-, and tripolyphosphate, the molar ratio of calcium to phosphorus, pH, and the injection order to optimize emplacement of the amendment and the extent of treatment, reduction in aqueous uranium concentration, and the formation of autunite and apatite. Sodium orthophosphate ($Na_3PO_4 \cdot 12H_2O$), sodium pyrophosphate ($Na_4P_2O_7 \cdot 10H_2O$), and sodium tripolyphosphate ($Na_5P_3O_{10}$) provided the source of each respective phosphate for all phosphorus amendment formulations and calcium-chloride ($CaCl_2$) as the source of calcium. Calcium rapidly precipitates with orthophosphate; therefore, all injections were conducted in two phases by injecting either the calcium solution followed by the phosphorus solution or vice versa. Details regarding the amendment formulation, injection order, calcium-to-total phosphorus molar ratio, amendment pH, and concentrations are summarized in Table 8.

Table 8. Experimental Parameters for Polyphosphate Amendment Optimization Column Tests

Column No.	Amendment Source	Wt% Phosphate Source	Injection Order	$Ca:P_{total}$	pH	Conc., M
1	Ortho $[P]_{aq}$	0.25	1	2.2	7	1.32 H 10^{-3}
	Pyro $[P]_{aq}$	0.25				6.58 H 10^{-4}
	Tripoly $[P]_{aq}$	0.5				8.77 H 10^{-4}
	Calcium		2			1.15 H 10^{-2}
2	Ortho $[P]_{aq}$	0.25	1	2.2	7	1.97 H 10^{-3}
	Pyro $[P]_{aq}$	0.25				9.87 H 10^{-4}
	Tripoly $[P]_{aq}$	0.5				1.32 H 10^{-3}
	Calcium		2			1.74 H 10^{-2}
3	Ortho $[P]_{aq}$	0.25	1	2.2	No adj.	1.97 H 10^{-3}
	Pyro $[P]_{aq}$	0.25				9.87 H 10^{-4}
	Tripoly $[P]_{aq}$	0.5				1.32 H 10^{-3}
	Calcium		2			1.74 H 10^{-2}
4	Ortho $[P]_{aq}$	0.375	1	2.2	No adj.	2.63 H 10^{-3}
	Pyro $[P]_{aq}$	0.25				1.32 H 10^{-3}
	Tripoly $[P]_{aq}$	0.375				1.75 H 10^{-3}
	Calcium		2			2.32 H 10^{-2}
5	Ortho $[P]_{aq}$	0.25	1	1.67	No adj.	3.47 H 10^{-3}
	Pyro $[P]_{aq}$	0.25				1.74 H 10^{-3}
	Tripoly $[P]_{aq}$	0.5				2.32 H 10^{-3}
	Calcium		2			2.32 H 10^{-2}
6	Ortho $[P]_{aq}$	0.25	1	1.67	7	3.47 H 10^{-3}
	Pyro $[P]_{aq}$	0.25				1.74 H 10^{-3}
	Tripoly $[P]_{aq}$	0.5				2.32 H 10^{-3}
	Calcium		2			2.32 H 10^{-2}
7/11	Ortho $[P]_{aq}$	0.25	1	2.2	No adj./7	2.63 H 10^{-3}
	Pyro $[P]_{aq}$	0.25				1.32 H 10^{-3}
	Tripoly $[P]_{aq}$	0.5				1.75 H 10^{-3}
	Calcium		2			2.32 H 10^{-2}
8/12	Ortho $[P]_{aq}$	0.25	1	2.2	No adj./7	6.58 H 10^{-3}
	Pyro $[P]_{aq}$	0.25				3.29 H 10^{-3}
	Tripoly $[P]_{aq}$	0.5				4.39 H 10^{-3}
	Calcium		2			5.79 H 10^{-2}
9/13	Ortho $[P]_{aq}$	0.25	1	2.2	No. Adj/7	9.21 H 10^{-3}
	Pyro $[P]_{aq}$	0.25				4.61 H 10^{-3}
	Tripoly $[P]_{aq}$	0.5				6.14 H 10^{-3}
	Calcium		2			8.10 H 10^{-2}
10/14	Ortho $[P]_{aq}$	0.25	1	2.2	No Adj./7	1.32 H 10^{-2}
	Pyro $[P]_{aq}$	0.25				6.58 H 10^{-3}
	Tripoly $[P]_{aq}$	0.5				8.77 H 10^{-3}
	Calcium		2			1.16 H 10^{-1}

Table 8. (contd)

Column No.	Amendment Source	Wt% Phosphate Source	Injection Order	$Ca:P_{total}$	pH	Conc., M
15	Ortho $[P]_{aq}$	0.25	2	1.9	No Adj.	1.32 H 10^{-2}
	Pyro $[P]_{aq}$	0.25				6.58 H 10^{-3}
	Tripoly $[P]_{aq}$	0.5				8.77 H 10^{-3}
	Calcium		1			9.98 H 10^{-2}
16	Ortho $[P]_{aq}$	0.25	2	1.9	7	1.32 H 10^{-2}
	Pyro $[P]_{aq}$	0.25				6.58 H 10^{-3}
	Tripoly $[P]_{aq}$	0.5				8.77 H 10^{-3}
	Calcium		1			9.98 H 10^{-2}
17	Ortho $[P]_{aq}$	0.25	2	2.2	7	9.21 H 10^{-3}
	Pyro $[P]_{aq}$	0.25				4.61 H 10^{-3}
	Tripoly $[P]_{aq}$	0.5				6.14 H 10^{-3}
	Calcium		1			8.10 H 10^{-2}
18	Ortho $[P]_{aq}$	0.25	2	2.2	7	1.32 H 10^{-2}
	Pyro $[P]_{aq}$	0.25				6.58 H 10^{-3}
	Tripoly $[P]_{aq}$	0.5				8.77 H 10^{-3}
	Calcium		1			1.16 H 10^{-1}

Several uranium mineral phases will fluoresce under UV radiation. This property can be a useful means to rapidly and efficiently evaluate the presence of uranium phases within large sedimentary matrices. A control column was conducted to confirm no other fluorescent phases may be present within the sediment or formed as a result of saturating the column with 1 ppm uranium. There was no evidence of any phase that would fluoresce at 254 nm within the uranium-saturated sediment indicating fluorescence spectroscopy could be used for qualitative evaluation of uranium-phosphate mineral phase formation. Visual inspection of sediment removed from columns 1 through 4 after application of the associated amendment formulations illustrated the formation of fluorescent green precipitates under shortwave UV radiation, 254 nm, indicative of uranium-phosphate phases (Figure 13). Qualitatively the precipitate appeared to be within or coating ~50% of the sediment particles Analysis of effluent solution samples by ICP-MS from columns 1 through 4 demonstrated ~50% reduction in the aqueous uranium concentration. This suggests that to treat 100% of the aqueous uranium a higher concentration of phosphorus and calcium in the amendment formulation was necessary. Comparison of columns 2 and 3 suggested there was little effect of pH in reducing the aqueous uranium concentration; however, precipitation of calcium-phosphate was more significant under pH conditions ~7.

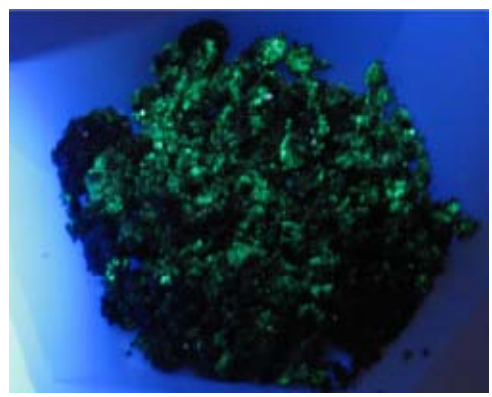

Figure 13. Representative Photo of Sediment Sectioned from the Effluent End of Column 1 Illustrating the Visual Identification of Uranium-Phosphate under Shortwave UV Radiation

Precipitation of apatite from homogeneous matrices has been suggested to proceed through initial precipitation of amorphous calcium-phosphate which serves as a template for the heterogeneous nucleation of octacalcium-phosphate (OCP) (Feenstra and de Bruyn 1979). In turn, OCP serves as a template for epitaxial growth of hydroxyapatite (Feenstra and de Bruyn 1979; Brown et al. 1962; Eanes et al. 1965; Eanes and Posner 1965; Eanes and Meyer 1977). The conversion of amorphous to crystalline phases involving an epitaxial matching of the depositing phase onto the hydroxyapatite crystalline substrate is consistent with a hypothesized autocatalytic conversion mechanism (Boskey and Posner 1973; 1976; Eanes and Posner 1965); this explains the significance of apatite seed crystals for accelerated precipitation of hydroxyapatite from solution (Boskey and Posner 1973; Nancollas and Mohan 1970; Nancollas and Tomazic 1974; Inskeep and Silvertooth 1988; Brown 1981a; 1980; 1981b; Amjad et al. 1981). Once the reservoir of non-apatitic calcium-phosphate is depleted during the conversion process, the increase in size of apatite crystals proceeds by Ostwald ripening in which the overall number of apatite crystals is reduced by consolidation and recrystalization (Eanes and Posner 1970). The Gibbs-Kelvin effect states the thermodynamic driving force for this mechanism is that the equilibrium solubility of smaller particles decrease with increasing particle size. Therefore, in a suspension of heterogeneously sized particles, the smaller particles have a higher solubility than larger particles, which causes the smaller particles to dissolve and the larger particles continue to grow (Eanes et al. 1965; Eanes and Posner 1970). However, the growth rate of apatite is controlled by surface nucleation and/or dislocation mechanisms (Eanes and Posner 1970). As such, hydroxyapatite growth is limited by process that occur at the crystal interface (Nancollas and Mohan 1970) and, therefore, are dependent on the surface area (Inskeep and Silvertooth 1988). Christoffersen and Christoffersen (1982) proposed that protonation of phosphate groups at the crystal surface catalyzes the exchange of phosphate between the apatite surface and the bulk solution, thereby accelerating growth. At pH 7.4, hydroxyapatite is the least soluble phase and most thermodynamically stable, in the absence of kinetic complications (Nancollas and Tomazic 1974). This is consistent with findings regarding the growth of fluorapatite (FAP) wherein a direct relationship between the growth rate of FAP and pH was observed (van Cappellen and Berner 1991). For a given degree of supersaturation, the growth rate of FAP at pH 7 was twice that measured at pH 8.

This underscores the complex series of elementary reactions in the precipitation of hydroxyapatite which suggests either 1) direct precipitation from solution on the surface of hydroxyapatite seed crystals, or 2) precipitation from surface or absorbed calcium and phosphate whose concentrations are dependent on the solution calcium-to-phosphate ratio (Inskeep and Silvertooth 1988). The compactness of the heterogeneous nucleus is more conducive to the formation of hydroxyapatite than the diffuse homogeneous ionic nucleus (Garten and Head 1966). However, macromolecules can influence both the initial formation of amorphous calcium-phosphate and the conversion to apatite (Termine et al. 1970; Termine and Posner 1970). These macromolecules contain sites within their internal or solvation-shell which favors nucleation and growth (Termine et al. 1970; Termine and Posner 1970). Additionally, a decreased dielectric constant enhances initial mineral phase separation and amorphous-crystalline conversion. Thus, a partially apolar region within a macromolecule, as well as more polar regions, may provide a local milieu favorable for amorphous calcium-phosphate formation or crystal conversion (Termine et al. 1970). Sodium tripolyphosphate serves as a favorable nucleating surface toward initial mineral phase separation and formation of amorphous calcium-phosphate with orthophosphate. When mineralization nucleation is considered relative to the initial mineral phase depositions pyrophosphate will serve as a strong nucleating agent (Termine and Posner 1970).

Schmid and McKinney (1968) identified key processes involved in the formation of apatite from mixtures of ortho-, pyro-, and tripolyphosphate. Results of sorption studies illustrated orthophosphate sorbs onto polyphosphate near pH ~7 to 9. Although, tripolyphosphate does not readily precipitate in the absence of orthophosphate, sorption of orthophosphate onto tripolyphosphate serves as a heterogeneous nucleating surface to promote precipitation. As orthophosphate begins to precipitate the pH of the solution increases slightly, while the degradation of tripolyphosphate is accelerated to form ortho- and pyrophosphate. This further enhances precipitation by providing additional orthophosphate. Furthermore, pyrophosphate produces a heavy, fast-settling precipitate with calcium, which increases the settling rate of the finer precipitates formed from tripolyphosphate. In the absence of orthophosphate, precipitation from tripolyphosphate is only ~50% of that under the same conditions in the presence of both ortho- and tripolyphosphate.

A key additional consideration regarding the use of a polyphosphate amendment in the precipitation of calcium-phosphate under conditions present within the 300 Area is the effect of carbonate. Precipitation of calcium-phosphate from monophosphate solutions is strongly influenced by competing reactions to produce calcium-carbonates (Lindsay and Moreno 1960; Diaz et al. 1994). Jenkins et al. (1971) demonstrated that in $Ca\text{-}PO_4\text{-}CO_3\text{-}H^+\text{-}H_2O$ system precipitation of calcium-carbonate competes with the precipitation of calcium-phosphate under the pH range of 9 to 10.5. Between pH 7.5 to 8.5 and above pH 10.5 calcium-phosphate precipitation controls the phosphorus concentration. For example, precipitation of calcium-phosphate at pH 8 initiated with an induction period of a couple hours followed by a period of rapid precipitation and prolonged slow removal of phosphorus from solution. As the bicarbonate concentration increased, the initial induction period required for precipitation of calcium-phosphate increased and the subsequent rate of removal as a function of bicarbonate concentration decreased.

By complexing calcium and sorbing to mineral surfaces, polyphosphate compounds effectively reduce both the rate and extent of calcium-carbonate precipitation, while simultaneously enhancing the rate of calcium-phosphate precipitation by reducing the competing reaction and "directing" calcium to participate in reactions resulting in calcium-phosphate precipitation (Ferguson et al. 1973).

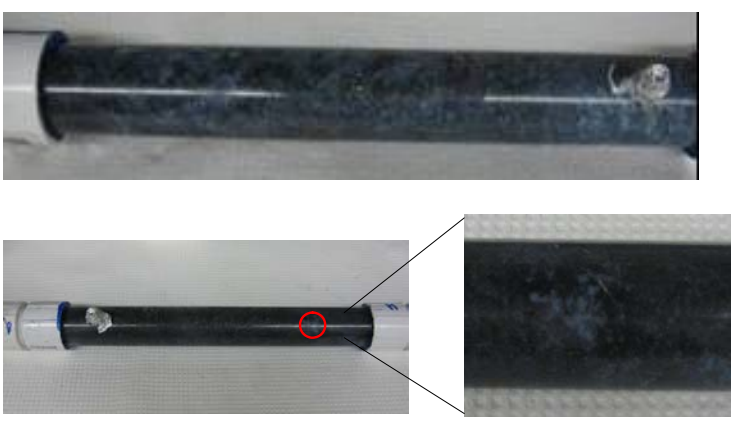

Figure 14. Photo Showing Disperse Precipitation of Calcium-Phosphate Throughout Column 1 (top) and Discrete Precipitation of Calcium-Phosphate within Column 4 (bottom)

Column 4 highlighted the significance of the complex relationship between ortho-, pyro-, and tripolyphosphate. Although the concentration of aqueous uranium was decreased ~50%, the formation of calcium-phosphate was restricted to a discrete region with in the sediment matrix (Figure 14).

Columns 5 and 6 (Ca:P molar ratio = 1.67) in comparison to columns 2 and 3 (Ca:P molar ratio = 2.2) illustrated the significance of the calcium-to-phosphorus molar ratio. Qualitatively, the Ca:P molar ratio of 2.2 (columns 2 and 3) afforded more precipitation than

a Ca:P molar ratio of 1.67 (columns 5 and 6), which gave no visual indication of calcium-phosphate precipitation. Although batch testing indicated the optimal Ca:P molar ratio for removal of calcium and phosphorus in the presence of both ortho-, and pyrophosphate was ~1.5, columns 1 through 4 illustrate the significance of the Ca:P ratio of 2.4 indicated by tripolyphosphate batch testing. This supports batch test results, which indicated an optimal Ca:P molar ratio of ≥1.9.

The calcium and phosphorus formulations were conducted in duplicate with columns 7 through 10 at the unadjusted pH (pH 7), and columns 11 through 14 at the adjusted pH with a Ca:P molar ratio = 2.2 for all columns. For these experiments the concentration of calcium varied from 2.32 H 10^{-2} M to 1.16 H 10^{-1} M, andphosphorus concentrations ranged from 1.05 H 10^{-2} M to 5.26 H 10^{-2} M. Precipitation of calcium-phosphate in columns 7 through 10 was limited, eliminating consideration of non-adjusted amendment solutions. Alternatively, the degree of calcium-phosphate precipitation increased utilizing the same amendment formulation adjusted to pH ~7, columns 11 through 14. In columns 11 and 12 the concentration of aqueous uranium in the effluent solution increased over the first 0.5 to 1 pore volume during remedy injection to concentrations between 1.2 to 3 times the influent uranium concentration (Figure 15a, b). However, increasing the concentration of phosphorus and calcium in the amendment formulation (column 14) precluded this phenomenon. Additionally, the concentration of aqueous uranium was reduced to below the MCL, 30 μg/L, within 0.5 to 1 pore volumes of treatment, and remained well below 30 μg/L for the remainder of the experiment (Figure 15d).

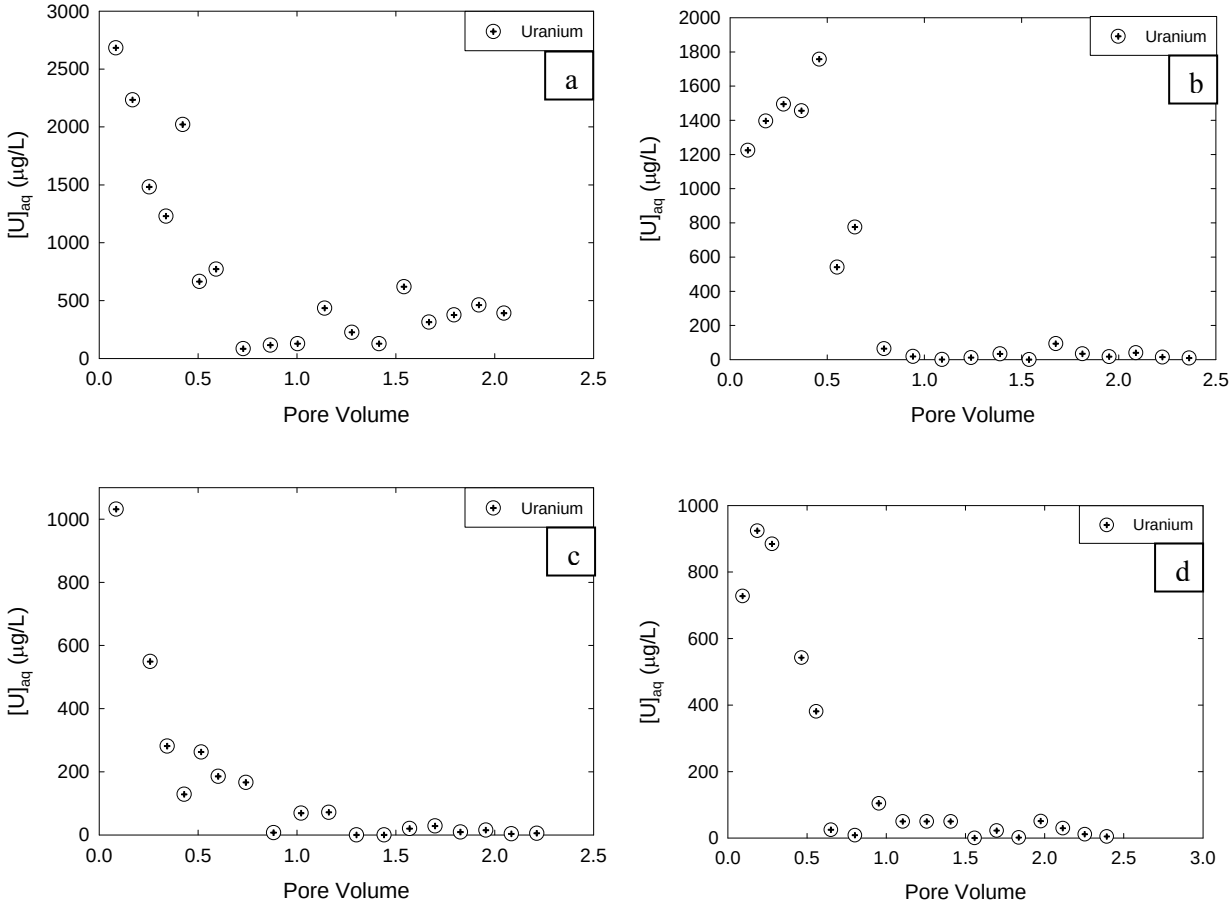

Figure 15. Graphs Depicting Aqueous Uranium Concentrations from Columns Saturated with 1,000 µg/L Uranium as a Function of the Number of Pore Volumes of Polyphosphate Remedy Displaced Through Columns a) 11, b) 12, c) 13, and d) 14 (Table 8).

Columns 15 through 18 used the optimum formulations identified through previous tests (columns 13 and 14) as well as two additional formulations that contained equivalent total phosphorus concentrations, but maintained total calcium-to-phosphorus ratios of 1.9 (columns 17 and 18). The order of injection was altered for all columns (15 through 18) such that calcium was injected prior to phosphorus. Qualitative visual inspection of the columns following treatment suggests the most complete distribution within the column and removal of uranium occurred in column 16, using a calcium-to-phosphorus molar ratio of 1.9, pH 7 (Figure 16).

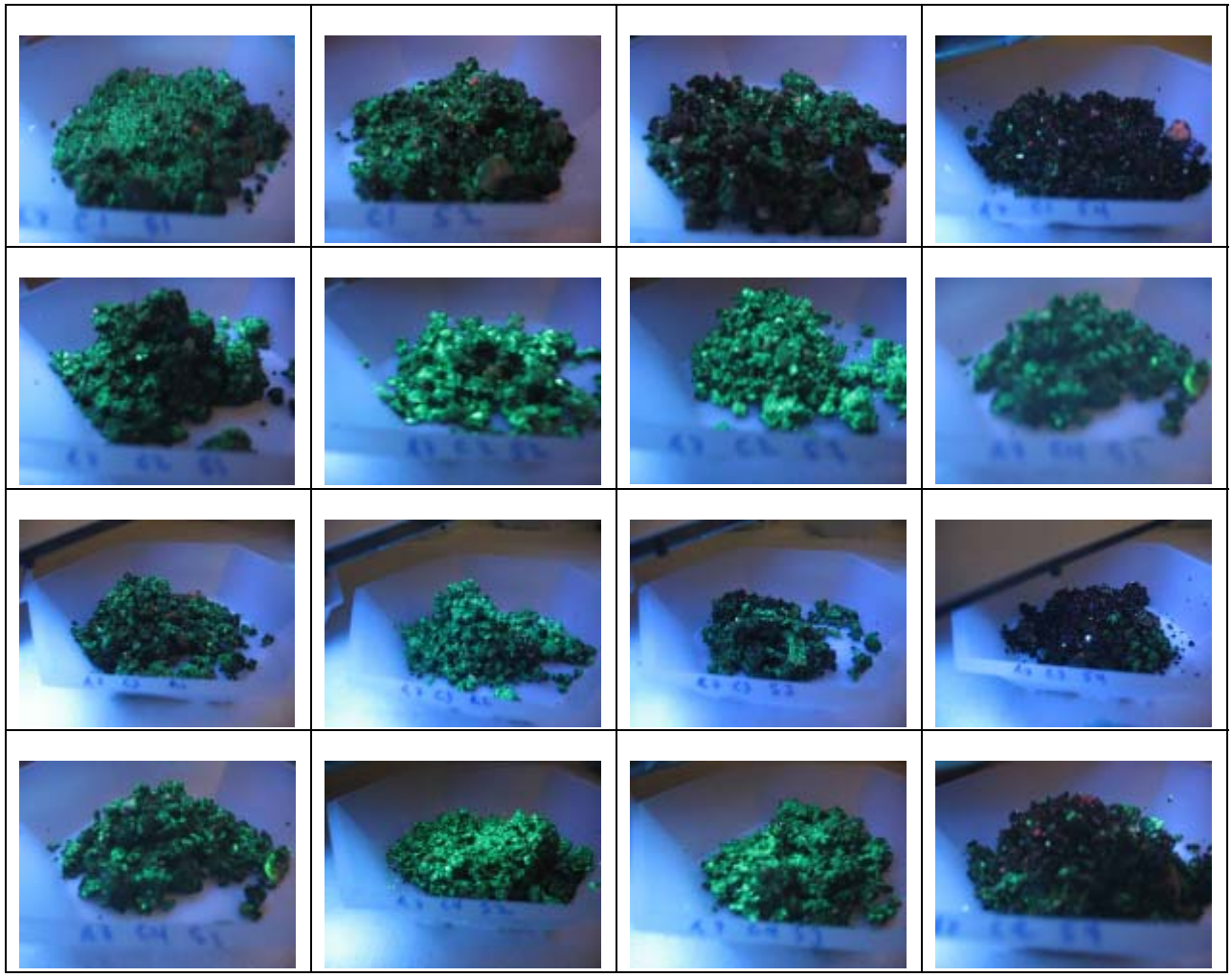

Figure 16. Photos of Column Sections Taken under Shortwave UV Radiation. Orientation: top-down, columns 15 through 18; left to right, influent to effluent.

However, with the exception of column 17, quantitative analysis of effluent uranium concentrations do not decline as rapidly as those measured in the previous set of columns, 11 through 14, wherein phosphorus was injected first followed by calcium (Figure 17). Additionally, the efficacy and long-term

performance of columns 15 through 18 is less than that of columns 11 through 14 where uranium concentrations remain well below 30 µg/L. The aqueous concentration of uranium measured in the effluent solutions collected from columns 15 through 18 decline to below 30 µg/L, but then exhibit a number of fluctuations above and below the MCL for the remainder of the experiment. It is hypothesized that these fluctuations can be attributed to the initial formation of precursor calcium-uranate phases, which are more soluble than uranium-phosphate phases. Upon injection of the phosphorus phase, the calcium-uranate phases likely undergo rapid dissolution to release soluble uranium that re-precipitates as a uranium-phosphate phase. Although both injection schemes ultimately result in formation of uranium-phosphate, precipitation and dissolution of calcium-uranate phases may afford undesirable fluctuations in uranium concentration above 30 µg/L.

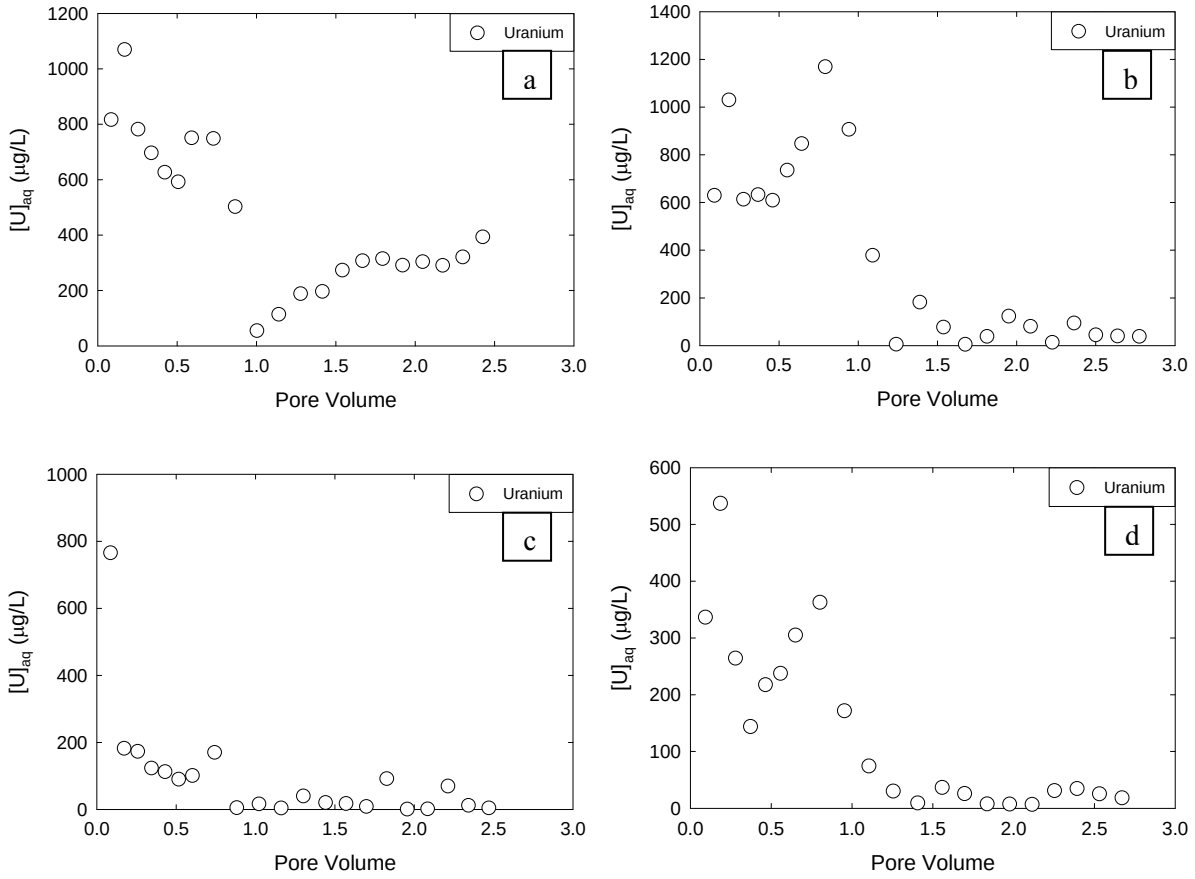

Figure 17. Graphs Depicting Aqueous Uranium Concentrations from Columns Saturated with 1,000 µg/L Uranium as a Function of the Number of Pore Volumes of Polyphosphate Remedy Displaced Through Columns a) 15, b) 16, c) 17, and d) 18 (Table 8). Remedy injection order was calcium followed by phosphorus.

Regardless of the injection order or concentration of phosphorus and calcium used in the amendment formulation all phosphorus, including degradation products, was removed via sorption and precipitation reactions. Figure 18 is a representative plot for the removal of phosphorus during treatment of a uranium contaminant column with results being comparable for all column tests conducted. Effluent concentra-

tions of phosphorus are at or below background groundwater concentrations. Thus, the potential for downgradient transport and potential migration to the river is minimal.

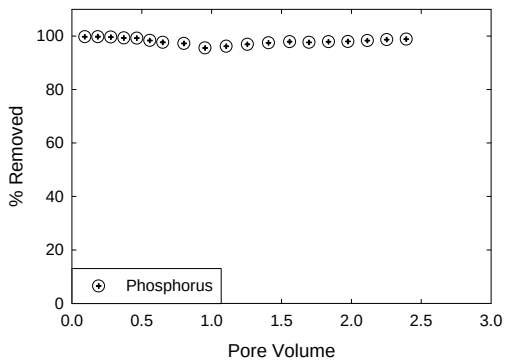

Figure 18. Representative Plot Depicting the Removal of Phosphorus by Sorption and Precipitation Reactions

3.2.2.2 Transport

Column experiments were conducted to quantify the mobility of ortho-, pyro-, and tripolyphosphate, individually and as a mixed formulation, to evaluate differences in retardation due to interaction between the various phosphate compounds and to evaluate the mobility of calcium to determine the volume of remedy necessary to treat the desired zone. Saturated column tests were conducted with the <2-mm sediment fraction from 300 Area cores. The conditions and measured parameters for all of the transport experiments are summarized in Table 9. Recovery (%) reflects the percentage of solute recovered in the effluent. R is the retardation factor analysis and K_d is the apparent distribution coefficient calculated from R. Transport experiments were conducted at a v of ~20 cm h^{-1}.

Table 9. Transport Parameters Determined by Direct Measurement or from Laboratory-Derived Breakthrough Curve on the <2-mm Sediment Fraction[(a)]

Expt.[(b)]	F (cm^3/hr)	ρ_b (g/cm^3)	θ	V_w (mL)	v (cm/hr)	t_o (V_w)	R	K_d (mL/g)
Ortho	30.37	1.478	0.386	20.89	16.01	11.22	5.54	1.19
Pyro	41.93	1.444	0.385	20.33	22.18	15.90	7.61	1.76
Tripoly	40.80	1.460	0.392	21.27	21.22	14.70	5.17	1.12
Calcium	31.41	1.478	0.386	20.89	16.57	11.95	14.14	3.44
Amend7	30.61	1.444	0.385	20.33	16.19	12.26	5.83	1.29
Amend	30.88	1.460	0.392	21.27	16.05	11.82	5.23	1.13

(a) F = flow rate; ρ_b = bulk density; θ = average volumetric water content (standard deviation); V_w = average pore volume; v = average pore water velocity; t_o = step input; R = retardation factor; K_d = sediment water distribution coefficient based on R.
(b) Columns appeared saturated and had reached a stable water content.

The results of transport in near-saturated columns for sodium ortho-, pyro-, tripolyphosphate, calcium, the phosphorus amendment formulation as mixed, and the phosphorus amendment formulation pH adjusted to ~7 are shown in Figure 19. Note that columns were saturated until a stable water content was attained. Calculation of the percent of saturation based on total porosity indicated that the conventional columns were approximately 90% saturated. A full breakthrough curve (BTC) for sodium orthophosphate was attained and recovery of phosphorus in the effluent was ~100% (Figure 19). BTCs for sodium pyro- and tripolyphosphate, conducted under the same conditions as sodium orthophosphate, only afforded ~75% recovery of the influent pulse (Figure 19). Possible mechanisms that may have resulted in increased sorption are 1) sorption of degradation products onto sediment-bound polymerized phosphate molecules, and/or 2) degradation of polymerized phosphate compounds and subsequent sorption to the sediment matrix. This suggests the significance of reactions occurring between sodium

ortho-, pyro-, and tripolyphosphate. In the absence of precipitation reactions (i.e., formation of calcium- and uranium-phosphate phases), the mobility of the phosphorus amendment is comparable to the

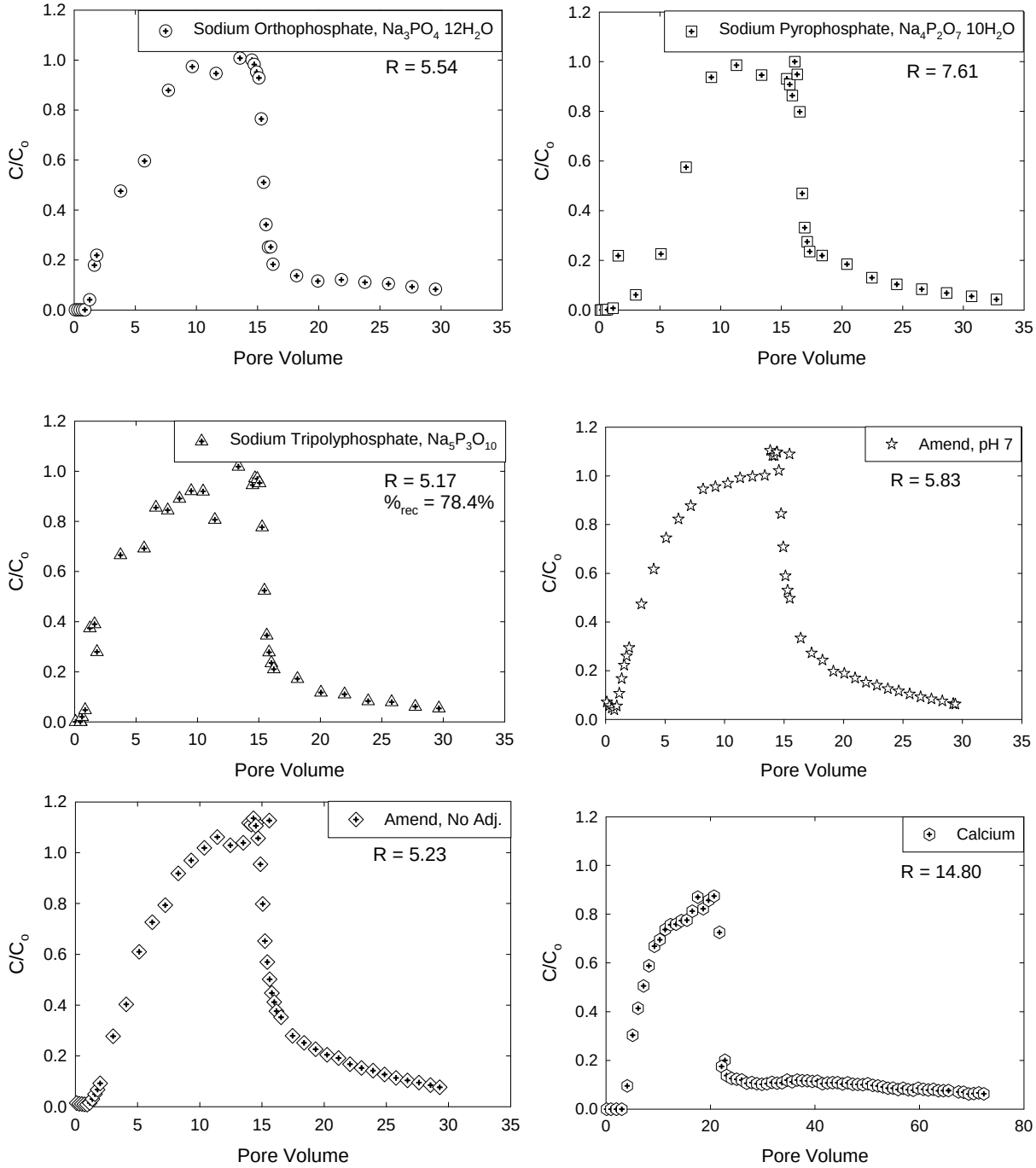

Figure 19. Breakthrough Curves for Sodium Ortho-, Pyro-, Tripolyphosphate, Calcium, the Phosphorus Amendment Formulation as Mixed, and the Phosphorus Amendment Formulation pH Adjusted to ~7. The breakthrough curves are based on total P measure in the column effluent solution.

individual phosphate compounds (Figure 19). The apparent retardation factor within the <2-mm sediment fraction is 5.23 for the non-pH-adjusted amendment and 5.83 for the pH-adjusted amendment (Table 9). To adjust these values for field conditions it was assumed retardation was due to the <2-mm fraction and the <2-mm fraction composed ~10% of the total sediment matrix. The field K_d and retardation values were calculated using the porosity value of 0.2 and bulk density value of 2.19, which were quantified within the LFI (Table 10).

Table 10. Field Transport Parameters Calculated from Laboratory-Derived Transport Parameters

Compound	*v* (ft/d)	*R*	K_d (mL/ g)
Sodium Orthophosphate	53.18	2.30	0.12
Sodium Pyrophosphate	74.88	2.93	0.18
Sodium Tripolyphosphate	71.66	2.23	0.11
Calcium	56.64	4.76	0.34
Amendment, pH 7	57.74	2.41	0.13
Amendment, no pH Adj.	57.61	2.24	0.11

Figure 19 also displays the result of calcium transport under saturated conditions. Unlike the anionic phosphate species, calcium is cationic and strongly retarded within the anionic sedimentary and aqueous conditions present within the Hanford 300 Area subsurface (Table 9). Injection of a calcium pulse required a greater number of pore volumes to be delivered in order to afford a $C/C_o = 1$. Moreover, the desorption, or later half of the calcium BTC, displayed prolonged tailing for more than 40 pore volumes without reaching zero. The same assumptions as described previously for calculating the field K_d and retardation values for phosphate were used to calculate the field values for calcium (Table 10).

3.3 Immobilization of Uranium via Apatite

Hydroxyapatite has been demonstrated to be highly efficient for the sequestration of heavy metals and radionuclides including the following uranium (Jeanjean et al. 1995; Thakur et al. 2005; Arey et al. 1999; Naftz et al. 2000; Fuller et al. 2003; Fuller et al. 2002a; Fuller et al. 2002b), nickel (Seaman et al. 2001), neptunium (Moore et al. 2003), plutonium (Moore et al. 2005; Conca et al. 2002), cesium (Park et al. 2002), lead (Ma et al.; Ma et al. 1993; Ma et al. 1994; Ruby et al. 1994; Xu and Schwartz 1994; Stanforth and Chowdhury 1994; Davis et al. 1992; Mavropoulos et al. 2002), rare earth metals (McArthur 1985), other heavy metals (Conca et al. 2002; Conca 1996; Conca et al. 2000; Lee et al. 1995; Seaman et al. 2001; Seaman et al. 2003; Wright et al. 1995; Wright et al. 1991; Jeanjean et al. 1995; Moore et al. 2004). Metal sequestration processes include sorption via ion exchange or surface complexation, incorporation in the apatite structure, and precipitation of metal phosphates. Ion exchange is the dominant mechanism for sorption of monovalent and divalent cations. However, complexation reactions and hydrolysis preclude actinides from intracrystalline sites (Cotton 2006); whereas, surface sorption is a significant mechanism for the sequestration of actinides to mineral surfaces.

Fuller et al. (2002a; 2003) demonstrated the efficacy of hydroxyapatite for reducing the aqueous uranium concentration to <0.05 μM under the pH range of 6.3 to 6.9 in the presence of carbonate. Results suggested binding of uranium, irrespective of dissolved carbonate concentration or aqueous

uranium concentration, occurred via surface complexation. Long-term retention occurs through the transformation of sorbed apatite to chernikovite. Additionally, Thakur et al. (2005) recently reported the sequestration of uranium to hydroxyapatite at pH = 2 to 8 in 0.001 to 1.0 M $NaClO_4$. The results indicate the sorption of uranium increases as a function of pH, reaching a maximum (100%) at pH 6 to 8, which occurs in <1 hour, further increasing the pH results in a sharp decrease in the sorption of uranium due to formation of soluble uranyl-carbonate species at higher pH. There was little effect of ionic strength on the sequestration of uranium and sorption kinetics followed Lagergren's first order rate equation over the temperature range of 298 to 333 K.

These results suggests that hydroxyapatite could serve as an efficient sorbent for the quantitative sequestration of uranium under conditions relevant to the 300 Area following the dispersion and dissipation of the polyphosphate remedy within the subsurface. However, hydroxyapatite is highly insoluble and far from equilibrium with natural waters. Moreover, apatite surfaces are hypothesized to have two different types of surface groups: $\equiv$Ca-OH_2^+ and $\equiv$P-OH, affording a pH_{pzc} of 8.15 or 7.13 upon exposure to atmospheric CO_2 (Wu et al. 1991). Below a pH of 4 the phosphate sites are predicted to be fully protonated, $\equiv$P-OH; however, above pH 4 the phosphate sites begin to deprotonate affording a fraction of $\equiv$P-OH and $\equiv$P-O^- sites dependent upon the pH. Near pH $\cong$ 6.6 the surface speciation is predicted to be approximately 50% $\equiv$P-OH and 50% $\equiv$P-O^-. At a pH of ~7, $\equiv$Ca-OH_2^+ surface sites begin to deprotonate and pH $\cong$ 9.7 affords approximately 50% $\equiv$Ca-OH_2^+ and 50% $\equiv$Ca-OH (Wu et al. 1991). The complexities of surface speciation exhibit a pronounced effect on the sorption of aqueous metal ions. This is further confounded by complex hydrolysis and complexation reactions experienced by actinides in aqueous matrices.

The interaction of uranium with hydroxyapatite may be complicated by geochemical reactions occurring between hydroxyapatite and the aqueous matrix that will change during initial infiltration through long-term monitoring. Initially, during the injection of the polyphosphate remedy, aqueous geochemical conditions will be oversaturated with respect to the formation of hydroxyapatite. But as the amendment is dispersed and concentrations within the subsurface dissipate the system will become undersaturated with respect to hydroxyapatite. This shift in aqueous geochemistry could significantly influence the speciation within the aqueous media and the speciation of reactive surface sites for the sequestration and retention of uranium.

Quantitative removal and sequestration of uranium has not been considered previously in the context of dynamic aqueous uranium speciation and/or hydroxyapatite surface speciation as will be encountered during remediation within the 300 Area subsurface. To evaluate the effectiveness of an apatite barrier for immobilizing uranium under dynamic pH and geochemical conditions relevant to remediation of the 300 Area subsurface, it is necessary to understand the effects of aqueous uranium speciation and changes to the hydroxyapatite surface groups on: 1) the rate at which hydroxyapatite barrier immobilizes uranium, 2) the capacity of hydroxyapatite for immobilizing uranium, and 3) the long-term stability of uranium sequestered by hydroxyapatite.

3.3.1 Sorption Kinetics

Sorption of uranium by hydroxyapatite has been investigated previously in aqueous matrices similar in composition to Hanford groundwater (Thakur et al. 2005; Fuller et al. 2003; Fuller et al. 2002a; Fuller et al. 2002b). However, there is no information regarding the sequestration of uranium by hydroxyapatite in an aqueous medium that has been equilibrated with hydroxyapatite. Kinetics experiments were

conducted in apatite equilibrated groundwater to evaluate the rate of uranium uptake by hydroxyapatite. Figure 20 shows the dependence of uranium uptake expressed as aqueous uranium concentration and percent of sorption by hydroxyapatite under the pH range of 6 to 7.5. Because the hydroxyapatite solid phase was pre-equilibrated with the aqueous matrix, the apatite was in thermodynamic equilibrium with the aqueous matrix. This allowed the reaction between aqueous uranium and solid hydroxyapatite to be isolated from other geochemical reactions that could occur within the system. The rate of uranium sorption to hydroxyapatite was rapid and equilibrium was attained within the first two minutes of the reaction. It is evident that the extent of uranium uptake decreases significantly above pH 7.

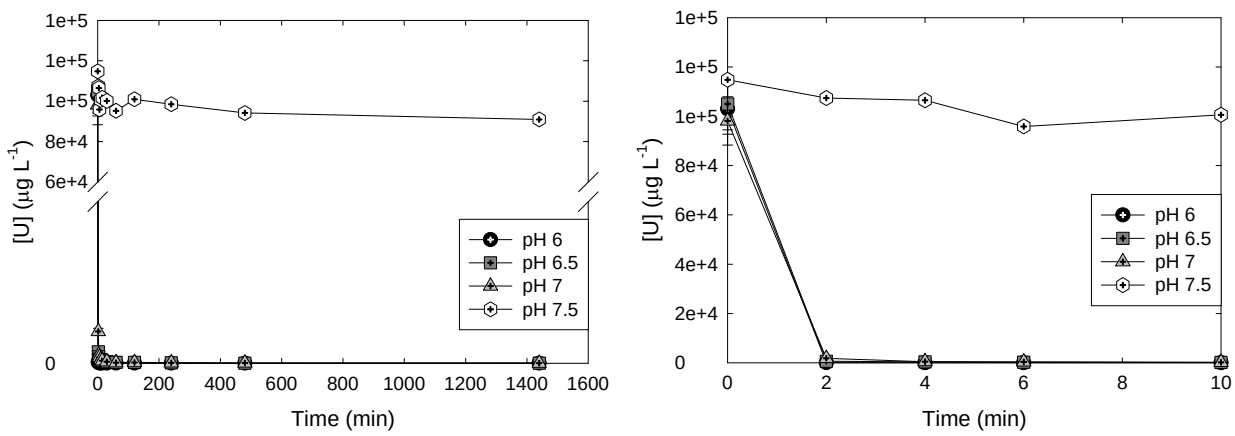

Figure 20. Rate of Aqueous Uranium Sorption on Hydroxyapatite in Apatite Equilibrated Water. The bottom figure is an expansion of the data collected for the first 10 minutes.

The thermodynamic geochemical code EQ3/6 version 8.0 (Wolery and Jarek 2003) was used to evaluate the aqueous speciation of uranium in solutions equilibrated with apatite over the pH range being investigated (6 to 7.5) (Table 11). It is important to note that because of the complex chemistry of uranium, there is significant debate within the literature regarding the stoichiometry and the thermodynamic values assigned to aqueous uranium species and secondary mineral phases. The model predictions are based on current knowledge, but may have significant uncertainty associated with them and are considered semi-quantitative. The table in Appendix A summarizes logK values for uranium species contained in the EQ3/6 version 8.0 database. Under the pH range of 6 to 7.5 the aqueous speciation of uranium changes from a predominantly $UO_2(CO_3)_2^{2-}$ to the more weakly charged species $(UO_2)_2(CO_3)(OH)_3^-$.

Coupling the predicted surface speciation, as discussed above, with the aqueous speciation, the sorption of uranium to hydroxyapatite can be explained by the dominance of the $\equiv Ca\text{-}OH_2^+$ surface complex sorbing anionic uranyl complexes over the pH range of 5 to approximately 7.5. However, the increase in $\equiv P\text{-}O^-$ surface sites from pH $\geq$7.5, inhibits the sorption of anionic uranyl complexes to the hydroxyapatite surface.

Table 11. Uranium Speciation in Sorption Experiments at 23°C Were Calculated Using the EQ3NR Code V8.0 Database. Aqueous calcium and phosphorus concentrations in equilibrium with hydroxyapatite.

pH	Uranium Species	% Composition
6	$UO_2(CO_3)_2^{2-}$	72.18
	$UO_2(CO_3)^{4-}$	18.08
	UO_2CO_3	3.25
	UO_2HPO_4	2.24
	$UO_2PO_4^-$	1.14
	$(UO_2)_3(CO_3)_6^{6-}$	2.10
	$(UO_2)_2(CO_3)(OH)_3^-$	9.42 H 10^{-1}
	Total	99.94
6.5	$UO_2(CO_3)_2^{2-}$	69.33
	$UO_2(CO_3)^{4-}$	18.29
	$(UO_2)_2(CO_3)(OH)_3^-$	8.05
	UO_2CO_3	2.20
	$UO_2PO_4^-$	7.03 H 10^{-1}
	UO_2HPO_4	4.52 H 10^{-1}
	Total	99.03
7	$UO_2(CO_3)_2^{2-}$	44.81
	$(UO_2)_2(CO_3)(OH)_3^-$	33.93
	$UO_2(CO_3)^{4-}$	15.10
	UO_2CO_3	1.04
	$UO_2(OH)_2$	5.88 H 10^{-1}
	Total	99.48
7.5	$(UO_2)_2(CO_3)(OH)_3^-$	64.77
	$UO_2(CO_3)_2^{2-}$	24.10
	$UO_2(CO_3)^{4-}$	9.50
	$UO_2(OH)_2$	1.13
	Total	99.50

3.3.2 Loading and Sorption Isotherms

Figure 21 shows the dependence of uranium sorption on hydroxyapatite as a function of the volume-to-mass ratio (*V:m*) in apatite-equilibrated groundwater. The loading of uranium on apatite is invariant as a function of pH under the range of 6 to 7 and increases linearly over the solution-to-solid ratio of 0 to 1,000. This reflects the abundance of available surface sites for sorption of uranium per gram of hydroxyapatite. At pH > 6 the mass of uranium that can be loaded onto hydroxyapatite reaches a maximum value given a solution-to-solid ratio of 1,000, ~100 mg uranium per gram of apatite. Once the aqueous uranyl species deplete the limited surface sites for sorption, a further increase in the *V:m* ratio does not affect the sorption for uranium. However, the amount of uranium that can be loaded onto apatite at pH 6 continued to increase linearly as a function of the solution-to-solid ratio in excess of 20,000. This

reflects the greater abundance of positively charged sites on the apatite surface available for sorption of anionic uranium species.

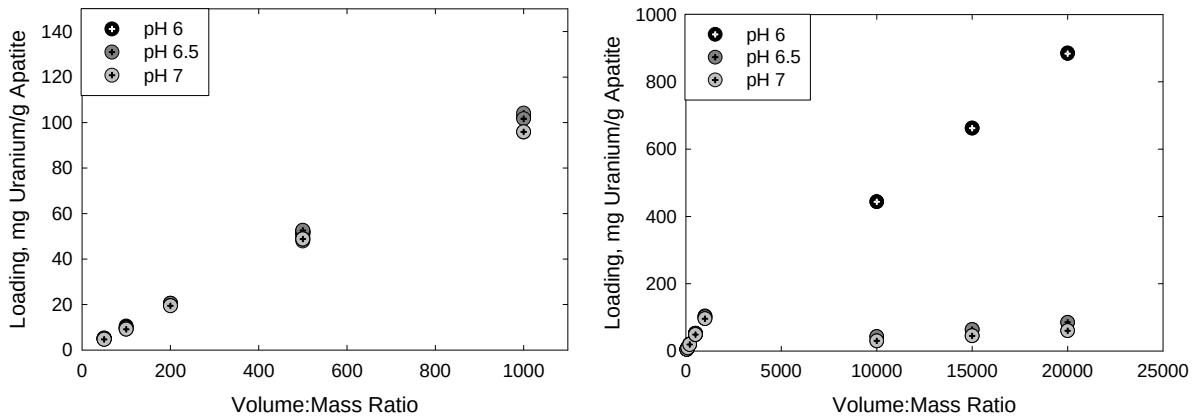

Figure 21. Sorption of Aqueous Uranium on Hydroxyapatite as a Function of the Solution-to-Solid Ratio under the pH Range of 6 to 7

3.3.3 Desorption of Uranium

Figure 22 illustrates the desorption of uranium, based on the total amount of uranium sorbed, from hydroxyapatite as a function of the cumulative volume of 1) apatite-equilibrated water and 2) Hanford groundwater. Desorption of uranium in apatite-equilibrated water exhibits an inverse relationship with increasing pH. After one month, ~10% of the sorbed uranium had been released at pH 6; whereas, at pH 8, <1% had been desorbed after one month. Conversely, the release of uranium in Hanford groundwater and deionized water matrices showed a direct relationship with increasing pH. The maximum uranium desorbed in Hanford groundwater was <1%. In addition, there was no quantifiable difference in the amount of uranium desorbed at pH 7.5 and 8, or over the pH range of 6 to 7. There was comparable desorption of uranium in apatite-equilibrated water and Hanford groundwater at pH 8, but increased desorption in apatite-equilibrated water at lower pH values. This is likely due to the increased concentration of aqueous calcium and phosphate in the apatite-equilibrated water. The high affinity of uranium for phosphate affords preferential reaction with aqueous phosphate over sorption with $\equiv Ca\text{-}OH_2^+$ surface sites.

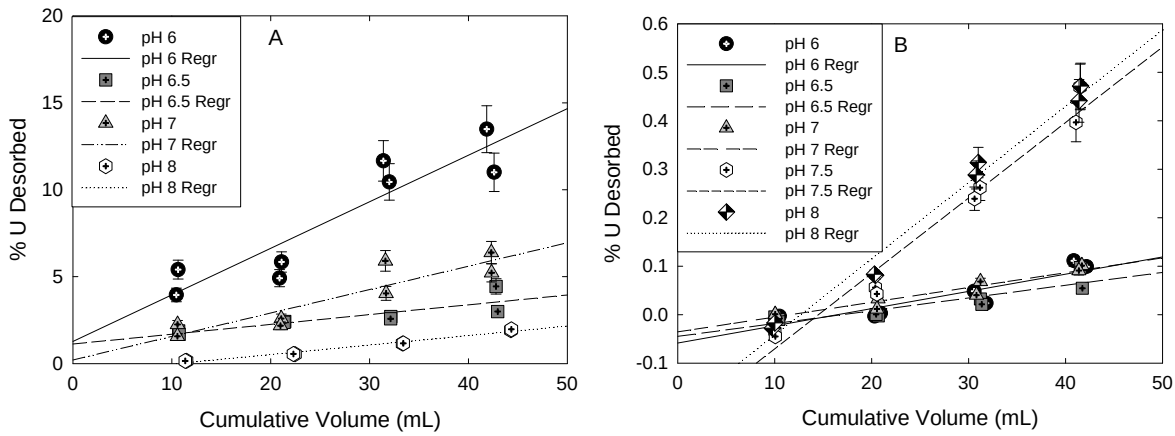

Figure 22. Percent Desorption of Uranyl from Hydroxyapatite as a Function of the Cumulative Volume of A) Apatite-Equilibrated Water and B) Hanford Groundwater

Thermodynamic geochemical modeling of aqueous solution from pH 7 apatite-equilibrated sorption-desorption testing suggests the formation of $(UO_2)_3(PO_4)_2 \bullet 4H_2O$, a precursor phase in the paragenetic sequence leading to autunite formation, with a saturation index (SI) of 1.67. The saturation indices continued to increase with decreasing pH, the saturation index at pH 6.5 = 2.91 and pH 6 = 3.68. The SI compares the ion activity product (Q) to the equilibrium constant (K) and can be expressed mathematically by

$$SI = \log_{10}\left(\frac{Q}{K}\right) \tag{15}$$

If $Q < K$ then $SI < 0$ and the solution is under saturated, if $Q > K$ then $SI > 0$ and the solution is super saturated, but if $Q = K$ then $SI = 0$ and the solution is in equilibrium (or near-saturated) with respect to a potential solid phase.

Results from thermodynamic modeling also suggest the formation of $(UO_2)_3(PO_4)_2 \bullet 4H_2O$ between the pH values of 4.75 and 7.25 with 10^{-6} M uranium and 10^{-4} M phosphate in systems devoid of sorbing solids (Payne et al. 1998). SEM analyses (Figure 23) of reacted solid phase material from pH 7 apatite equilibrated sorption-desorption testing clearly revealed the formation of a secondary precipitate on the apatite surface which did not possess a well defined morphology. Energy dispersive spectroscopy indicated the composition of the secondary phase was highly variable, 4 to 16 wt% calcium, 24 to 50 wt% uranium and 7 to 12 wt% phosphate. Thus, under test conditions that are supersaturated or near equilibrium with respect to hydroxyapatite, uranium will remain sequestered in stable uranium-phosphate solid phases. Additionally, under the predominant conditions of Hanford groundwater, the limited desorption suggests that hydroxyapatite will serve as an efficient agent for the quantitative sequestration of uranium under conditions relevant to the 300 Area subsurface.

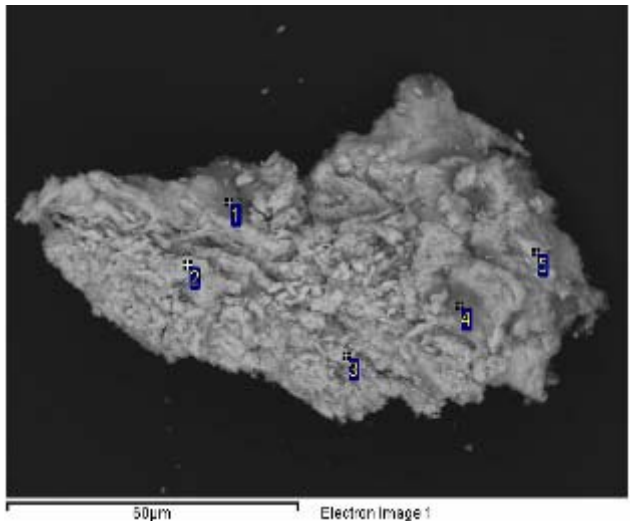

Spectrum	O	Na	Al	P	Ca	Cu	U	Total
1	47.717	0.805		11.899	16.003		23.576	100
2	32.031		0.259	8.470	5.800	0.465	52.976	100
3	39.003		0.252	7.634	4.749		48.361	100
4	38.778	0.765	0.156	11.88	15.03		33.389	100
5	34.351		0.282	8.274	6.311	0.511	50.272	100
Max.	47.717	0.805	0.282	11.899	16.003	0.511	52.976	
Min.	32.031	0.765	0.156	7.634	4.749	0.462	23.576	

All results in weight%.

Figure 23. A Scanning Electron Photomicrograph of Hydroxyapatite in Apatite-Equilibrated Water Reacted with 100 ppm Uranium at pH 7

3.3.4 Column Transport Experiments

Column experiments were conducted to quantify the efficacy of an in situ hydroxyapatite barrier on the retardation and retention of uranium. Sorption of uranium during transport, or retardation, R_{ef}, was calculated from the experimental BTC using moment analysis, which is based on the center-of-mass and area under the BTC (Valocchi 1984; 1985). Apparent K_d values, $K_{d\text{-}ap}$, were calculated from R_{ef}, as follows

$$K_{d-ap} = (R_{ef} - 1)\frac{\theta}{\rho_b} \tag{16}$$

where θ is the volumetric water content and ρ_b is the bulk density.

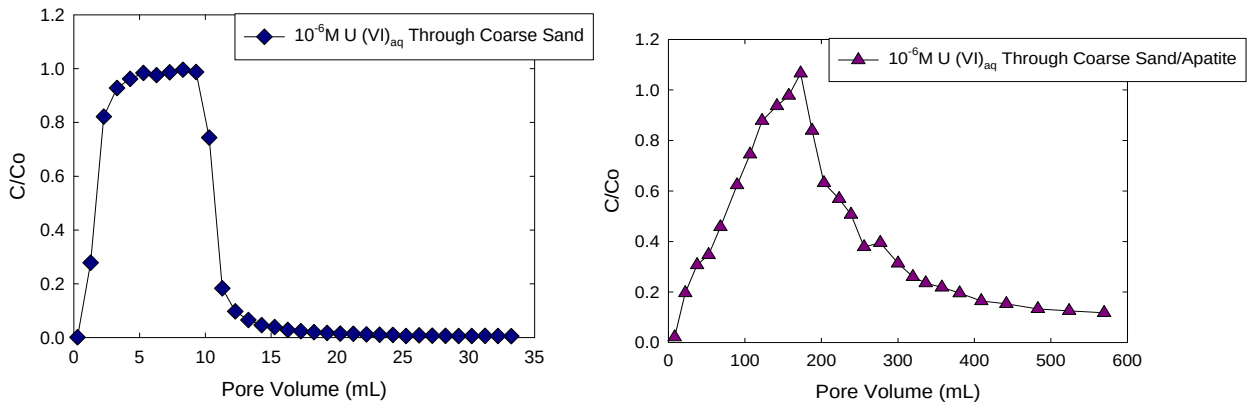

Figure 24. Experimental Migration of Uranium in Hydraulically Saturated Columns Through 300 Area Sediment (top) and Sediment Containing an Apatite Barrier (bottom)

The top graph in Figure 24 illustrates the migration of uranium and breakthrough under saturated conditions in the <2-mm fraction of sediment obtained from the 300 Area. Complete breakthrough occurred within the first five pore volumes. An effective retardation of 2.1 was calculated from moment analysis and afforded an apparent K_d of 0.29. Alternatively, complete breakthrough of uranium in a column containing a 5 wt% apatite barrier located in the center of the column did not occur until nearly 200 pore volumes had been displaced through the column (Figure 24, bottom). Approximately a 100-fold increase in sorption was observed, R_{ef} = 104.1 and $K_{d\text{-}ap}$ = 22.97.

3.4 Apatite Barrier Longevity

In dynamic systems the long-term stability of minerals is controlled by the solubility and the dissolution rate of the mineral. Under highly advective conditions where transport is greater than the solubility, the stability of the mineral is controlled by dissolution kinetics. Alternatively, in low to moderately advective environments where solubility is greater than transport and the long-term stability of the mineral is based on the solubility of the phase. The former conditions are relevant to the 300 Area saturated zone. As such, to quantify longevity of an apatite barrier and the performance of polyphosphate technology, it is necessary to determine the rate of apatite dissolution under conditions representative of the 300 Area aquifer.

3.4.1 Hydroxyapatite Single-Pass Flow-Through Dissolution Experiments

Although phosphate minerals are important in natural processes such as biomineralization, control of soil nutrients, and in industrial processes such as scale formation, phosphate mineral dissolution has not been investigated in detail. Until recently, the majority of the research has been conducted under conditions relevant to biology and focused on compositional analogues for skeletal apatite (Guidry and Mackenzie 2000). However, mineral composition and environmental conditions can control the mechanism and rate of dissolution. This is particularly noted for apatite minerals, such as fluorapatite [$Ca_5(PO_4)_3F$], hydroxyapatite [$Ca_5(PO_4)_3OH$], and carbonate apatite [$Ca_5(PO_4, CO_3)_3(OH, F)$], because significant cation and/or anion substitution can occur during the formation and long-term weathering of these phases. The environment within the 300 Area subsurface ranges from pH 6 to 7.5, contains 0.80 ppm carbonate, 21.0 ppm chloride, and 0.60 ppm fluoride. As such, all major apatite isomorphs of apatite, hydroxyapatite, fluorapatite, and chlorapatite [$Ca_{10}(PO_4)_6Cl_2$], have the potential to form with

varying degrees of cation and/or anion substitution. Given the potential number of phases, a conservative estimate of the longevity of an apatite barrier under representative dynamic conditions is limited by the dissolution rate of the least stabile apatite phase.

Guidry and Mackenzie (2003) previously quantified the dissolution of fluorapatite and carbonate fluorapatite as a function of pH (2 to 8.5) and temperature (23° to 55°C). Results of this investigation illustrated that the dissolution of fluorapatite and carbonate fluorapatite were highly dependent on pH, and that the dissolution of fluorapatite (ranging from 10^{-9} mol m^{-2} s^{-1} at pH 5 to 10^{-10} mol m^{-2} s^{-1} at pH 8) was faster than carbonate fluorapatite (ranging from 10^{-11} mol m^{-2} s^{-1} at pH 5 to $10^{-11.5}$ mol m^{-2} s^{-1} at pH 7). Although there are no known investigations regarding the dissolution rate of chlorapatite, the heat of dissolution for chlorapatite lies between that for fluorapatite and hydroxyapatite (Figure 25). A conservative estimate of the longevity of the apatite barrier should be limited by the formation and stability of the least stabile phase, hydroxyapatite.

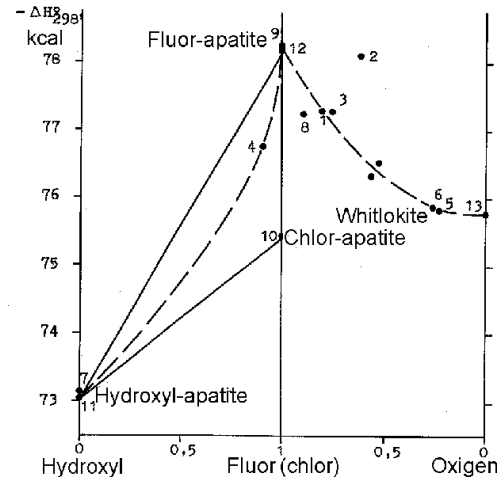

Figure 25. Heat of Dissolution for Fluor-, Chlor-, and Hydroxyapatite (Stolyarova 2003)

Results of numerous investigations of hydroxyapatite dissolution have provided valuable information regarding the mechanisms of hydroxyapatite corrosion as a function of relevant environmental variables, including temperature, pH, and solution species (Guidry and Mackenzie 2003; Dorozhkin 1997a; b; 2002; Guidry and Mackenzie 2000; Kohler et al. 2005; Misra 1991; de Leeuw 2004; Valsami-Jones et al. 1998; Schaad et al. 1997; Schaad et al. 1994; Christoffersen 1980; Christoffersen and Christoffersen 1982). Results of static dissolution studies identified the significance of surface processes during the dissolution of hydroxyapatite. Gramain et al. (1989; 1987) and Thomann et al. (1990) noted dissolution processes wherein limited mass transfer afforded the spontaneous formation at the solid interface of an adsorbed calcium-rich layer. Chistoffersen (1980) noted that under the pH range of $6.6 < pH < 7.2$ and $0.1 < C/C_s < 0.7$ where C is the stoichiometric concentration of hydroxyapatite, and C_S is the molar solubility of hydroxyapatite at the respective pH, the dissolution of hydroxyapatite is controlled by surface processes. Hydrogen ions catalyze the exchange of phosphate between the crystal surface and the solution (Christoffersen and Christoffersen 1982). Valsami-Jones et al. (1998) clarified the mechanism of dissolution and described two different surface groups: $\equiv Ca - OH_2^+$ and $\equiv P - O^-$, the latter of which is analogous to the $\equiv Si - O^-$ group found in silicates. Results of dissolution experiments conducted by Valsami-Jones et al. (1998) suggested deprotonation occurred at both sites, and within the pH range 5 to 7, $\equiv P - O^-$ was the significant site of deprotonation. In both instances, the charged species polarizes and weakens the phosphate bonds, $\equiv P\text{-}O^-$, ultimately leading to detachment of the phosphate molecule and subsequent degradation of the apatite structure. Results presented by Schaad et al. (1997) supported the significance of interfacial ionic exchange and calcium accumulation, which afford a pseudo-steady state dissolution of hydroxyapatite. Therefore, the long-term performance of an apatite barrier will be determined by the rate of dissolution of the least stable potential apatite phase to precipitate during polyphosphate remediation, hydroxyapatite, as well as the rate of mass transfer. Depending on the rate of dissolution and precipitation, mass transfer may limit the

degradation of an apatite barrier such that rapid reprecipitation of apatite will sustain the barrier beyond what would be possible if conditions were conducive to the forward rate of dissolution.

Figure 26 presents the release of calcium and phosphorus as a function of time over the pH range of 7 to 12, at a temperature of 40°C. The results are representative for dissolution experiments conducted under the pH range of 7 to 12 at temperatures ranging from 23°C to 90°C. The graphs illustrate that steady-state conditions are met for calcium and phosphorus under all temperatures investigated. The concentration of calcium (Figure 26, left) initially started out at low values and increased to steady-state values (concentrations invariant with time); whereas, the release of phosphorus (Figure 26, right) initiated at high values and rapidly decreased to steady-state values.

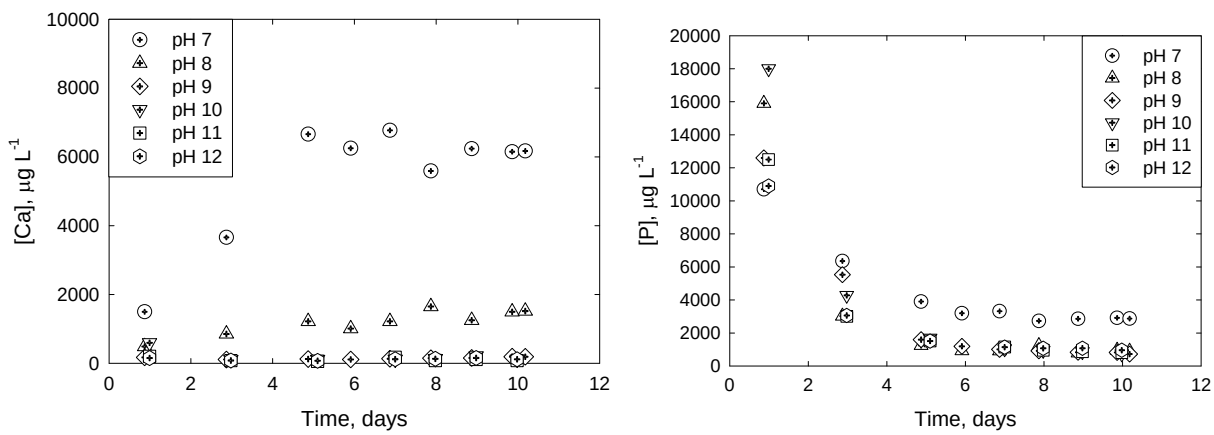

Figure 26. Aqueous Effluent Concentration of Calcium (left) and Phosphorus (right) as a Function of Reaction Time

The maximum dissolution rate for a given mineral is referred to as the forward rate of reaction or forward dissolution rate, which is typically attained by maximizing the ratio of flow rate to surface area, *q/S*. This minimizes the concentrations of elements released into solution and decreases the chemical affinity within the system. This effect is expressed mathematically as the chemical affinity of the following reaction:

$$ChemicalAffinity, A, = R\,T\ \ \ln\left(\frac{K}{Q}\right) = -\Delta G_r \tag{15}$$

where ΔG_r = the free energy of reaction
R = the gas constant
T = the temperature
K = the equilibrium constant
Q = the ion activity product.

In other words, the chemical affinity is a measure of the departure from equilibrium. Therefore, as the ion activity product, *Q*, approaches the value of the equilibrium constant, *K*, the chemical affinity term goes to zero, and the dissolution rate slows as the difference in chemical potential between the solid phase and the solution decreases. By increasing the flow rate or decreasing the surface area within the system, the value of *q/S* can be increased, which increases the difference in chemical potential between the solid

phase and the solution. This allows quantification of the maximum ratio of *q/S* necessary to attain the dissolution plateau, which is equated to the forward rate of dissolution (Nagy 1995). Accordingly, once the forward rate of reaction has been quantified, the effects of various environmental factors (e.g., effect of temperature, pH, and saturation state) on dissolution rate can be quantified independently by conducting experiments under the respective conditions to preclude dissolution rates from being influenced by solution saturation state.

Figure 27 illustrates the effect of varying the ratio of *q/S*. Dissolution rates based on the steady-state concentration of calcium (Figure 27, left) and phosphorus (Figure 27, right) are plotted for the conditions of 40°C, pH (23°C) = 9. At high *q/S* values (i.e., dilute conditions), the dissolution rate as indexed by calcium (Figure 27, left) appears to be independent of solution saturation state and at the maximum (or forward) rate of reaction [3.5 H 10^{-12} mol m^{-2} s^{-1} at $\log_{10}$ (*q/S*) = -10.10] (Aagaard and Helgeson 1982). However, the dissolution rate indexed by phosphorus is, within experimental error, invariant as a function of *q/S* (Figure 27, right), which could suggest that the solution saturation state was oversaturated with respect to secondary phases.

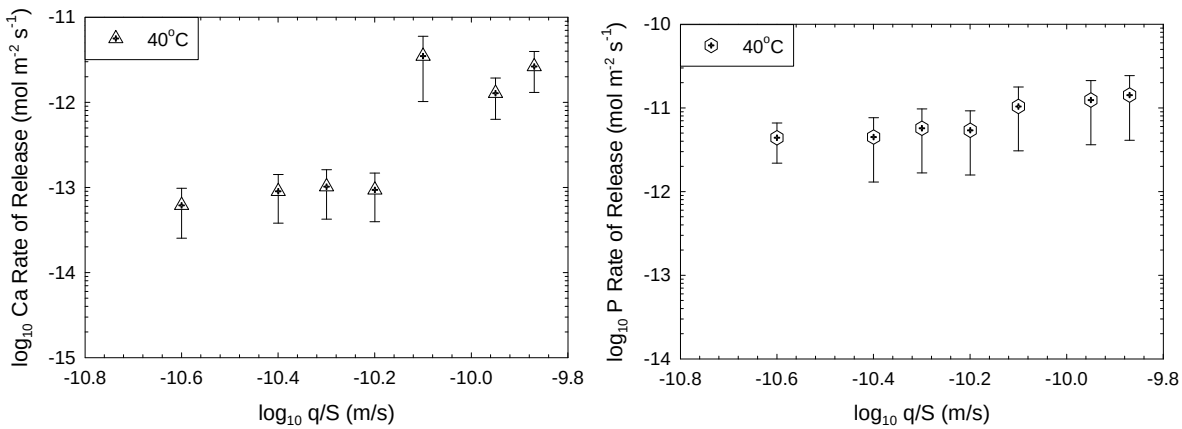

Figure 27. Effect of the Variation in *q/S* as Indexed by the Release of Calcium ($\log_{10}$) (left), and Phosphorus ($\log_{10}$) (right), from Hydroxyapatite

The dissolution profiles when indexed based on the release of calcium ($\log_{10}$) (Figure 28, left) exhibited a negative pH dependence (η = -0.36) and no dependence on temperature. The apparent dissolution rate as indexed by the release of phosphorus ($\log_{10}$) from hydroxyapatite displayed a similar negative dependence on pH over the pH range of 5 to 7. Under pH values greater than 7, within experimental error, there was no measurable dependence on pH or temperature (Figure 28, right).

Figure 29 displays the average ratio of calcium to phosphorus as a function of pH as measured in the effluent solutions during dissolution. Within experimental error, the ratio of calcium to phosphorus is stoichiometric at pH 6 and 8. However, the ratio of Ca:P at pH 7 is 1.97. The presence of more calcium than phosphorus into solution suggests either 1) formation of a calcium-rich surface layer is inhibiting the release of phosphorus or 2) the aqueous concentration of phosphorus is being controlled by secondary phase precipitation.

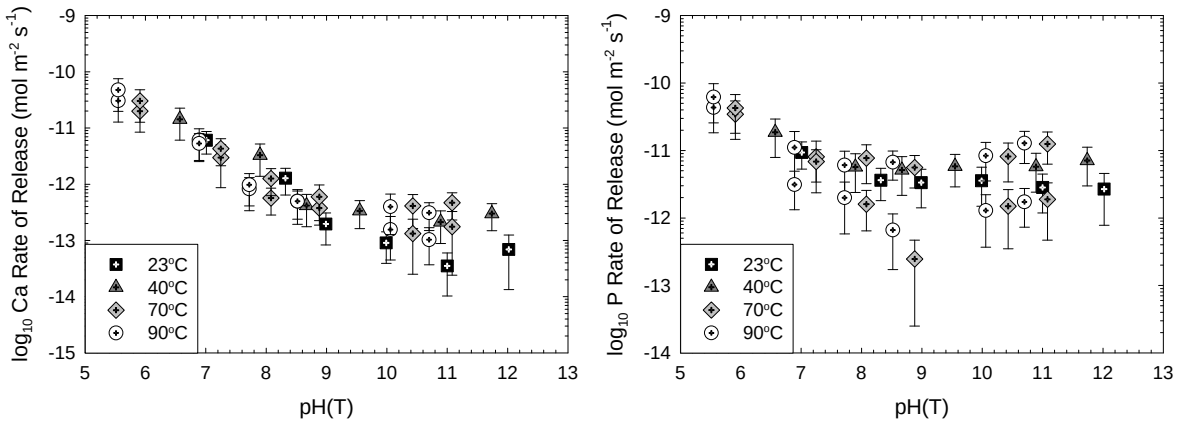

Figure 28. Rate of Hydroxyapatite Dissolution as Indexed by the Release of Calcium (log_{10}) (left) and Phosphorus (log_{10}) (right) as a Function of Temperature-Corrected pH

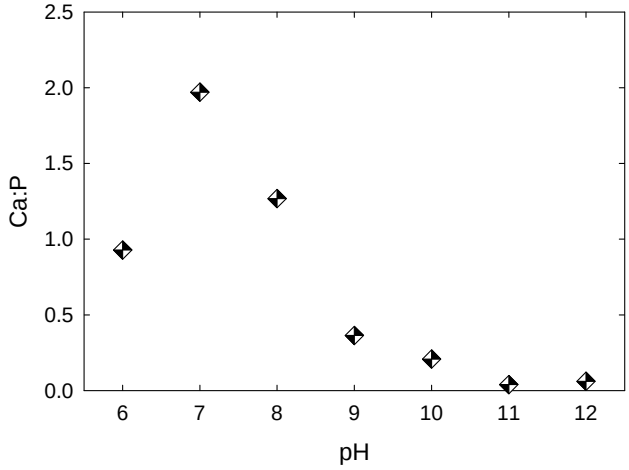

Figure 29. The Ca:P ratio as a Function of pH as Measured in Effluent Samples During Dissolution Testing

Geochemist's Workbench®, version 3.2.2, (Bethke 1992) was used to predict the solid-phase stability based on the concentrations of calcium and phosphorus in the effluent solution. Figure 30 indicates that, given the concentration of calcium and phosphorus in solution, the system is undersaturated with respect to any calcium-phosphate solid phases. Similar analyses for conditions at 23°, 70°, and 90°C were conducted and yielded comparable results. This suggests quantification of the dissolution rate of hydroxyapatite is not confounded by the formation of calcium-phosphate solid phases. However, geochemical modeling of solution concentrations to predict solid-phase saturation implies the formation of secondary solid phases is via homogeneous precipitation from solution. This neglects the potential catalytic effects afforded by interactions with the dissolving solid phase, such as heterogeneous nucleation, topotaxy, and epitaxy, all of which have been shown to play a significant role in the formation of silicate minerals during dissolution (Nagy 1995; Putnis and Putnis 2007) and phosphate phase formation (Harlov et al. 2002; Yanagisawa et al. 1999; Renden-Angeles et al. 2000; Manecki et al. 2000).

Although, hydroxyapatite is frequently the most thermodynamically stable solid phase predicted to control the activities of calcium and phosphate (Lindsay 1979; Lindsay and Moreno 1960), natural waters remain oversaturated with respect to hydroxyapatite due to the exceedingly slow rate of hydroxyapatite precipitation (Inskeep and Silvertooth 1988). Numerous investigations regarding the precipitation of hydroxyapatite have demonstrated the efficacy of seed crystal precipitation for the formation of hydroxyapatite (Brown 1981a; Ferguson et al. 1970; Inskeep and Silvertooth 1988; van Cappellen and Berner 1991; Nancollas et al. 1979; Nancollas and Tomazic 1974; Tomazic and Nancollas 1975; Moreno and Varughese 1981; Koutsoukos et al. 1980; Aoba and Moreno 1985; Boskey and Posner 1976; Kato

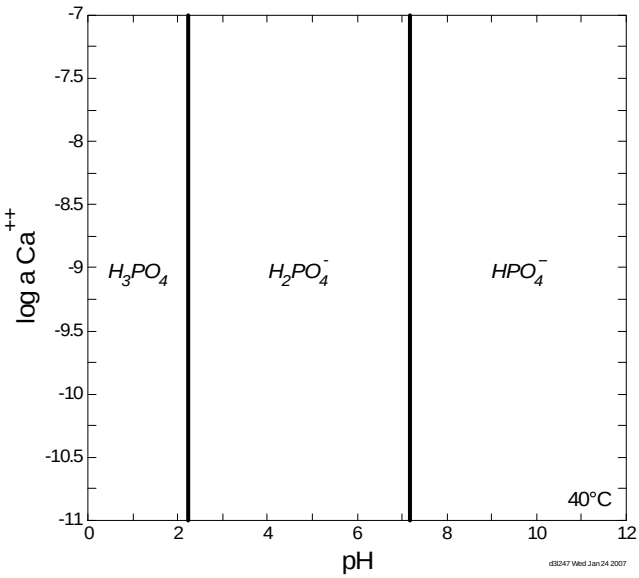

Figure 30. Predicted Saturation State Based on Effluent Solution Concentrations for the Dissolution of Hydroxyapatite in 0.05 M THAM at 40°C

et al. 1997; Amjad et al. 1981). The presence of seed crystals limits spontaneous nucleation of amorphous precursor phases (i.e., dicalcium phosphate dehydrate and octacalcium-phosphate) (Grossl and Inskeep 1992). As such, precipitation of hydroxyapatite can occur under conditions at low saturations with respect to hydroxyapatite (Koutsoukos et al. 1980; Moreno and Varughese 1981; Aoba and Moreno 1985; Boskey and Posner 1973; Kato et al. 1997).

Figure 31 illustrates the saturation state of calcium-phosphate minerals during the reaction of hydroxyapatite at 40°C. The input concentration of phosphorus and calcium were set to values measured in effluent solution samples, as discussed above. In contrast to results of geochemical modeling of solution chemistry, the presence of hydroxyapatite crystals significantly decreases the aqueous concentration of calcium and phosphorus necessary to promote precipitation of hydroxyapatite. Additionally, the system is saturated with respect to the thermodynamically less stable calcium-phosphate phase whitlockite [$Ca_9(Mg,Fe^{2+})(PO_4)_6(PO_3OH)$] , which is frequently a precursor to the formation of hydroxyapatite.

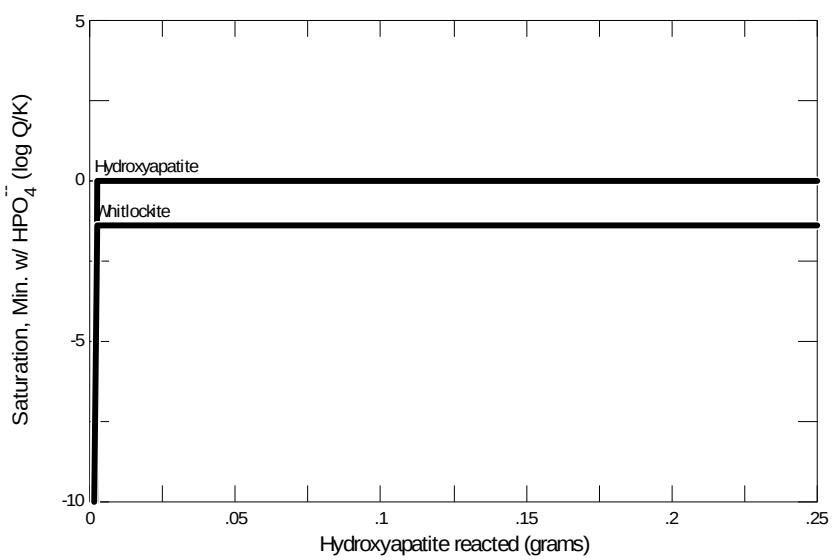

Figure 31. Predicted Phosphorus Mineral Saturation Indices Based on the Reaction of Hydroxyapatite at 40°C, pH 8

Scanning electron microscopy conducted on hydroxyapatite following dissolution testing (T = 40°C, pH 8) clearly illustrates precipitation on the surface of the reacted starting phase (Figure 32). The fact that XRD of the reacted material does not reveal any reflections other than those attributable to hydroxyapatite suggests that during the dissolution of hydroxyapatite, the dissolving surface also acts as a nucleating surface for the precipitation of hydroxyapatite. Comparable results were observed during the analysis of reacted hydroxyapatite from all temperature and pH values investigated. Thus, given the average flow rate within the 300 Area aquifer, the performance of an apatite barrier may be sustained beyond that predicted based on solubility or dissolution kinetics.

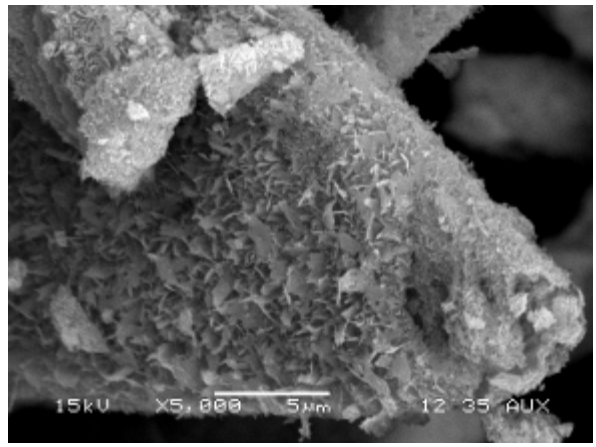

Figure 32. Scanning Electron Photomicrograph of Hydroxyapatite Reacted at 40°C, pH = 8, Illustrating the Re-Precipitation of Hydroxyapatite on the Surface of the Starting Material

At pH values > 9 the ratio of Ca:P is less than one (Figure 29), suggesting that secondary precipitation of calcium-rich secondary phases may be controlling the aqueous concentration of calcium. Figure 33 displays the saturation state with respect to calcium-bearing phases during the dissolution of hydroxyapatite at 40°C. In addition to the calcium-phosphate phases, saturation indices for lime, portlandite, and calcium hydroxide are exceeded under the test conditions. Rapid precipitation and dissolution of these phases, which are more soluble than hydroxyapatite, may influence the apparent dissolution rate such that a plot to evaluate the forward rate of dissolution appears to have attained the maximum rate of dissolution when, in fact, the system is being strongly influenced by rapid precipitation/dissolution of secondary solid phases (Figure 27). No evidence of these phases was observed during SEM analyses. However, formation of secondary phases typically proceeds through initial formation of an amorphous phase. This precludes identification via XRD and, depending on the rate of reaction, may not be visible using SEM due to rapid redissolution or transformation to more stable crystalline phases. The only distinct crystalline phase, aside from the starting material, was hydroxyapatite in post-test material.

3.4.2 Column Experiments

A column experiment was conducted to evaluate the stability of an in situ hydroxyapatite barrier. Figure 34 displays the release of calcium and phosphorus in Hanford groundwater at 23°C. The apparent release rate as indexed by the release of calcium and phosphorus ($\log_{10}$) from hydroxyapatite indicates rapid attainment of steady state. Unlike results obtained by SPFT testing, wherein the calculated release rates for calcium and phosphorus were within experimental error, the release of calcium (1.42 H 10^{-11} mol m^{-2} sec^{-1}) from the sedimentary column experiment was approximately 1,000 times faster than that measured for phosphorus (7.14 H 10^{-14} mol m^{-2} sec^{-1}). Moreover, the release of calcium measured here was within experimental error of that quantified by SPFT testing; however, the release of phosphorus was approximately two orders of magnitude lower than SPFT results. It has been previously noted that the

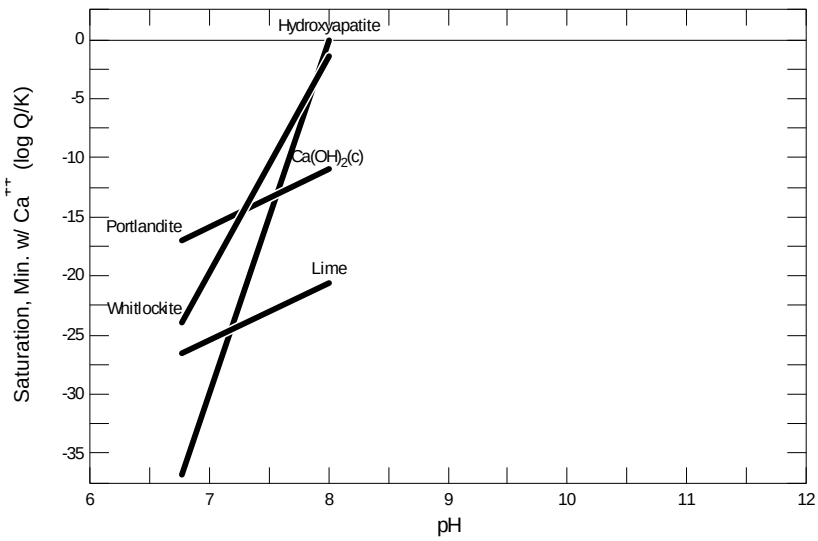

Figure 33. Predicted Calcium Mineral Saturation Indices Based on the Reaction of Hydroxyapatite at 40°C

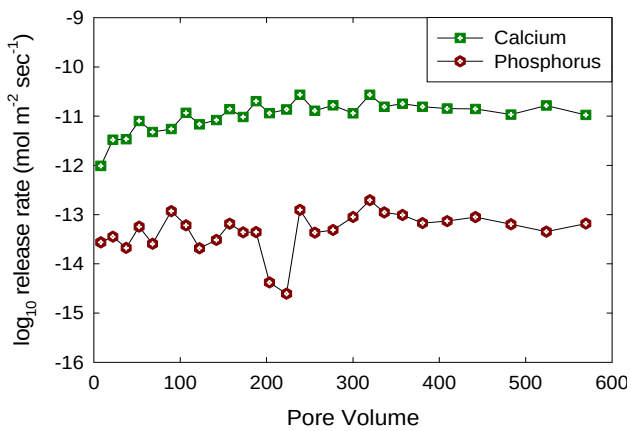

Figure 34. Experimental Release of Calcium and Phosphorus from 300 Area Sediment Containing a 5-wt% Hydroxyapatite Barrier

evolution of the hydroxyapatite surface is responsible for attainment of pseudo-steady state rather than true steady state, which affords decreased rates of dissolution as indexed by phosphorus were due to the formation of a semi-permeable layer of interfacial calcium accumulation (Gramin et al. 1989; Gramin et al. 1987; Thomann et al. 1990). Moreover, thermodynamic equilibrium of hydroxyapatite may be reached under non-stoichiometric conditions (Schaad et al. 1997). In summary, it is likely that dissolution/reprecipitation reactions will sustain an in situ apatite barrier providing a long-term sorbent for uranium and source of phosphate for the formation of uranium-phosphate phases under the geochemical and hydraulic conditions present within the 300 Area an apatite barrier.

3.5 Effect of pH and Temperature on the Dissolution Kinetics of Meta-Autunite Minerals, $(Na, Ca)_{2-1}[(UO_2)(PO_4)]_2 \cdot 3H_2O$

Uranyl phosphate phases are advanced secondary uranium minerals formed during the oxidized weathering of primary UO_2 deposits (Garrels and Christ 1965). The general paragenetic sequence of secondary mineral formation has been well-documented (Finch and Murakami 1999); however, uranyl silicates and phosphates are typically the solubility-limiting minerals that persist in locales geographically removed from the primary deposit (Murakami et al. 1997). The presence of phosphate in groundwater,

even in minor concentrations (10^{-8} M), promotes the formation of autunite group minerals $X_{3-n}^{(n)^+}$ $[(UO_2)(PO_4)]_2 \cdot xH_2O$; thereby, limiting the mobility of the uranyl cation (UO_2^{2+}) in subsurface environments.

In addition to natural settings, operations related to nuclear energy and weapons production have resulted in widespread uranium contamination of geologic media in surface and subsurface environments (Abdelouas et al. 1999). Within the United States, uranium has been recognized as one of the two most frequently occurring radionuclides in groundwater, and it is the most frequently occurring radionuclide in soils/sediments at DOE facilities (Riley et al. 1992). Characterization of sediments from contaminated sites has identified discrete uranyl-phosphate minerals, autunite, (Buck et al. 1996; Buck et al. 1995; Buck et al. 1994; Bertsch et al. 1994; Morris et al. 1996; Tidwell et al. 1996) for which autunite solubility has been suggested to be the dominant control on uranium concentration in the underlying aquifer (Elless and Lee 1998).

Previous experimental results have established the low solubility of many uranyl-phosphate minerals (Moskvin et al. 1967; Vesely et al. 1965; Chukhlantsev and Stepanov 1956; Scheyer and Baes 1954; Karpov 1961). However, knowledge of the stability of the uranyl-phosphate phases is restricted to a narrow range of experimental conditions involving low pH media with high concentrations of phosphoric acid (Scheyer and Baes 1954; Vesely et al. 1965; Karpov 1961). Further, all known studies related to autunite stability and solubility are based on synthetic, rather than natural, phases (Giammar 2001; Sowder et al. 2000; Vesely et al. 1965; Pekarek and Vesely 1965; Scheyer and Baes 1954; Karpov 1961), and interpretations of dissolution studies have been confounded by impurities present within the starting material (Giammar 2001).

Figure 35a illustrates the release rate of uranium from Na-autunite, across the pH range 7 to 10 and the temperature range of 5° to 70°C. Release rates of uranium increase by ~100-fold over the pH interval of 7 to 10. Under the temperature range of 5° to 40°C the increase in rate as a function of pH is constant, and is quantified as the power law coefficient, $\eta = 0.91 \pm 0.08$. The constant value of the slope over the temperature interval indicates that the power law coefficient, η, is independent of temperature. However, the constant release of uranium as a function of pH deviates at the higher pH values of 9 and 10 at 70°C. This suggests the formation of a secondary phase(s), which would result in slower release of uranium at conditions of high pH and temperature.

Geochemical modeling suggests that experiments with Na-autunite are under-saturated with respect to all possible secondary phases over the pH range of 7 to 10 from 5° to 40°C. However, at 70°C the system becomes saturated with respect to schoepite, β - $UO_2(OH)_2$, α - $UO_3 \cdot 9H_2O$, at pH 9 and 10, and, additionally, clarkeite (sodium uranyl oxy-hydroxide) at pH 10. These results support the validity of autunite dissolution rates obtained over the temperature interval 5° to 40°C. However, the results at 70°C indicate that the concentration of uranium is not due solely to dissolution of Na-autunite; secondary phases control net uranium concentrations.

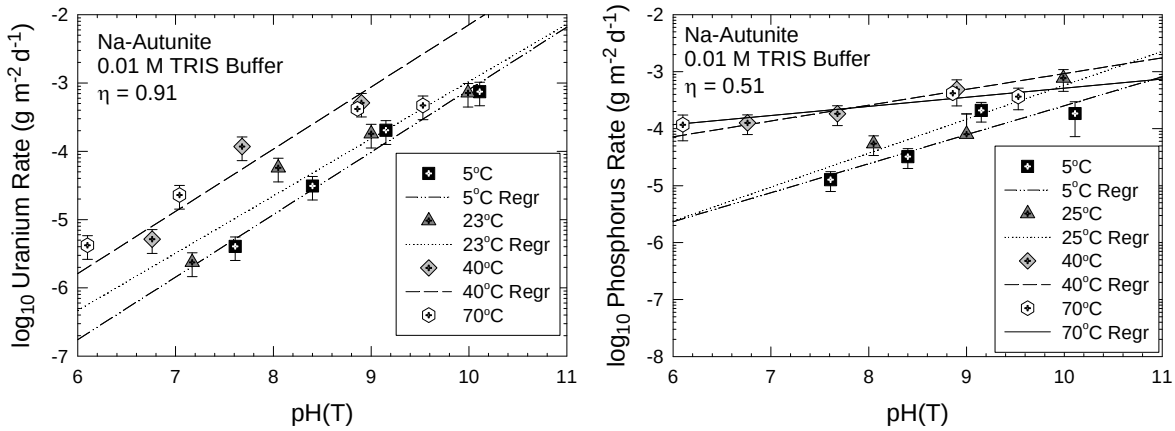

Figure 35. A) $\log_{10}$ Uranium Release Rate as a Function of Temperature-Corrected pH for Na-Autunite in 0.01 M THAM solution, and B) $\log_{10}$ Uranium Release Rate as a Function of Temperature-Corrected pH for GHR in 0.01 M THAM Solution

Figure 35b depicts the release rate of phosphorus across the pH range 7 to 10 over the temperature range of 5° to 70°C. The release of phosphorus is less dependent on pH ($\eta = 0.51 \pm 0.17$), than observed for uranium ($\eta = 0.91 \pm 0.08$); yet, the rate of phosphorus release is faster by approximately 30 times. Release of phosphorus follows the same pH- and temperature-dependent patterns exhibited by uranium. Over the temperature range of 5° to 40°C the increase in rate as a function of pH is constant; however, at 70°C, the slope of the line decreases. Yet, geochemical modeling did not suggest saturation with respect to any phosphorus-bearing phases. This suggests that dissolution of the autunite structure is dependent on initial removal of uranium from the uranium-phosphate sheet.

The pH dependence for uranium release, $\eta = 0.88 \pm 0.04$, measured across the pH range 7 to 10 from 5° to 40°C from GHR was identical within error to the release of uranium from Na-autunite, $\eta = 0.91 \pm 0.08$ (Figure 35a and Figure 36a). An inflection in pH dependence was again observed at 70°C, suggesting saturation limits with respect to secondary uranyl minerals may also be controlling the release of uranium in GHR tests.

Table 12 summarizes the geochemical modeling results based on steady-state effluent concentrations for GHR. The presence of calcium has a noticeable effect on the chemical affinity of the system. At pH = 10, the system becomes saturated with respect to $CaUO_4$ across the temperature range investigated. At the two highest temperatures investigated, 40° and 70°C, the system becomes saturated with respect to $CaUO_4$ at pH = 9. The pattern of element release rates, coupled with geochemical modeling results, explain the convergence of apparent uranium release rates to a common value, $3.57 \cdot 10^{-4}$ g · m-^{2} d^{-1} at pH = 10, across the investigated temperature range. Results at 70°C indicate the system also becomes saturated with respect to schoepite, β - $UO_2(OH)_2$, and α - $UO_3 \cdot 0.9H_2O$ at pH 10, which is similar to that predicted for Na-autunite. Thus, uranium dissolution data from 5° to 40°C are representative of the dissolution of GHR. However, uranium release rates at 70°C are subject to solubility limits for secondary minerals, and cannot be attributed solely to dissolution of GHR.

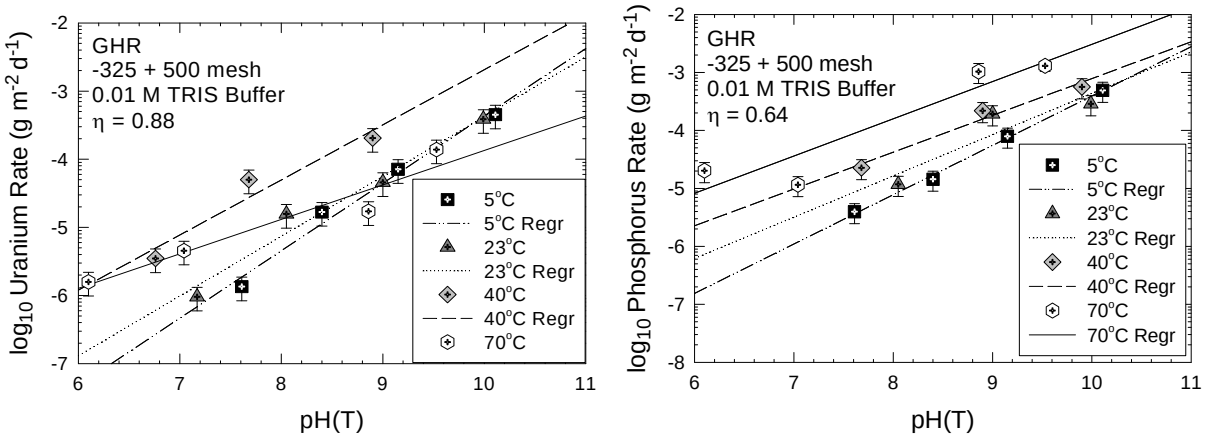

Figure 36. A) $\log_{10}$ Phosphorus Release Rate as a Function of Temperature-Corrected pH for Na-Autunite in 0.01 M THAM Solution, and B) $\log_{10}$ Phosphorus Release Rate as a Function of Temperature-Corrected pH GHR in 0.01 M THAM Solution

Table 12. Mineral Saturation Indices Based on Effluent Solution Compositions from Dissolution of GHR in 0.01 M THAM Buffer

Temp., °C	pH	Mineral Saturation Indices					
		Schoepite	β - $UO_2(OH)_2$	α - $UO_3 \cdot 9H_2O$	$CaUO_4$	Hydroxyapatite	Whitlockite
5	7-9	Undersaturated with respect to all potential secondary minerals					
	10				2.608	4.151	-0.238
23	7-9	Undersaturated with respect to all potential secondary minerals					
	10				3.696	4.648	0.096
40	7-8	Undersaturated with respect to all potential secondary minerals					
	9				1.094		
	10				4.517	6.228	1.079
70	7-8	Undersaturated with respect to all potential secondary minerals					
	9				2.756	3.134	-0.187
	10	-0.122	-0.067	-0.229	4.984	8.245	2.640

Phosphorus release rates from GHR are shown in Figure 36b. In accordance with phosphorus release from Na-autunite, the pH-dependent release of phosphorus was less than that quantified for uranium, 0.64 ± 0.04 versus 0.88 ± 0.03, respectively. However, release of phosphorus from GHR exhibits no deviation in phosphorus release with increasing temperature and pH, which is contrary to the pattern of phosphorus release displayed by Na-autunite (c.f. pH 9 and 10 at 70°C). This suggests secondary mineral solubility may be influencing the apparent phosphorus concentrations. Geochemical modeling results suggest that the system exceeds the saturation index for hydroxylapatite at pH 10 under all temperatures investigated. Thus, the apparent release of phosphorus at all temperatures and high pH is not solely attributable to the dissolution of GHR under these conditions.

3.5.1 Interlayer Cation Release Rates

Contrary to uranium and phosphorus release rates, which were shown to increase as a function of pH and also with increasing temperature (Figure 35), release of sodium is shown here to be independent of pH and temperature. Release of sodium is ~9,800 times faster than uranium at the lower pH values of 7 and 8. As pH increases, the difference in the release rate of sodium relative to uranium is significantly less; sodium release is only ~7 times greater than uranium at pH 10. Moreover, release rates for calcium from GHR display similar characteristics to sodium release from Na-autunite, in that both are independent of temperature and pH (Figure 37). Comparing release of calcium from GHR to sodium release from Na-autunite illustrates that the rates are identical within experimental error (Figure 37).

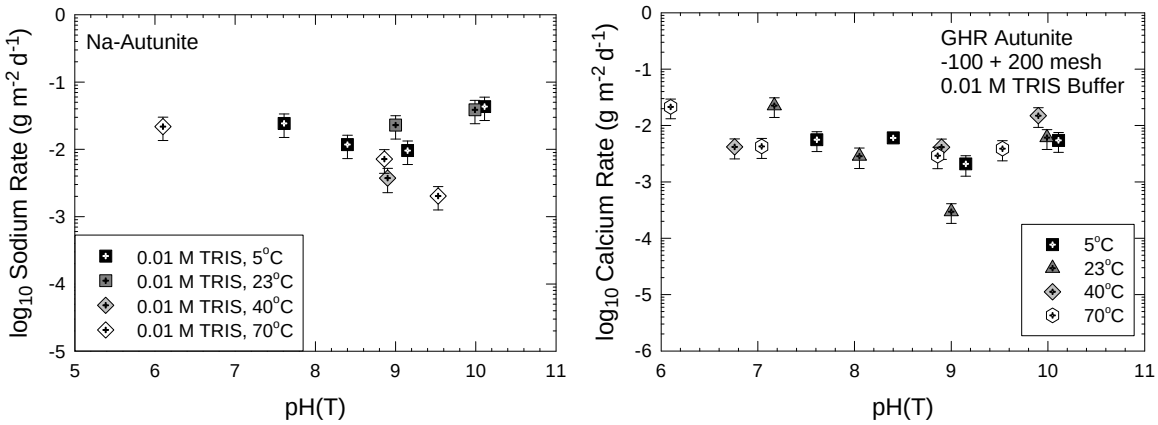

Figure 37. A) $\log_{10}$ Sodium Release Rate as a Function of Temperature-Corrected pH for Na-Autunite in 0.01 M THAM solution, and B) $\log_{10}$ Calcium Release Rate as a Function of Temperature-Corrected pH for GHR in 0.01 M THAM Solution

Release of interlayer cations (i.e., Na^+ or Ca^{2+}) from minerals is generally subject to two separate reactions: matrix dissolution and alkali-hydrogen exchange. Based on the saturation state of the system, one or both of these mechanisms may contribute to release of interlayer cations from the structure. For example, when the system is near saturation, the activities of dissolved species near and/or in contact with the solid phase increase, thereby resulting in a decrease in the matrix dissolution rate. Concurrently, the chemical potential difference between autunite and solution will be the driving force for cation diffusion. Concentrations of both Na^+ and Ca^{2+} appear to be constant across the range of pH values, but this is misleading. Dissolution of the autunite matrix will also contribute to the concentration of dissolved cations in solution; therefore, two distinct mechanisms, ion exchange and matrix dissolution, account for Na^+ or Ca^{2+} release.

3.5.2 Structural Dissolution

SPFT experiments suggested the dissolution of autunite occurs via attack and removal of the uranium polyhedra. To provide a more thorough understanding of the autunite dissolution mechanism, select SPFT experiments were conducted at 40°C in D_2O-based solutions. The test solution was a 0.1 M

deuterated ammonium hydroxide (ND_4OD) solution. The pD of the solution was adjusted using deuterated hydrochloric acid (DCl). The pH and pD scales are related through the following equation:

$$pD = pH + 0.4 \tag{16}$$

Steady-state release rates in H_2O and D_2O-based solutions are listed in (Figure 37). Uranium release rates from both autunite minerals are approximately an order of magnitude slower in D_2O than quantified in H_2O. In contrast, phosphorus rates are statistically within error between H_2O and D_2O-based solutions.

Table 13. Release Rates from Autunite Samples in H_2O and D_2O at pH(D) = 8, T = 40°C

Autunite	Solution Composition	U Release Rate ($g \cdot m^{-2}\ d^{-1}$)	P Release Rate ($g \cdot m^{-2}\ d^{-1}$)	Na/Ca Release Rate ($g \cdot m^{-2}\ d^{-1}$)
Na-Autunite $[Na_2(UO_2)_2(PO_4)_2 \cdot 3H_2O]$	H_2O	2.3 H 10^{-6} (±2.1 H 10^{-5})	1.41 H 10^{-5} (±7.3 H 10^{-6})	9.4 H 10^{-3} (±4.4 H 10^{-3})
	D_2O	8.3 H 10^{-8} (±2.2 H 10^{-8})	3.8 H 10^{-5} (±7.3 H 10^{-6})	3.2 H 10^{-3} (±5.6 H 10^{-4})
GHRI $[Ca(UO_2)_2(PO_4)_2 \cdot 3H_2O]$	H_2O	2.7 H 10^{-7} (±4.5 H 10^{-8})	2.8 H 10^{-5} (±1.8 H 10^{-5})	2.8 H 10^{-3} (±1.1 H 10^{-3})
	D_2O	7.2 H 10^{-8} (±2.7 H 10^{-8})	5.3 H 10^{-6} (±2.0 H 10^{-6})	1.8 H 10^{-3} (±7.0 H 10^{-4})

The decrease in uranium release rates with no effect on phosphorus release rates supports the hypothesis that the dissolution of autunite minerals is controlled by a surface-mediated reaction with the uranium polyhedra. The mean bond enthalpy of H_2O is 463.5 kJ mol^{-1} compared to 470.9 kJ mol^{-1} for D_2O reflecting the greater strength of the D_2O bond compared to H_2O. The observed decrease in the release rate of uranium in D_2O reflects a surface complex that requires the breakage of an O-H (O-D) bond. Thus, the slower reaction rates in D_2O are contributed to by a rate-limiting step in the hydrolysis of uranium within the autunite sheet.

Release rates of interlayer cationic elements show no dependence on the identity of the cation or variation in release rate based on the solution media (i.e., H_2O versus D_2O). This is significant because if the rates of release were governed solely by ion exchange with H^+ or H_3O^+ an isotopic effect would be detectable and proportional to the square root of the ratio of the masses of the isotopic atoms, $\sqrt{\frac{H}{D}}$ = 0.71. Thus, a 71% difference in the release would be detected in the results.

Experiments conducted in D_2O-based buffer solutions exhibited a decrease in uranium release rates by approximately an order of magnitude, relative to rates calculated in H_2O-based buffer solutions, while phosphorus rates were consistent between buffer systems. This supports a proposed mechanism in which autunite dissolution proceeds via attack at the uranium polyhedral units by •OH, rather than at the phosphate tetrahedra.

The autunite structure is characterized by perfect (*001*) basal cleavage with relatively weak forces holding successive sheets together, thereby increasing the probability that dissolution of the autunite mineral could occur through structural attack by water molecules along cleavage planes. Separation of the autunite sheets during dissolution would readily release the interlayer cations into solution. Na-autunite material used in dissolution experiments did not exhibit any cleavage planes prior to dissolution. However, SEM analyses of reacted Na-autunite revealed the formation of cleavage planes during the dissolution process (Figure 38). This supports the proposed hypothesis that dissolution occurs through attack of the crystal from the edges and along the cleavage planes. Additionally, this affords a significant contribution to the release of interlayer cations. Thus, interlayer cation release behavior is a combination of structural dissolution and ion exchange, but imparts no effect on the overall stability of autunite.

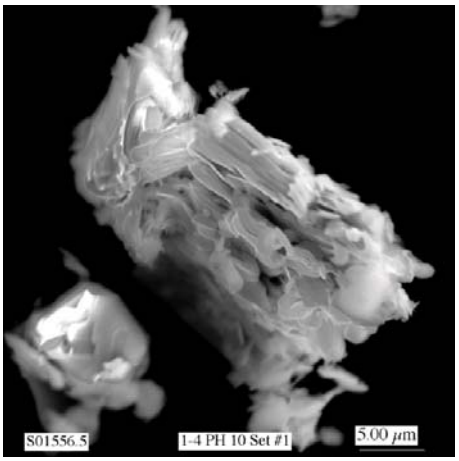

Figure 38. A SEM Photomicrograph of Reacted Na-Autunite Illustrating Basal Cleavage of the Autunite Plates from Attack During Dissolution

3.6 Polyphosphate Amendment

Based on the results of column transport experiments, a three-phase injection strategy was identified as an effective approach to obtain both direct treatment of the uranium contamination in groundwater (i.e., autunite formation) and secondary formation of calcium-phosphate. This will provide the long-term treatment capacity within the amended zone to address uranium solubilized and released from the deep vadose zone and capillary fringe during future high water table conditions. The three-part injection strategy consists of the following:

- Initial polyphosphate amendment injection to precipitate aqueous uranium within the treatment zone as autunite. This will prevent the formation of soluble calcium-uranate, which may redissolve, thereby releasing a pulse of uranium into the groundwater upon injection of the soluble polyphosphate.

- The initial polyphosphate injection will be directly followed by injection of a calcium-chloride ($CaCl_2$) solution to provide a sufficient calcium source for apatite formation during a subsequent polyphosphate injection. Due to the higher K_d of the $CaCl_2$ solution as measured on site-specific sediments, a larger injection volume will be required to reach the full radial extent of the targeted treatment zone for this component of the amendment formulation. However, this same increased retardation will help to facilitate mixing between the calcium and polyphosphate amendments during the third and final injection phase.

- The $CaCl_2$ injections will be directly followed by a final polyphosphate injection. This will provide additional time-released phosphorus for lateral precipitation of calcium-phosphate as the remedy migrates downfield, and additional hydraulic driving force to achieve the maximum lateral distribution of solid-phase calcium-phosphate.

Table 14 presents the final polyphosphate remediation amendment formulation. The solubility values listed in Table 2.7 were experimentally determined in tap water, filtered through a 0.45-µm filter at room temperature. Moreover, the values are not independent solubility values; rather, they are the maximum solubility within the total polyphosphate formulation. Results of batch and column tests demonstrated optimum performance is achieved using a formulation to which the contribution of phosphorus is 25% orthophosphate, 25% pyrophosphate, and 50% tripolyphosphate. Anhydrous forms of pyrophosphate and tripolyphosphate were used to maximize solubility and minimize cost. The mixture of the various components of the polyphosphate solution will be used to achieve a solution pH of ~7. The amendment solution will be prepared by mixing, in order, the sodium orthophosphate, sodium pyrophosphate, and sodium tripolyphosphate to achieve a pH of 7 and prevent degradation of polymerized phosphate molecules during preparation of the remedy solution. The total Ca:P molar ratio is 1.9.

Table 14. Pilot Scale Field Test Amendment Formulation

Injection	Amendment	Formula	CAS #	Formula Wt, g/mol	Solubility, g/L 23°C H_2O	Density, g/cm^3 (25°C)	Conc., g/L	Conc., M
1	Sodium phosphate, monobasic	NaH_2PO_4	7558-80-7	119.98	29.63	1.004	0.59	4.94 H 10^{-3}
	Sodium pyrophosphate	$Na_4P_2O_7$	7722-88-5	265.9	32.81		0.66	2.47 H 10^{-3}
	Sodium tripolyphosphate	$Na_5P_3O_{10}$	7758-29-4	367.86	60.40		1.21	3.29 H 10^{-3}
	Sodium bromide	NaBr		102.90			0.103	1.00 H 10^{-3}
2	Calcium chloride	$CaCl_2$	10043-52-4	110.98	800	1.005	3.41	3.07 H 10^{-2}
3	Sodium phosphate, monobasic	NaH_2PO_4	7558-80-7	119.98	29.63	1.004	0.59	4.94 H 10^{-3}
	Sodium pyrophosphate	$Na_4P_2O_7$	7722-88-5	265.9	32.81		0.66	2.47 H 10^{-3}
	Sodium tripolyphosphate	$Na_5P_3O_{10}$	7758-29-4	367.86	60.40		1.21	3.29 H 10^{-3}
	Sodium bromide	NaBr		102.90			0.103	1.00 H 10^{-3}

The viscosity of the amendment solutions was quantified using a TA Instruments AR2000 rheometer with a steel standard recessed end concentric cylinder. The procedure used to measure the viscosity had two ramp steps separated by a hold step. During the first step, the shear rate of the instrument was ramped from 0 to 150 s^{-1} over a 15-minute period collecting 300 data points. During the hold step, the shear rate was held at 150 s^{-1} for one minute collecting 60 data points. The shear rate was then ramped back to 0 s^{-1} over a 15-minute period collecting another 300 data points during the last step. Using the TA Instruments Rheology Advantage data analysis software, each ramp step was fit to the Newtonian equation to obtain the viscosity of 1.051 cP (Figure 39).

Newtonian Equation $$\tau = \eta \times \gamma \tag{18}$$

where τ = shear stress (Pascal, Pa)
γ = shear rate (per second, $^1/_s$)
η = viscosity (Pascal-seconds, Pa-s;).

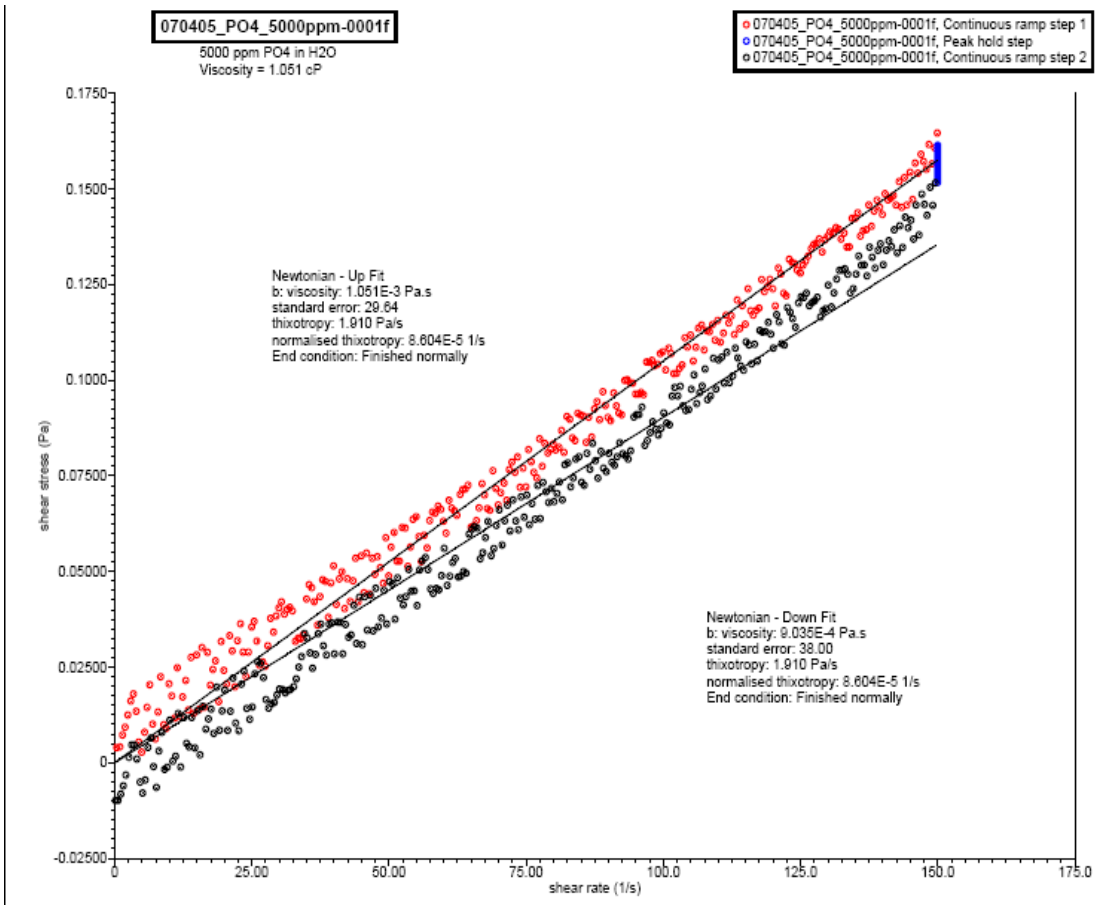

Figure 39. Viscosity of Polyphosphate Amendment

4.0 Conclusions

In this report a large body of data is presented from bench-scale treatability studies conducted under site-specific conditions in order to optimize the polyphosphate amendment for implementation of a field-scale technology demonstration to treat aqueous uranium within the 300 Area aquifer on the Hanford Site. The general treatability testing approach consisted of conducting studies with site sediment to develop an effective chemical formulation for the polyphosphate amendments and evaluate the transport properties of these amendments under site conditions. ^{31}P NMR was used to determine the effects of Hanford groundwater and sediment on the degradation of inorganic phosphates. Static batch tests were used to optimize the composition of the polyphosphate formulation for the precipitation of apatite and autunite, and to quantify the kinetics, loading, and stability of apatite as a long-term sorbent for uranium. Dynamic column tests further optimized the polyphosphate formulation for emplacement within the subsurface and the formation of autunite and apatite. Single-pass flow-through testing quantified the stability of apatite under conditions relevant to the 300 Area subsurface. The results of this investigation provide the necessary information for designing a full-scale remediation of uranium from the groundwater in the 300 Area aquifer on the Hanford Site.

5.0 References

Aagaard P and H Helgeson. 1982. "Thermodynamic and Kinetic Constraints on Reaction Rates among Minerals and Aqueous Solutions. I. Theoretical Considerations." *American Journal of Science* 282:237-285.

Abdelouas A, W Lutze, and HE Nuttall. 1999. "Uranium Contamination in the Subsurface: Characterization and Remediation." In *Uranium: Mineralogy, Geochemistry and the Environment*. PC Burns and RJ Finch, Eds., Mineralogical Society of America, Washington, D.C. 38:679.

Alwan AK and PA Williams. 1980. "The Aqueous Chemistry of Uranium Minerals. Part 2. Minerals of the Liebigite Group." *Mineralogical Magazine* 43:665-667.

Amjad Z, PG Koutsoukos, and GH Nancollas. 1981. "Crystallization of Fluoroapatite. A Constant Composition Study." *Journal of Colloid and Interface Science* 82(2):394-400.

Aoba T and EC Moreno. 1985. "Adsorption of Phosphoserine onto Hydroxyapatite and Its Inhibitory Activity on Crystal Growth." *Journal of Colloid and Interface Science* 106:110-121.

Arey JS, JC Seaman, and PM Bertsch. 1999. "Immobilization of Uranium in Contaminated Sediments by Hydroxyapatite Addition." *Environmental Science and Technology* 33:337-342.

American Society for Testing and Materials (ASTM). 2001. *Standard Test Method for Distribution Ratios by the Short-Term Batch Method*, D 4319-93, ASTM International, West Conshohocken, Pennsylvania.

American Society for Testing and Materials (ASTM). 2002. *Standard Test Method for Particle-Size Analysis of Soils*, D422-63, ASTM International, West Conshohocken, Pennsylvania.

Avrami M. 1939. "Kinetics of Phase Change, I." *Journal of Chemistry and Physics* 7:1103-1112.

Avrami M. 1940. "Kinetics of Phase Change, Ii." *Journal of Chemistry and Physics* 8:212-224.

Bertsch PM, DB Hunter, SR Sutton, S Bajt, and ML Rivers. 1994. "In Situ Chemical Speciation of Uranium in Soils and Sediments by Micro X-Ray Absorption Spectroscopy." *Environmental Science and Technology* 28:980-984.

Bethke CM. 1992. *The Geochemist's Workbench*. University of Illinois, Urbana-Champaign, Illinois.

Boskey AL and AS Posner. 1973. "Conversion of Amorphous Calcium Phosphate to Microcrystalline Hydroxyapatite. A pH-Dependent, Solution-Mediated, Solid-Solid Conversion." *Journal of Physics and Chemistry* 77:2313-2317.

Boskey AL and AS Posner. 1976. "Formation of Hydroxyapatite at Low Supersaturation." *Journal of Physics and Chemistry* 80:40-45.

Brown JL. 1980. "Calcium Phosphate Precipitation in Aqueous Calcite Limestone Suspensions." *Journal of Environmental Quality* 9(4):641-644.

Brown JL. 1981a. "Calcium Phosphate Precipitation: Effect of Common and Foreign Ions on Hydroxyapatite Crystal Growth." *Soil Science Society of America Journal* 45:482-486.

Brown JL. 1981b. "Calcium Phosphate Precipitation: Identification of Kinetic Parameters in Aqueous Limestone Suspensions." *Soil Science Society of America Journal* 45:475-477.

Brown WE, JP Smith, JR Lehr, and AW Frazier. 1962. "Crystallographic and Chemical Relations between Octacalcium Phosphate and Hydroxyapatite." *Nature* 196(4859):1050.

Brunauer S, PH Emmett, and E Teller. 1938. "Adsorption of Gases in Multimolecular Layers." *Journal of the American Chemical Society* 60:300-319.

Buck EC, NR Brown, and NL Dietz. 1996. "Contaminant Uranium Phases and Leaching at the Fernald Site in Ohio." *Environmental Science and Technology* 30:81-88.

Buck EC, NL Dietz, JK Bates, and JC Cunnane. 1994. *Uranium-Contaminated Soils: Ultramicrotomy and Electron Beam Analysis*. ANL/CMT/PP-82412, Argonne National Laboratory, Argonne, Illinois.

Buck EC, NL Dietz, JA Fortner, JK Bates, and NR Brown. 1995. *Characterization of Uranium- and Plutonium-Contaminated Soils by Electron Microscopy*. ANL/CMT/CP-85758; CONF-950216-65, Argonne National Laboratory, Argonne, Illinois.

Chen F, RC Ewing, and SB Clark. 1999. "The Gibbs Free Energies and Enthalpies of Formation of U^{6+} Phases: An Empirical Method of Prediction." *American Mineralogist* 84:650-664.

Christoffersen J. 1980. "Kinetics of Dissolution of Calcium Hydroxyapatite. Iii. Nucleation-Controlled Dissolution of a Polydisperse Sample of Crystals." *Journal of Crystal Growth* 49:29-44.

Christoffersen J and MR Christoffersen. 1982. "Kinetics of Dissolution of Calcium Hydroxyapatite: V. The Acidity Constant for the Hydrogen Phosphate Surface Complex." *Journal of Crystal Growth* 57:21-26.

Chukhlantsev VG and SI Stepanov. 1956. "Solubility of Uranyl and Thorium Phosphates." *Russian Journal of Inorganic Chemistry* 1(3):478-484.

Conca J, E Strietelmeier, N Lu, SD Ware, TP Taylor, JP Kaszuba, and J Wright. 2002. "Treatability Study of Reactive Materials to Remediate Groundwater Contaminated with Radionuclides, Metals, and Nitrates in a Four-Component Permeable Reactive Barrier." In *Handbook of Groundwater Remediation Using Permeable Reactive Barriers*. Academic Press, San Diego, California.

Conca JL. 1996. *Phosphate-Induced Metal Stabilization*. StARS Program, National Center for Environmental Research, Office of Research and Development, U.S. Environmental Protection Agency, Washington, D.C.

Conca JL, N Lu, G Parker, B Moore, A Adams, J Wright, and P Heller. 2000. "Pims - Remediation of Metal Contaminated Waters and Soils." In *Proceedings of the Second International Conference on Remediation of Chlorinated and Recalcitrant Compounds*.

Cotton S. 2006. *Lanthanide and Actinide Chemistry*, Wiley, West Sussex, England.

Davis A, MV Ruby, and PD Bergstrom. 1992. "Bioavailability of Arsenic and Lead in Soils from the Butte, Montana, Mining District." *Environmental Science and Technology* 26:461-468.

de Leeuw NH. 2004. "Resisting the Onset of Hydroxyapaite Dissolution through the Incorporation of Fluoride." *Journal of Physical Chemistry B* 108:1809-1811.

DeFord DH, RW Carpenter, and MW Finan. 1994. *300-FF-2 Operable Unit Technical Baseline Report*. BHI-00012, Rev. 00, Bechtel Hanford, Inc., Richland, Washington.

Diaz OA, KR Reddy, and PA Moore, Jr. 1994. "Solubility of Inorganic Phosphorous in Stream Water as Influenced by pH and Calcium Concentration." *Water Resources* 28(8):1755-1763.

Dorozhkin SV. 1997a. "Acidic Dissolution Mechanism of Natural Fluorapatite Ii. Nanolevel of Investigations." *Journal of Crystal Growth* 182:133-140.

Dorozhkin SV. 1997b. "Surface Reactions of Apatite Dissolution." *Journal of Colloid and Interface Science* 191:489-497.

Dorozhkin SV. 2002. "A Review on the Dissolution Models of Calcium Apatites." *Progress in Crystal Growth and Characterization of Materials* 44:45-61.

Eanes ED, IH Gillessen, and AS Posner. 1965. "Intermediate States in the Precipitation of Hydroxyapatite." *Nature* 208:365-367.

Eanes ED and JL Meyer. 1977. "Maturation of Crystalline Calcium Phosphates in Aqueous Suspensions at Physiologic pH." *Calcified Tissue Research* 23(3):259.

Eanes ED and AS Posner. 1965. "Kinetics and Mechanism of Conversion of Noncrystalline Calcium Phosphate to Crystalline Hydroxyapatite." In *Transactions New York Academy of Sciences*, New York.

Eanes ED and AS Posner. 1970. "A Note on the Crystal Growth of Hydroxyapatite Precipitated from Aqueous Solutions." *Materials Research Bulletin* 5(6):377-384.

Elless MP and SY Lee. 1998. "Uranium Solubility of Carbonate-Rich Uranium-Contaminated Soils." *Water, Air, and Soil Pollution* 107:147-162.

U.S. Environmental Protection Agency (EPA). 1996. *Record of Decision for Hanford 300-FF-1 and 300-FF-5 Operable Units Remedial Actions*, Agreement Between U.S. Department of Energy and EPA, with concurrence by the Washington State Department of Ecology, EPA, Washington, D.C.

Feenstra TP and PL de Bruyn. 1979. "Formation of Calcium Phosphates in Moderately Supersaturated Solutions." *Journal of Physical Chemistry* 83(4):475-479.

Ferguson JF, D Jenkins, and J Eastman. 1973. "Calcium Phosphate Precipitation at Slightly Alkaline pH Values." *Water Pollution Control Federation* 45(4):620-631.

Ferguson JF, D Jenkins, and W Stumm. 1970. "Calcium Phosphate Precipitation in Wastewater Treatment." *Chemical Engineering Progress Symposium Series* 107(67):279-287.

Finch RJ. 1997. "Thermodynamic Stabilities of U(Vi) Minerals: Estimated and Observed Relationships." *Material Research Society Symposium Proceedings* 465:1185-1192.

Finch RJ and T Murakami. 1999. "Systematics and Paragenesis of Uranium Minerals." In *Uranium: Mineralogy, Geochemistry and the Environment*. PC Burns and RJ Finch, Eds., Mineralogical Society of America, Washington, D.C. 38**:**91-180.

Fuller CC, JR Bargar, and JA Davis. 2003. "Molecular-Scale Characterization of Uranium Sorption by Bone Apatite Materials for a Permeable Reactive Barrier Demonstration." *Environmental Science and Technology* 37:4642-4649.

Fuller CC, JR Bargar, JA Davis, and MJ Piana. 2002a. "Mechanisms of Uranium Interactions with Hydroxyapatite: Implication for Groundwater Remediation." *Environmental Science and Technology* 36:158-165.

Fuller CC, MJ Piana, JR Bargar, JA Davis, and M Kohler. 2002b. "Evaluation of Apatite Materials for Use in Permeable Reactive Barriers for the Remediation of Uranium-Contaminated Groundwater." In *Handbook of Groundwater Remediation Using Permeable Reactive Barriers: Applications to Radionuclides, Trace Metals, and Nutrients*. DL Naftz, SJ Morrison, JA Davis and CC Fuller, Eds., Academic Press, San Diego, California.

Gamerdinger AP, DI Kaplan, DM Wellman, and RJ Serne. 2001a. "Two-Region Flow and Decreased Sorption of Uranium (Vi) During Transport in Hanford Groundwater and Unsaturated Sands." *Water Resources Research* 37(12):3155-3162.

Gamerdinger AP, DI Kaplan, DM Wellman, and RJ Serne. 2001b. "Two-Region Flow and Rate-Limited Sorption of Uranium (Vi) During Transport in an Unsaturated Silt Loam." *Water Resources Research* 37(12):3147-3153.

Gamerdinger AP, K van Rees, PSC Rao, and RE Jessup. 1994. "Evaluation of In Situ Columns for Characterizing Organic Contaminant Sorption During Transport." *Environmental Science and Technology* 28:376-382.

Garrels RM and CL Christ. 1965. *Solutions, Minerals and Equilibria*. Harper and Row Publishing Co., New York.

Garten VA and RB Head. 1966. "Philosophical Magazine." *14* 14(132):1243.

Gauglitz R and M Holterdorf. 1992. "Immobilization of Heavy Metals by Hydroxyapatite." *Radiochimica Acta* 58(59):253-257.

Gerber MS. 1992. *Past Practices Technical Characterization Study – 300 Area – Hanford Site*, WHC-MR-0388, Westinghouse Hanford Company, Richland, Washington.

Giammar DE. 2001. *Geochemistry of Uranium at Mineral-Water Interfaces: Rates of Sorption-Desorption and Dissolution-Precipitation Reactions*. California Institute of Technology, Pasadena, California.

Gramin P, JM Thomann, M Gumpper, and JC Voegel. 1989. *Journal of Colloid Interfacial Science* 128:370.

Gramin P, JC Voegel, M Gumpper, and JM Thomann. 1987. *Journal of Colloid Interfacial Science* 118:147.

Grenthe I, J Fuger, RJM Konings, RJ Lemire, AB Muller, C Nguyen-Trung, and H Wanner. 1992. *Chemical Thermodynamics of Uranium*. Organization for Economic Co-Operation and Development (OECD) Nuclear Energy Agency, Amsterdam, Holland.

Grossl PR and WP Inskeep. 1992. "Kinetics of Octacalcium Phosphate Crystal Growth in the Presence of Organic Acids." *Geochimica et Cosmochimica Acta* 56:1955-1961.

Guidry MW and FT Mackenzie. 2000. "Apatite Weathering and the Phanerozoic Phosphorus Cycle." *Geology* 28(7):631-634.

Guidry MW and FT Mackenzie. 2003. "Experimental Study of Igneous and Sedimentary Apatite Dissolution: Control of pH, Distance from Equilibrium, and Temperature on Dissolution Rates." *Geochimica et Cosmochimica Acta* 67(16):2949-2963.

Harlov DE, H-J Forster, and TG Nijland. 2002. "Fluid-Induced Nucleation of (Y+Ree)-Phosphate Minerals within Apatite: Nature and Experiment. Part I. Chlorapatite." *American Mineralogist* 87:245-261.

Inskeep WP and JC Silvertooth. 1988. "Kinetics of Hydroxyapatite Precipitation at pH 7.4 to 8.4." *Geochimica et Cosmochimica Acta* 52:1883-1893.

Jeanjean J, JC Rouchaud, L Tran, and M Fedoroff. 1995. "Sorption of Uranium and Other Heavy Metals on Hydroxyapatite." *Journal of Radioanalytical Nuclear Chemistry, Letters* 201(6):529-536.

Jenkins D, JF Ferguson, and AB Menar. 1971. "Chemical Processes for Phosphate Removal." *Water Research* 5:369-389.

Jensen MP, K Nash, JW Morse, EH Appelman, and MA Schmidt. 1996. "Immobilization of Actinides in Geomedia by Phosphate Precipitation." In *ACS Symposium Series 651,* American Chemical Society, Washington, D.C.

Kalmykov SN and GR Choppin. 2000. "Mixed $Ca^{2+}/Uo_2^{2+}/Co_3^{2-}$ Complex Formation at Different Ionic Strengths." *Radiochimica Acta* 88:603-606.

Karpov VI. 1961. "The Solubility of Triuranyl Phosphate." *Russian Journal of Inorganic Chemistry* 6:271-276.

Kato K, Y Eika, and Y Ikada. 1997. "In Situ Hydroxyapatite Crystallization for the Formation of Hydroxyapatite/Polymer Composites." *Journal of Materials Science* 32:5533-5543.

Kohler SJ, N Harouiya, C Chairat, and EH Oelkers. 2005. "Experimental Studies of Ree Fractionation During Water-Mineral Interaction: Ree Release Rates During Apatite Dissolution from pH 2.8 to 9.2." *Chemical Geology* 222:168-182.

Koutsoukos PG, Z Amjad, MB Tomson, and GH Nancollas. 1980. "Crystallization of Calcium Phosphates: A Constant Composition Study." *Journal of American Chemical Society* 102(5):1553-1557.

Kura G. 1987. "Alkaline Hydrolysis of Inorganic Cyclo-Polyphosphates." *Bulletin of Chemical Society of Japan* 60:2857-2860.

Kura G and T Tsukuda. 1993. "Effect of Copper(Ii), Nickel(Ii), and Aluminum(Iii) Ions on the Hydrolysis Rates of Inorganic Condensed Phosphate Oligomers." *Polyhedron* 12:865-870.

Langmuir D. 1978. "Uranium Solution-Mineral Equilibria at Low Temperatures with Applications to Sedimentary Ore Deposits." *Geochimica et Cosmochimica Acta* 42:547-569.

Lee SY, CW Francis, ME Timpson, and MP Elless. 1995. *Radionuclide Containment in Soil by Phosphate Treatment*. CONF-9503120-1, Oak Ridge National Laboratory, Oak Ridge, Tennessee.

Lindsay WL. 1979. "Phosphates." In *Chemical Equilibria in Soils*. JWa Sons, Ed., The Blackburn Press, Caldwell, New Jersey:163-209.

Lindsay WL and EC Moreno. 1960. "Phosphate Phase Equilibria in Soils." *Soil Science Society of America Proceedings* 24:177-182.

Ma QY, TJ Logan, and SJ Traina. "Effects of No_3, Cl and F on Pb Immobilization by Hydroxyapatite." *Environmental Science and Technology* .

Ma QY, SJ Traina, and TJ Logan. 1993. "In Situ Pb Immobilization by Apatite." *Environmental Science and Technology* 27:1803-1810.

Ma QY, SJ Traina, TJ Logan, and JA Ryan. 1994. "Effects of Aqueous Al, Cd, Cu, Fe(Ii), Ni, and Zn on Pb Immobilization by Hydroxyapatite." *Environmental Science and Technology* 28(7):1219-1288.

Manecki M, P Maurice, A., and SJ Traina. 2000. "Uptake of Aqueous Pb by Cl^-, F^-, and Oh^- Apatites: Mineralogic Evidence for Nucleation Mechanism." *American Mineralogist* 85:932-942.

Mavropoulos E, AM Rossi, AM Costa, CAC Perez, JC Moreira, and M Saldanha. 2002. "Studies on the Mechanisms of Lead Immobilization by Hydroxyapatite." *Environmental Science and Technology* 36:1625-1629.

McArthur JM. 1985. "Francolite Grochemistry – Compositional Controls on Formation, Diagenesis, Metamorphism, and Weathering." *Geochimica et Cosmochimica Acta* 49:23-25.

McGrail PB, JP Icenhower, PF Martin, DR Rector, HT Schaef, EA Rodriguez, and JL Steele. 2000. *Low-Activity Waste Glass Studies: FY 2000 Summary Report*. PNNL-13381, Pacific Northwest National Laboratory, Richland, Washington.

Misra DN. 1991. "Adsorption of Low Molecular Weight Poly(Acrylic Acid) on Hydroxyapatite: Role of Molecular Association and Apatite Dissolution." *Langmuir* **7**:2422-2424.

Moore RC, M Gasser, N Awwad, KC Holt, FM Salas, A Hasan, MA Hasan, H Zhao, and CA Sanchez. 2005. "Sorption of Plutonium(Vi) by Hydroxyapatite." *Journal of Radioanalytical and Nuclear Chemistry* 263(1):97-101.

Moore RC, K Holt, H Zhao, A Hasan, N Awwad, M Gasser, and C Sanchez. 2003. "Sorption of Np(V) by Synthetic Hydroxyapatite." *Radiochimica Acta* 91:721-727.

Moore RC, C Sanchez, K Holt, P Zhang, H Xu, and GR Choppin. 2004. "Formation of Hydroxyapatite in Soils Using Calcium Citrate and Sodium Phosphate for Control of Strontium Migration." *Radiochimica Acta* 92:719-723.

Moore RC, C Sanchez, J Schelling, J Jones, DR Anderson, F Salas, D Lucero, and K Holt. 2001. *Bench-Scale Testing of In-Situ Formation of Apatite in Hanford Soils for Sorption of Uranium and Technetium.* SAND2001-3001, Sandia National Laboratories, Albuquerque, New Mexico.

Moreno EC and K Varughese. 1981. "Crystal Growth of Calcium Apatites from Dilute Solutions." *Journal of Crystal Growth* 53:20-30.

Morris DE, PG Allen, JM Berg, CJ Chisholm-Brause, SD Conradson, RJ Donohoe, NJ Hess, JA Musgrave, and CD Tait. 1996. "Speciation of Uranium in Fernald Soils by Molecular Spectroscopic Methods: Characterization of Untreated Soils." *Environmental Science and Technology* 30(7):2322-2331.

Moskvin AI, AM Shelyakina, and PS Perminov. 1967. "Solubility Product of Uranyl Phosphate and the Composition and Dissociation Constants of Uranyl Phosphato-Complexes." *Russian Journal of Inorganic Chemistry* 12(12):1756-1760.

Murakami T, T Ohnuki, H Isobe, and T Sato. 1997. "Mobility of Uranium During Weathering." *American Mineralogist* 82:888-899.

Naftz DL, EM Feltcorn, CC Fuller, RG Wilhelm, JA Davis, SJ Morrison, GW Freethey, MJ Piana, RC Rowland, and JE Blue. 2000. *Field Demonstration of Permeable Reactive Barriers to Remove Dissolved Uranium from Groundwater, Fry Canyon, Utah*. EPA 402-C-00-001, Environmental Protection Agency, Washington, D.C.

Nagy KL. 1995. "Dissolution and Precipitation Kinetics of Sheet Silicates." In *Chemical Weathering Rates of Silicate Minerals*. AF White and SL Brantley, Eds., Mineralogical Society of America, Washington, D.C. 31:173-23.

Nancollas GH, Z Amjad, and P Koutsoukos. 1979. "Calcium Phosphates – Speciation, Sorption, Solubility, and Kinetics." In *Chemical Modeling in Aqueous Systems*. EA Jenne, Ed., American Chemical Society, Washington, D.C. 93:475-497.

Nancollas GH and MS Mohan. 1970. "The Growth of Hydroxyapatite Crystals." *Archives of Oral Biology* 15:731-745.

Nancollas GH and BB Tomazic. 1974. "Growth of Calcium Phosphate on Hydroxyapatite Crystals. Effect of Supersaturation and Ionic Medium." *Journal of Physics and Chemistry* 78:2218-2225.

Nash K. 2000. *Organophosphorous Reagents in Actinide Separations: Unique Tools for Production, Cleanup and Disposal*. ANL/CHM/CP-100858, Argonne National Laboratory, Argonne, Illinois.

Nash K, EJ Jensen, and MA Schmidt. 1998a. "In-Situ Actinide Immobilization of Actinides for Groundwater Cleanup: Laboratory Demonstration with Soil from the Fernald Environmental Management Project." In *Science and Technology for Disposal of Radioactive Tank Wastes*. WW Schultz and NJ Lombardo, Eds., Plenum Press, New York:507-518.

Nash K, MP Jensen, and MA Schmidt. 1997. "Actinide Immobilization in the Subsurface Environment by In-Situ Treatment with a Hydrolytically Unstable Organophosphorous Complexant: Uranyl Uptake by Calcium Phytate." In *International Conference on Actinides*, Baden-Baden, Germany.

Nash K, MP Jensen, and MA Schmidt. 1998b. "Actinide Immobilization in the Subsurface Environment by In-Situ Treatment with a Hydrolytically Unstable Organophosphorous Complexant: Uranyl Uptake by Calcium Phytate." *Journal of Alloys and Compounds* 271-273:257-261.

Nash K, LR Morse, MP Jensen, EH Appelman, MA Schmidt, S Friedrich, M Redko, and JJ Hines. 1999. *Water-Soluble Organophosphorous Reagents for Mineralization of Heavy Metals*. ANL/CHM/CP-98479, Argonne National Laboratory, Argonne, Illinois.

Nguyen SN, RJ Silva, HC Weed, and JE Andrews. 1992. "Standard Gibbs Free Energies of Formation at the Temperature 303.15k of Four Uranyl Silicates: Soddyite, Uranophane, Sodium Boltwoodite, and Sodium Weeksite." *Journal of Chemical Thermodynamics* 25:359-376.

O'Hare PAG, J Boerio, and HR Hoekstra. 1976. "Thermochemistry of Uranium Compounds: Vii. Solution Calorimetry of Alpha and Beta-Na_2uo_4, Standard Enthalpy of Formation of Beta-Na_2uo_4 and the Enthalpy of the Alpha to Beta Transition at 298.15 K." *Journal of Chemical Thermodynamics* 8:845-855.

O'Hare PAG, BM Lewis, and SN Nguyen. 1988. "Thermochemistry of Uranium Compounds Xvii. Standard Molar Enthalpy of Formation at 298.15 K of Dehydrated Schoepite Uo_3*0.9h_2o. Thermodynamics of (Schoepite+Dehydrated Schoepite+Water)." *Journal of Chemical Thermodynamics* 20:1287-1296.

Park H-S, I-T Kim, H-Y Kim, K-S Lee, S-K Ryu, and J-H Kim. 2002. "Application of Apatite Waste Form for the Treatment of Water-Soluble Wastes Containing Radioactive Elements. Part I. Investigation of the Possibility." *Journal of Industrial Engineering Chemistry* 8(4):318-327.

Payne TE, GR Lumpkin, and TD Waite. 1998. "Uranium (VI) Adsorption on Model Minerals." In *Adsorption of Metals by Geomedia*. EA Jenne, Ed., Academic Press, San Diego, California:75-130.

Pekarek V and V Vesely. 1965. "A Study on Uranyl Phosphates – II. Sorption Properties of Some 1- to 4-Valent Cations on Uranyl Hydrogen Phosphate Heated to Various Temperatures." *Journal of Inorganic and Nuclear Chemistry* 27:1151-1158.

Peterson REE, EJ Freeman, CJ Murray, RE Peterson, PD Thorne, MJ Truex, VR Vermeul, MD Williams, SB Yabusaki, JM Zachara, JL Lindberg, and JP McDonald. 2005. *Contaminants of Potential Concern in the 300-Ff-5 Operable Unit: Expanded Annual Groundwater Report for FY 2004*. PNNL-15127, Pacific Northwest National Laboratory, Richland, Washington.

Putnis A and CV Putnis. 2007. "The Mechanism of Re-Equilibration of Solids in the Presence of a Fluid Phase." *Journal of Solid State Chemistry* 180:1783-1786.

Renden-Angeles JC, K Yanagisawa, N Ishizawa, and S Oishi. 2000. "Topotaxial Conversion of Chlorapatite and Hydrocyapatite to Fluorapatite by Hydrothermal Ion Exchange." *Chemistry of Materials* 12:2143-2150.

Riley RG, JM Zachara, and FJ Wobber. 1992. *Chemical Contaminant on DOE Lands and Selection of Contaminant Mixtures for Subsurface Science Research*. DOE/ER-0547T, U.S. Department of Energy, Office of Energy Research, Washington, D.C.

Ruby MV, A Davis, and A Nicholson. 1994. "In-Situ Formation of Lead Phosphates in Soils as a Method to Immobilize Lead." *Environmental Science and Technology* 28:646-654.

Schaad P, F Poumier, JC Voegel, and P Gramain. 1997. "Analysis of Calcium Hydroxyapatite Dissolution in Non-Stoichiometric Solutions." *Colloids and Surfaces A: Physicochemical and Engineering Aspects* 121:217-228.

Schaad P, J-M Thomann, J-C Voegel, and P Gramain. 1994. "Inhibition of Dissolution of Hydroxyapatite Powder by Adsorbed Anionic Polymers." *Colloids and Surfaces A: Physicochemical and Engineering Aspects* 83:285-292.

Scheyer JM and CF Baes. 1954. "The Solubility of Uranium (Vi) Orthophosphates in Phosphoric Acid Solutions." *American Chemical Society Journal* 76:354-357.

Schmid LA and RR McKinney. 1968. "Phosphate Removal by a Lime-Biological Treatment Scheme." In *Water Pollution Control Federation*, Chicago, Illinois.

Seaman JC, JS Arey, and PM Bertsch. 2001. "Immobilization of Nickel and Other Metals in Contaminated Sediments by Hydroxyapatite Addition." *Journal of Environmental Quality* 30:460-469.

Seaman JC, J Hutchinson, BP Jackson, and VM Vulava. 2003. "In Situ Treatment of Metals in Contaminated Soils Using Phytate." *Journal of Environmental Quality* 32:153-161.

Sergeyeva EI, AA Nikitin, IL Khodakovkiy, and GB Naumov. 1972. "Experimental Investigation of Equilibria in the System Uo_3-Co_2h_2o in 25-200°C Temperature Interval." *Geochemistry International* 9:900-910.

Shen C and D Dyroff. 1966. "Hydrolytic Degradation of Sodium Tripolyphosphate in Concentrated Solutions and in the Presence of Foreign Ions." *Industrial & Engineering Chemistry Product Research and Development* 5:97-100.

Shen CY and FW Morgan. 1973. "Hydrolysis of Phosphorous Compounds." In *Environmental Phosphorous Handbook*. EJ Griffith, A Beeton, JM Spencer and DT Mitchell, Eds., John Wiley & Sons, New York:241.

Sowder AG, SB Clark, and RA Fjeld. 2000. "Dehydration of Synthetic Autunite Hydrates." *Radiochimica Acta* 88:533-538.

Stanforth R and A Chowdhury. 1994. "In-Situ Stabilization of Lead-Contaminated Soil." In *Federal Environmental Restoration III and Waste Minimization II Conference Proceedings*, New Orleans, Louisiana.

Termine JD, RA Peckauskas, and AS Posner. 1970. "Calcium Phosphate Formation in Vitro II. Effects of Environment on Amorphous-Crystalline Transformation." *Archives of Biochemistry and Biophysics* 140:318-325.

Termine JD and AS Posner. 1970. "Calcium Phosphate Formation in Vitro I. Factors Affecting Initial Phase Separation." *Archives of Biochemistry and Biophysics* 140:307-317.

Thakur P, RC Moore, and GR Choppin. 2005. "Sorption of U(Vi) Species on Hydroxyapatite." *Radiochimica Acta* 93:385-391.

Thomann JM, JC Voegel, and P Gramin. 1990. *Calcified Tissue Research* 46:121.

Tidwell VC, DE Morris, JC Cunnane, and SY Lee. 1996. "Characterizing Soils Contaminated with Heavy Metals: A Uranium Contamination Case Study." *Remediation Journal* 81-96.

Tomazic BB and GH Nancollas. 1975. "The Seeded Growth of Calcium Phosphates. Surface Characterization and the Effect of Seed Material." *Journal of Colloid and Interface Science* 50:451-461.

Valocchi AJ. 1984. "Describing the Transport of Ion-Exchanging Contaminants Using an Effective K_d Approach." *Water Resources Research* 20(4):499-503.

Valocchi AJ. 1985. "Validity of the Local Equilibrium Assumption for Modeling Sorbing Solute Transport through Homogeneous Soils." *Water Resources Research* 21(6):808-820.

Valsami-Jones E, KV Ragnarsdottir, A Putnis, D Bosboach, AJ Kemp, and G Cressey. 1998. "The Dissolution of Apatite in the Presence of Aqueous Metal Cations at pH 2-7." *Chemical Geology* 151:215-233.

van Cappellen P and RA Berner. 1991. "Fluorapatite Crystal Growth from Modified Seawater Solutions." *Geochimica et Cosmochimica Acta* 55:1219-1234.

Vermuel VR, JS Fruchter, DM Wellman, BA Williams, and MD Williams. 2006. *Site Characterization Plan: Uranium Stabilization through Polyphosphate Injection – 300 Area Uranium Plume Treatability Demonstration Project*. PNNL-16008, Pacific Northwest National Laboratory, Richland, Washington.

Vesely V, V Pekarek, and M Abbrent. 1965. "A Study on Uranyl Phosphates: Iii. Solubility Products of Uranyl Hydrogen Phosphate, Uranyl Orthophosphates and Some Alkali Uranyl Phosphates." *Journal of Inorganic and Nuclear Chemistry* 27:1159-1166.

Vochten R. 1990. "Transformation of Cherikovite and Sodium Autunite into Lehnerite." *American Mineralogist* 75:221-225.

Waichler SR and SB Yabusaki. 2005. *Flow and Transport in the Hanford 300 Area Vadose Zone-Aquifer-River System*. PNNL-15125, Pacific Northwest National Laboratory, Richland, Washington.

Watanabe M, S Sato, and H Saito. 1975. "The Mechanism of the Hydrolysis of Condensed Phosphates, Iii. The Mechanism of the Hydrolysis of Trimeta- and Tetrametaphosphates." *Bulletin of the Chemical Society of Japan* 48:3593-3597.

Wazer JV. 1958. *Phosphorus and Its Compounds*. Interscience Publishers, Inc., New York.

Wazer JV and E Griffith. 1955. "Structure and Properties of the Condensed Phosphates, Vii. Hydrolytic Degradation of Pyro- and Tripolyphosphate." *Journal of American Chemical Society* 77:287-291.

Wellman DM, JG Catalano, JP Icenhower, and AP Gamerdinger. 2005a. "Synthesis and Characterization of Sodium Meta-Autunite, $Na_2[(Uo_2)(Po_4)]_2$ $3h_2o$." *Radiochimica Acta* 93:1-7.

Wellman DM, JI Icenhower, EM Pierce, BK McNamara, SD Burton, KN Geiszler, SR Baum, and BC Butler. 2005b. "Polyphosphate Amendments for in Situ Immobilization of Uranium Plumes." In *Third International Conference on Remediation of Contaminated Sediments*, Battelle Press, Columbus, Ohio.

Wellman DM, JP Icenhower, AP Gamerdinger, and SW Forrester. 2006a. "Effects of pH, Temperature, and Aqueous Organic Material on the Dissolution Kinetics of Meta-Autunite Minerals, $(Na, Ca)_{2-1}[(Uo_2)(Po_4)]_2$ $3H_2o$." *American Mineralogist* 91:143-158.

Wellman DM, JP Icenhower, and AT Owen. 2006b. "Comparative Analysis of Soluble Phosphate Amendments for the Remediation of Heavy Metal Contaminants: Effect on Sediment Hydraulic Conductivity." *Environmental Chemistry* 3:219-224.

Wieker W and E Thilo. 1960. "The Catalytic Effect of Metal Ions on the Degradation of Polyphosphate in Aqueous Solutions." *Z. Anorg. Allgem. Chem.* 306:48-62.

Willard J, T Farr, and J Hatfield. 1975. "Hydrolysis of Ammonium Pyro-, Tripoly-, and Tetrapolyphosphate at 25° and 50°C." *Journal of Chemical and Engineering Data* 20:276-283.

Williams BA, CF Brown, W Um, MJ Nimmons, RE Peterson, BN Bjornstad, RJ Serne, FA Spane, and ML Rockhold. 2007. *Limited Field Investigation Report for Uranium Contamination in the 300 Area, 300-Ff-5 Operable Unit, Hanford Site, Washington*. PNNL-16435, Pacific Northwest National Laboratory, Richland, Washington.

Wolery TJ. 1992. *Eq3nr, a Computer Program for Geochemical Aqueous Speciation-Solubility Calculations: Theoretical Manual, User's Guide, and Related Documentation (Version 7.0)*. UCRL-MA-110662, Lawrence Livermore National Laboratory, Livermore, California.

Wolery TW and RL Jarek. 2003. *Eq3/6, Theoretical Manual, User's Guide, and Related Documentation (Version 8.0)*. Sandia National Laboratory, Albuquerque, New Mexico.

Wright J, LM Peurrung, TE Moody, JL Conca, X Chen, PP Didzerekis, and E Wyse. 1995. *In Situ Immobilization of Heavy Metals in Apatite Mineral Formulations*. Pacific Northwest Laboratory, Richland, Washington.

Wright J, HCW Skinner, SV Mattigod, and RJ Serne. 1991. *Solid Solution Apatite Mineral Formation Structure and Crystal Chemistry*. Pacific Northwest Laboratory, Richland, Washington.

Wu L, W Forsling, and PW Schindler. 1991. "Surface Complexation of Calcium Minerals in Aqueous Solution 1. Surface Protonation a Fluorapatite-Water Interfaces." *Journal of Colloid and Interface Science* 147(178).

Xu Y and FW Schwartz. 1994. "Lead Immobilization by Hydroxyapatite in Aqueous Solution." *Journal of Hydrology* 15:187-206.

Yanagisawa K, JC Renden-Angeles, N Ishizawa, and S Oishi. 1999. "Topotaxial Replacement of Chlorapatite by Hydroxyapatite During Hydrothermal Ion Exchange." *American Mineralogist* 84:1861-1869.

Young JS and JS Fruchter. 1991. *Addendum to Data Compilation Task Report for the Source Investigation of the 300-FF-1 Operable Unit Phase I Remedial Investigations*. EMO-1026, Environmental Management Operations for the U.S. Department of Energy, Richland, Washington.

Appendix A

Appendix A

Table A.1. The logK Values for Uranium Species at 25°C within the EQ3/6 Code V8.0 Database

Aqueous Species		Solid Species		Auxiliary Basis Set		Gaseous Species	
Formula	logK (25°C)	Formula	logK (25°C)	Formula	logK (25°C)	Formula	logK (25°C)
$(UO_2)_{11}(CO_3)_6(OH)_{12}^{+2}$	25.8549	$(UO_2)_2\ As_2O_7$	7.7285	U^{+3}	62.8818	U	294.0076
$(UO_2)_2(OH)_2^{+2}$	5.6565	$(UO_2)_2Cl_3$	12.7453		38.2257	U_2Cl_{10}	82.7628
$(UO_2)_2(PuO_2)(CO_3)_6^{-6}$	9.3821	$(UO_2)_2P_2O_7$	-14.6607	U^{+4}	32.5032	U_2Cl_8	82.4214
$(UO_2)_2CO_3(OH)_3^{-1}$	11.2448	$(UO_2)_3(AsO_4)_2$	9.3507		23.115	U_2F_{10}	-12.288
$(UO_2)_2NpO_2(CO_3)_6^{-6}$	8.4965	$(UO_2)_3(PO_4)_2$	-13.9912	UO^{+2}	-13.2003	UBr	221.9432
$(UO_2)_2OH^{+3}$	2.7291	$(UO_2)_3(PO_4)_2 : {}_4H_2O$	-27.0022		-12.1542	UBr_2	189.7405
$(UO_2)_3(CO_3)_6^{-6}$	8.093	$(UO_2)_3(PO_4)_2 : {}_6H_2O$	-27.8204			UBr_3	67.6501
$(UO_2)_3(OH)_4^{+2}$	11.9618	$Ba_2U_2O_7$	36.4643			UBr_4	54.3003
$(UO_2)_3(OH)_5^{+1}$	15.6191	Ba_3UO_6	94.382			UBr_5	61.4276
$(UO_2)_3(OH)_7^{-1}$	31.0836	BaU_2O_7	21.9795			UCl	218.8907
$(UO_2)_3O(OH)_2(HCO_3)^{+1}$	9.7457	$BaUO_4$	18.2117			UCl_2	180.9038
$(UO_2)_4(OH)_7^{+1}$	21.9946	$Be_{13}U$	1549.9856			UCl_3	58.3918
HUO_2 (aq)	21.2025	$CaUO_4$	15.953			UCl_4	46.4066
HUO_2^{+1}	5.0031	$Cs_2U_2O_7$	31.0483			UCl_5	54.5315
HUO_3^{-1}	16.5756	$CS_2U_4O_{12}$	18.9686			UCl_6	63.4902
HUO_4^{-1}	19.2454	Cs_2UO_4	35.9038			UF	203.3704
$U(CO_3)_4^{-4}$	6.2611	Li_2UO_4	27.8531			UF_2	169.4689
$U(CO_3)_5^{-6}$	17.8247	$MgUO_4$	23.0133			UF_3	47.0125
$U(NO_3)_2^{+2}$	-2.2533	$Na_2U_2O_7$	22.6135			UF_4	14.6056
$U(SCN)_2^{+2}$	-4.2585	Na_2UO_4	30.0341			UF_5	6.3805
$U(SO_4)_2$ (aq)	-10.3431	Na_3UO_4	56.2577			UF_6	18.2645
UBr^{+3}	-1.4163	$Na_4UO_2(CO_3)_3$	4.0504			UI	227.9182
UCl^{+3}	-1.6997	$NaUO_3$	8.3374			UI_2	191.6521
UF^{+3}	-9.2327	Rb_2UO_4	34.0198			UI_3	75.3615
UF_2^{+2}	-16.1429	UO_3: $2H_2O$ (Schoepite)	4.8443			UI_4	64.3349
UF_3^{+1}	-21.4731	$SrUO_4$ (alpha)	19.176			UO	208.7712
UF_4 (aq)	-25.4332	Uranium	208.4445			UO_2	124.1645
UF_5^{-1}	-26.8034	$U(HPO_4)_2{:}4H_2O$	-32.8574			UO_2Cl_2	47.974
UF^{-2}	-28.8336	$U(OH)_2SO_4$	-3.0654			UO_2F_2	34.6784
UI^{+3}	-1.2074	$U(SO_3)_2$	-36.7421			UO_3	70.9589
UNO_3^{+3}	-1.4429	$U(SO_4)_2$	-11.9785			UOF_4	24.2957
UO^{+1}	12.7087	$U(SO_4)_2{:}4H_2O$	-11.5208				
UO^{+2}	2.0068	$U(SO_4)_2{:}8H_2O$	-12.5479				
$UO_2(CO_3)_2^{-2}$	3.7577	U_2C_3	441.7818				
$UO_2(CO_3)_3^{-5}$	23.6245	U_2F_9	-45.4942				
$UO_2(CO_3)_3^{-4}$	9.4411	$U_2O_2Cl_5$	19.2832				
$UO_2(H_2PO_4)(H_3PO_4)^{+1}$	-22.7428	$U_2O_3F_6$	-2.4845				
$UO_2(H_2PO_4)_2$ (aq)	-21.7328	U_2S_3	10.4341				
$UO_2(IO_3)_2$ (aq)	-2.986	U_2Se_3	234.5112				

Aqueous Species		Solid Species		Auxiliary Basis Set		Gaseous Species	
Formula	logK (25°C)	Formula	logK (25°C)	Formula	logK (25°C)	Formula	logK (25°C)
$UO_2(N_3)_2$ (aq)	-4.3192	U_2As_4	471.7386				
$UO_2(N_3)_3^{-1}$	-5.7291	$U_3O_5F_8$	-2.7107				
$UO_2 (N_3)_4^{-2}$	-4.9091	U_3P_4	805.8205				
$UO_2(SCN)_2$ (aq)	-1.2553	U_3S_5	-0.8439				
$UO_2(SCN)_3^{-1}$	-2.0984	U_3Sb_4	515.1151				
$UO_2(SO_4)_2^{-2}$	-4.7419	U_3Se_4	356.4425				
UO_2 (aq)	4.5633	U_3Se_5	354.8366				
UO_2^{-1}	31.6845	U_4F_{17}	-104.7424				
UO_2Br^{+1}	-0.1731	$U_5O_{12}Cl$	-18.7778				
$UO_2BrO_3^{+1}$	-0.5401	UAs	144.416				
UO_2CO^3 (aq)	0.6838	UAs_2	182.3429				
UO_2Cl^{+1}	-0.1463	UBr_2Cl	17.5379				
UO_2Cl_2 (aq)	1.1362	UBr_2Cl_2	26.2262				
$UO_2ClO_3^{+1}$	-0.481	UBr_3	19.9367				
UO_2F^{+1}	-5.0393	UBr_3Cl	29.1254				
UO_2F_2 (aq)	-8.5294	UBr_4	31.2328				
$UO_2F_3^{-1}$	-10.7697	UBr_5	41.6317				
$UO_2F_4^{-2}$	-11.5298	$UBrCl_2$	14.2631				
$UO_2H_2PO_4^{+1}$	-11.661	$UBrCl_3$	23.5335				
$UO_2H_3PO_4^{+2}$	-11.301	UC	189.5102				
UO_2HPO_4 (aq)	-8.4288	$UC_{1.94}$ (alpha)	249.1236				
$UO_2IO_3^{+1}$	-1.6926	UCl_2F_2	-3.5008				
$UO_2N_3^{+1}$	-2.569	UCl_2I_2	30.3038				
$UO_2NO_3^{+1}$	-0.2696	UCl_3	13.0401				
UO_2OH (aq)	18.1622	UCl_3F	10.3277				
UO_2OH^{+1}	5.2173	UCl_3I	25.5465				
$UO_2OSi(OH)_3^{+1}$	2.481	UCl_4	21.9229				
$UO_2PO_4^{-1}$	-2.0688	UCl_5	33.8207				
$UO_2S_2O_3$ (aq)	35.1793	UCl_6	53.1432				
UO_2SCN^{+1}	-1.3922	$UClF_3$	-17.5044				
UO_2SO_3 (aq)	-6.7422	$UClI_3$	35.2443				
UO_2SO_4 (aq)	-3.0594	UF_3	-20.9385				
UO_3 (aq)	10.3117	UF_4	-30.3553				
UO_3^{-1}	36.4874	$UF_4{:}2.5H_2O$	-33.3607				
UO_4^{-2}	33.0259	UF_5 (alpha)	-12.8372				
UOH^{+2}	6.1849	UF_5 (beta)	-13.1683				
UOH^{+3}	0.5408	UF_6	17.5678				
$USCN^{+3}$	-2.9655	UH_3 (beta)	195.179				
USO_4^{+2}	-6.4927	UI_3	29.9408				
		UI_4	40.4934				
		UN	41.4712				
		$UN_{1.59}$ (alpha)	38.2266				
		$UN_{1.73}$ (alpha)	27.4312				
		$UO_2(AsO_3)_2$	6.9487				
		$UO_2(IO_3)_2$	-7.2761				
		$UO_2(NO_3)_2$	11.9709				
		$UO_2(NO_3)_2{:}2H_2O$	4.9556				

Aqueous Species		Solid Species		Auxiliary Basis Set		Gaseous Species	
Formula	logK (25°C)	Formula	logK (25°C)	Formula	logK (25°C)	Formula	logK (25°C)
		$UO_2(NO_3)_2:3H_2O$	3.7272				
		$UO_2(NO_3)_2:6H_2O$	2.33				
		$UO_2(NO_3)_2:H_2O$	8.5214				
		$UO_2(OH)_2$(beta)	4.9567				
		$UO_{2.25}$	-4.7626				
		$UO_{2.25}$(beta)	-4.7553				
		$UO_{2.3333}$(beta)	-26.7364				
		$UO_{2.6667}$	-41.6576				
		UO_2Br_2	16.488				
		$UO_2Br_2:3H_2O$	9.4224				
		$UO_2Br_2:H_2O$	12.1343				
		$UO_2BrOH:2H_2O$	4.2136				
		UO_2Cl	-0.5151				
		UO_2Cl_2	12.1037				
		$UO_2Cl_2:3H_2O$	5.6275				
		$UO_2Cl_2:H_2O$	8.299				
		$UO_2ClOH:2H_2O$	2.3174				
		UO_2F_2	-6.2647				
		$UO_2F_2:3H_2O$	-7.358				
		$UO_2FOH:2H_2O$	-2.6497				
		$UO_2FOH:H_2O$	-2.2729				
		$UO_2HPO_4:4H_2O$	-13.0122				
		UO_2SO_3	-15.9702				
		UO_2SO_4	2.4282				
		$UO_2SO_4:2.5H_2O$	-1.4803				
		$UO_2SO_4:3.5H_2O$	-1.4695				
		$UO_2SO_4:2H_2O$	-1.3919				
		UO_3 (alpha)	8.6501				
		UO_3 (beta)	8.3205				
		UO_3 (gamma)	7.8659				
		$UO_3:.9H_2O$ (alpha)	5.0276				
		$UOBr_2$	7.9817				
		$UOBr_3$	23.5777				
		UOCl	-9.7309				
		$UOCl_2$	5.8869				
		$UOCl_3$	8.5736				
		UOF_2	-18.1396				
		$UOF_2:H_2O$	-18.6942				
		UOF_4	4.5848				
		UOFOH	-8.9196				
		$UOFOH:.5H_2O$	23.1287				
		UP	227.4544				
		UP_2	350.9182				
		UP_2O_7	-32.9847				
		UPO_5	-19.5751				
		US	45.6883				
		$US_{1.9}$	-2.3238				

Aqueous Species		Solid Species		Auxiliary Basis Set		Gaseous Species	
Formula	logK (25°C)	Formula	logK (25°C)	Formula	logK (25°C)	Formula	logK (25°C)
		US_2	-2.3248				
		US_3	-16.626				
		USb	204.0673				
		USb_2	257.2654				
		USe	120.2947				
		USe_2 (alpha)	117.2323				
		USe_2 (beta)	117.0747				
		USe_3	136.111				
		Uraninite (UO_2)	-4.8295				
		Uranophane(alpha) $Ca(UO_2SiO_3OH)_2{:}5H_2O$	11.6891				
		Na-Weeksite $Na_2(UO_2)_2Si_5O_{13}{:}3H_2O$	4.0525				

Distribution

No. of Copies		
3	**DOE-Richland Operations Office**	
	K. M. Thompson	A6-38
	Public Reading Room (2)	H2-53

No. of Copies		
14	**Pacific Northwest National Laboratory**	
	J. S. Fruchter	K6-96
	V. R. Vermeul	K6-96
	D. M. Wellman	K3-62
	E. M. Pierce	K3-62
	S. D. Burton	K8-98
	E. L. Richards	K6-96
	K. E. Parker	K3-62
	E. A. Rodriguez	K3-62
	S. R. Baum	P7-22
	E. T. Clayton	P7-22
	B. A. Williams	K6-75
	M. D. Williams	K6-96
	Hanford Technical Library (2)	P8-55